ARTERIAL HEMODYNAMICS AND ITS INTERACTION WITH THE LEFT VENTRICLE IN HEART FAILURE

By

GINA N. HEGYI

A thesis submitted to the

Graduate School-New Brunswick

And

The Graduate School of Biomedical Sciences

Rutgers, The State University of New Jersey

In partial fulfillment of the requirements

For the degree of

Master of Science

Graduate Program in Biomedical Engineering

Written under the direction of

Professor John K-J. Li

Approved by

_____

_____

_____

New Brunswick, New Jersey

October 2015

ABSTRACT OF THE THESIS

Arterial Hemodynamics and Its Interaction with the Left Ventricle in Heart Failure

By GINA N. HEGYI

Thesis Director: Professor John K-J. Li

Monitoring heart-arterial system (LV-AS) interactions of cardiovascular patients is important in achieving successful diagnosis and treatment. This is particularly true in the cases of hypertension and heart failure. However, there has been limited quantitative hemodynamic analysis aimed at improving the outcome for the 70-million hypertensive patients and millions of heart failure patients. This thesis develops a model-based strategy to provide a comprehensive evaluation of the state of the vascular system and its coupling to the heart, and ultimately aims to distinguish patient groups of heart failure with preserved or reduced ejection fraction (HFpEF and HFrEF).

The first aspect of this study is analysis of arterial hemodynamics from animal experimental data collected during normotensive, vasodilation, and induced hypertension conditions. Total arterial compliance (C), peripheral resistance (R_s), and aortic characteristic impedance (Z_0) based on the 3-element Windkessel model were obtained, together with frequency-domain impedance, wave reflection information, and parameters for assessing global cardiac function. Subsequently, clinical human data were collected and analyzed, focusing on the LV-AS interactions. We identified critical parameters in LV-AS interaction, i.e. effective arterial system elastance, Ea, LV systolic elastance, Emax, LV-AS coupling index, k (=Ea/Emax), and C.

Results characterized hypertension by a significantly reduced C and increased R_s, confirmed by increased vascular impedance and wave reflections. Unloading the heart reversed these observations via vasodilator treatment. For human studies, we found C to be more effective than Ea in distinguishing groups of HFpEF and HFrEF patients. It was found that HFpEF patients tended to have a relatively independent coupling index, k, with respect to arterial parameter changes.

The findings in this work can be incorporated into larger scale clinical studies that implement the use of pulse waveform analysis and the identified critical LV-AS interaction parameters to improve patient treatment and outcome.

Acknowledgements

I would like to first and foremost thank God for giving me the opportunity, knowledge, and perseverance to complete this work; it is through Him that I am able to do all things.

Secondly, to Dr. John K-J. Li, I thank you for the patience and kindness you have shown me through teaching, guiding, challenging, and encouraging me during the past two years. It is truly a pleasure working with you.

I would like to thank Dr. Kenneth Khaw for his willingness to collaborate by providing clinical patient data for my thesis studies.

Lastly, I would like to acknowledge my parents, Jack and Laura Hegyi, and my fiancé, Lucas Galey, for their unending support, love, and prayers. I cannot thank you all enough.

Table of Contents

Chapter 1. Introduction

The cardiovascular system is complex and vital. Vascular networks distribute blood throughout the entire human body, and are responsible for exchanging nutrients and waste in the body's tissues and organs. Because of the complex and robust nature of these interactions, it can be difficult to identify or detect early signs of cardiovascular disease. Advances in medical equipment, procedures, and education are needed to address these diagnostic and treatment problems.

1.1 Physiological Background

The cardiovascular system (CVS) is composed of the heart and the many distributing blood vessels found in the body, namely, arteries, veins, and capillaries. The main functions of the CVS are to: (1) efficiently deliver nutrients to the entire body system, as well as remove waste; (2) act as a control system by regulating hormones to tissues; (3) maintain and distribute body temperature; and (4) control reproductive mechanisms (Levick, 2010).

The pumping of the heart induces rapid movement of blood by means of convective transport, or bulk flow. This flow is used to move blood distances greater than 0.1 millimeters, and moves the fluid at a rate of about 3 centimeters/second, covering a meter or more from the lungs to the smallest capillaries in roughly 30 seconds (Levick, 2010). In convection, blood flows through the arteries like a wave, which significantly influences the fluid dynamics and kinetics of bulk transport. The concepts of wave propagation and reflection will be covered in more detail in chapter 3, and are a focus of this study.

The other type of transport found in the CVS is diffusion, which occurs for the exchange of gases between the lungs and pulmonary circulation, as well as in the capillaries to the surrounding tissue. Diffusion is described as a voluntary transport of molecules down a concentration gradient. Diffusion in the CVS happens over distances of 0.3 to 10 microns, and

happens at a significantly slower rate than bulk flow (Levick, 2010). Convection and diffusion serve different, and important, roles in providing efficient and thorough transportation of fluids, nutrients, and gasses in the body — convection for energy-expensive, rapid, mass transport over long distances, and diffusion for energy-free, slower, passive transport over microscopic distances.

Arteries, arterioles, capillaries, venules, and veins are the CVS's pipelines. Varying levels of endothelium (thin cell linings), elastic and fibrous tissues, and smooth muscle cells make up each different type of vessel. Starting with the body's main artery, the aorta, these types of vessels move oxygenated blood away from the heart. As the aorta extends away from the heart, it branches into smaller, narrower, arteries, which continue to narrow and change composition, becoming arterioles and then capillaries. Once nutrients and waste are exchanged in the tissues in the capillary beds, veins carry partially deoxygenated blood back to the heart. The capillary beds transition and form more distinct vessels and grow in size as they move proximally and become venules, veins, and then the largest vein connected directly to the heart, the vena cava.

The composition of each vessel type varies to serve different functions. Large arteries have more elastic and fibrous components, allowing for better volume capacitance and support against higher pressures. Smaller arteries contain more smooth muscle, which provide a control mechanism to change vessel diameter. This allows smaller arteries to regulate flow dynamics in local areas by either relaxing or constricting the smooth muscle embedded in their walls. The capillaries and venules are the only classes that do not contain any elastic or muscle components; capillaries are made entirely of a thin layer of endothelium, allowing for quick and easy diffusion of nutrients to the surrounding tissue, whereas venules are only made of endothelium and fibrous tissue (Li, 2004).

In order for blood to travel through the circulation, the heart needs to pump. The heart, a hollow conically shaped organ with walls made of cardiac muscle tissue (myocytes), consists of four chambers: two upper atria and two lower ventricles (Figure 1.1). These chambers contract

and relax in a sequence that produces pressure and flow of blood through the heart, out to the body, and then back to the heart in a cycle. The left half of the heart receives oxygenated blood from the lungs and pumps to the rest of the body. The right half of the heart receives partially deoxygenated blood from the body and sends it to the lungs to become oxygenated. Therefore, the circulation of blood can be classified into two branches: the pulmonary circulation (path taken: heart to lungs to heart) and systemic circulation (heart to body to heart) (Figure 1.2). There are valves in the heart and veins that ensure flow occurs in the proper direction, and the heart valves help identify the phases of the ventricular cycle (Widmaier et al., 2007).

The beating of the heart is synchronized and rhythmic. This rhythm is maintained by electro-chemical stimulation produced by specialized pacemaker cells found in the sino-atrial node (SA node) that induce the relaxation and contraction of the cardiac muscle (Figure 1.3). Cardiac relaxation, or diastole, is the time when a chamber of the heart fills with blood. Contraction of the muscle is called systole, and is when the blood-filled chamber ejects some of its volume into the next pathway of the circulation (Figure 1.4).

The ventricular cycle consists of four phases: filling, isovolumetric contraction, ejection, and isovolumetric relaxation. Due to the cyclic pumping of the heart, pressure and flow are also oscillatory and cyclic (Figure 1.5). The end result of the ejection phase is the release of blood into the aorta. This ejection is called ventricular outflow, Q, which is defined as the change of ventricular volume over time (Li, 2004).

There are three main control/regulatory mechanisms of the heart: mechanical, electrical, and chemical. The mechanical control can be summarized by the Frank-Starling principle, which states that muscle contractile force increases directly with the amount of stretch the muscle undergoes before contraction (Caro et al., 2012). In application to the heart, if the cardiac muscle is stretched due to increase in venous blood volume into the heart, the muscle will respond with a stronger contractile force to eject a proportional volume of blood out of the heart. As described above, the electrical control mechanisms of the heart are vital to pacing the rhythmic beating. The

autonomic nervous system plays a role in the electrical regulation of the heart as well, specifically, the vagus nerve. Stimulation or inhibition of the firings of this nerve affects the cardiac output and heart rate beyond the normal self-stimulated pacemaker cells found in the SA node. Lastly, chemicals, for example hormones or dietary compounds, can affect heart rate and contractility. Chemical control is used mainly to regulate the heart in accordance to other systems in the body, for example the chemical compound caffeine stimulates the nervous system. But chemical pathways can be slow, especially hormones, but result in strong changes in average cardiac performance.

Understanding the basic physiological functions of each component of the cardiovascular system allows us to better identify and treat abnormalities and chronic illness. A major area of interest among physicians is heart failure (HF), which is a chronic and progressive syndrome. HF affects the heart's ability to supply an adequate supply of blood to the rest of the body. It should be noted that heart failure does not imply that the heart can no longer beat, but that the ventricles, due to either functional or structural abnormalities, cannot fill with or eject enough blood (Yancy et al., 2013).

The normal ways the body tries to combat the decreased blood flow is by stretching the size of the heart chambers to be able to fill with more blood, and increasing the strength of the heart's contractions to eject more blood. The heart may also increase its pumping rate to increase blood output, or it may increase the chamber wall's muscle mass (hypertrophy) to increase contractility. Peripherally, blood vessels narrow to maintain a constant blood pressure and the body's regulatory systems may divert blood from nonessential organs to maintain blood flow to vital systems like the brain and heart. However, these naturally occurring remedies do not solve the heart failure problem, and over time the body begins to show signs of fatigue and difficulty breathing. HF can affect either one side of the heart or both though it is most commonly seen in the left ventricle.

1.2 Risk Factors for Cardiovascular Disease

There are many factors linked to the development of cardiovascular diseases (CVDs), such as diabetes, obesity, aging, ethnicity, stress, life-style choices, and genetic predisposition. The World Health Organization has identified unhealthy diet, physical inactivity, tobacco use, and excessive alcohol consumption as the leading causes of CVD, and concluded that behavioral risk factors were responsible for ~80% of CVDs (World Health Organization, 2011a, 2013). Factors that increase the likelihood of developing a CVD include high levels of blood glucose, hypertension, elevated levels of blood lipids, and being overweight (World Health Organization, 2011b). There are some risk factors, however, that are beyond behavioral influences, such as social, cultural, hereditary, and economic determinants. For example, populations in poverty (low- and middle-income countries) account for ~80% of total CVD-related deaths in the world (World Health Organization, 2013). Increased world population life expectancy suggests that people are no longer dying of communicable disease, but rather more advanced non-communicable diseases due to old age and systematic failures like CVD.

Focusing on heart failure, certain conditions may lead to heart failure more often than others, and include coronary arterial disease, myocardial infarction, hypertension, abnormal heart valves, diabetes, cardiomyopathy, and sever lung disease ("Understand Your Risk for Heart Failure", n.d.). Coronary artery disease is a build up of cholesterol and fatty deposits (atherosclerosis) in the arteries that supply blood to the heart. This buildup can block blood flow to the heart muscle, and can lead to chest pain (angina), heart attack (myocardial infarction), high blood pressure, and heart failure. Myocardial infarction (MI) occurs when heart muscle tissue dies, or is damaged due to a cutoff of blood to the heart. The damaged tissue then cannot contract effectively and weakens the heart's pumping ability leading to possible heart failure. Having high blood pressure, or hypertension, increases the likelihood of having heart failure by two or three times due to the gradual weakening or thickening of the myocardium (American Heart Association, 2014).

1.3 Observed Hemodynamic Changes

Under healthy conditions, the CVS effectively regulates the pressure and flow of blood in the body by communication and feedback with the parasympathetic nervous system (part of the autonomic nervous system discussed previously). Pressure, flow, heart contractility and rate are kept in homeostasis via feedback of the nervous system and circulating hormones. Under disease conditions, however, the CVS struggles to maintain stable hemodynamic levels, and if not identified or treated expeditiously, chronic illness and heart failure may result.

As priorly mentioned, there are three main regulatory mechanisms used to maintain hemodynamic homeostasis (mechanical, electrical, and chemical). One of the most prominent control mechanisms, and one of high interest for our studies, is the mechanical contraction and relaxation of smooth muscle in blood vessel walls. This physical flexing and relaxing is used to regulate vessel diameter, and ultimately controls the flow, pressure, and distribution of blood in local areas (Levick, 2010).

Many regulatory pathways utilize vasoconstriction and dilation to influence circulation under extraneous conditions or disease states. Recall that smaller vessels, like capillaries and venues, have fewer regulation mechanisms in place to control diameter size. Resultantly, smaller vessels have more rigid walls. As the vessel walls stiffen, hemodynamic waveforms change in response to increased wall forces and decreased elasticity. Due to the body's inability to control these regions, under disease conditions, the unregulated regions can propagate disadvantageous hemodynamic components onto normally well-maintained regions to a point beyond control even for the most regulated systems. This leads to the complex clinical problems often associated with CVD. An example of this interconnectivity and disease progression is seen in chronic hypertension with the progressive stiffening of large elastic arteries, the narrowing of small resistive arteries, and the decrease in regulatory responsiveness and sensitivity to pressure change, all of which are normally well-regulated (Caro et al., 2012; Levick, 2010). These changes affect many CVS functions, including increased peripheral resistance and mean arterial pressure,

increased pulse pressure and pulse wave velocity, and peripheral resetting of the baroreflex (Joyner, 2006; Levick, 2010; Li, 2004; Parati and Esler, 2012).

Many parameters used to measure heart and vascular system health are inter-related, and understanding how physiological changes affect these measures is important in understanding the causes and possible treatments for disease. For example, in high blood pressure conditions, the systemic (peripheral) vascular system begins to resist blood flow more and arterial stiffness increases (by the changes just described). Cardiologists created parameters based on physically measureable variables that describe both changes: total peripheral resistance (R_s) and total arterial compliance (C) (the inverse of arterial stiffness), shown in equations (1.1) and (1.2).

$$Rs \approx \frac{\overline{P}}{\overline{Q}} \tag{1.1}$$

$$C = \frac{dV}{dP} \tag{1.2}$$

It can be seen that peripheral resistance increases as mean pressure increases ($\overline{P}$) and/or mean flow decreases ($\overline{Q}$). Compliance will decrease (hence, stiffness will increases) as change in distending pressure (dP) increases and/or change in volume (dV) decreases.

Another standard clinical measure of heart health is ejection fraction (EF)—the ratio of stroke volume (SV) to left ventricle end-diastolic volume (LV-EDV). The mathematics behind these measures are covered in more detail in chapter 3. Left ventricular EF is the standard measure of systolic function of the heart, and can be measured both invasively and noninvasively (Iwano and Little, 2013). A healthy EF is considered >0.50, and indicates that the heart is able to produce adequate pressure to eject blood from the LV into the aorta. Therefore, if the left ventricle is pumping 65% of its total chamber volume out per beat then EF is 0.65. Changes in EF are used to indicate disease and heart failure (HF). When EF is less than 0.40, a patient is diagnosed with heart failure with reduced ejection fraction (HFrEF). What causes EF to decrease in these patients can be described by an increase in LV-EDV relative to SV, and a dilation

(ballooning) of the left ventricle. A reduced EF is a clear signal of systolic dysfunction and heart failure; however, another type of heart failure can take place with a normal, or preserved, ejection fraction (HFpEF). Here, EF >0.05 and there is an equal ratio of SV to LV-EDV. Though a normal EF exists, that does not lessen the impacts of HFpEF, and recent studies have indicated that HFpEF patients display an increase in both LV and arterial elastance (Iwano and Little, 2013).

1.4 Model-Based Analysis

Due to the inter-connected nature of our body, being able to simulate specific systems, or parts of a system, is valuable in expanding our understanding of how individual components interact and function. Theoretical or experimental models allow us to accurately and confidently simplify complex networks of interactions, and help reveal prominent mechanisms or pathways that influence the overall system's behavior. These models can be mathematical, physical, electrical, or computer based, and depending on the focus of a study, different models are more appropriate than others.

Historically, mathematic, analog, physical, computer-based, and combinations of these, have been used to simulate wave propagation and cardiovascular function (Burattini and Gnudi, 1982; Chau et al., 1979; Hardy et al., 1982; Jager et al., 1965; Lee et al., 2004; McIlroy et al., 1986; Noordergraaf, 1978; Shim et al., 2004; Sud et al., 1992; Westerhof et al., 1969). These models range from complex branching and lumped parameter electrical analog networks (Hardy et al., 1982; Jager et al., 1965; O'Rourke and Avolio, 1980; Westerhof et al., 1971) to simple vessel and T-tube models (Berger et al., 1996; Burattini et al., 1991; O'Rourke, 1967). Mathematically and physically, all models make assumptions and simplifications, such as lumping similarly behaving components, excluding minor changes, or assuming ideal conditions or steady states. The model used in this study is no exception to necessary simplifications.

The model that allows description of the hemodynamic behaviors in the arterial system is the lumped Windkessel model (Li, 2004; Westerhof et al., 2009). The basic Windkessel model

consists of two elements, an electrical resistor and capacitor, and was proposed mathematically by Otto Frank in 1899. The two-element Windkessel simulates the arterial blood flow ejected from the heart as it travels through the large elastic arteries, i.e. the aorta and resistive peripheral systemic vasculature. The two components of the model are total arterial compliance, C, and peripheral resistance, R_s. To be able to simplify such a complex network into these two parameters, it is required to lump similar components together (Figure 1.6). Therefore, the two-element model describes pulsatile pressure and flow through the entire arterial system in terms of R_s and C. This description is too basic to let us understand the details within the arterial system such as wave reflection and propagation. In order to study this, a more complex model is needed.

To study flow and wave propagation, the two-element model was adapted with the addition of another element, the aortic characteristic impedance, Z_0. This change came with advancements in technology to physically measure aortic flow, and computational power to perform Fourier analysis on pressure and flow waveforms to calculate input impedance (the concept of impedance is covered in more detail in chapter 3). Making a simple assumption about the observed characteristic impedance at high frequencies, the three-element Windkessel model was developed. This proposed model demonstrates the link between resistance, compliance, and wave propagation, because characteristic impedance is defined as wave speed multiplied by blood density and divided by aortic cross-sectional area. Figure 1.8 gives a visual representation of the two- and three-element Windkessel models in both hydraulic (physical) and electrical terms.

The use of the three-element Windkessel, though successful in describing the arterial system, is not sufficient in studying the coupling of the heart and the arterial system. A goal of this thesis is to study the interactions of the heart and arterial system and how they relate in heart failure. Additional components have been introduced to the three-element model to allow investigators to study the coupling that occurs between the left ventricle (LV) and the arterial system (AS). This expanded model will be used in this thesis to study the LV-AS coupling and interactions, and is covered in more detail in chapter 3. The hemodynamic changes that occur in

the two main classes of HF (HFpEF and HFrEF) can therefore be studied more closely using this model.

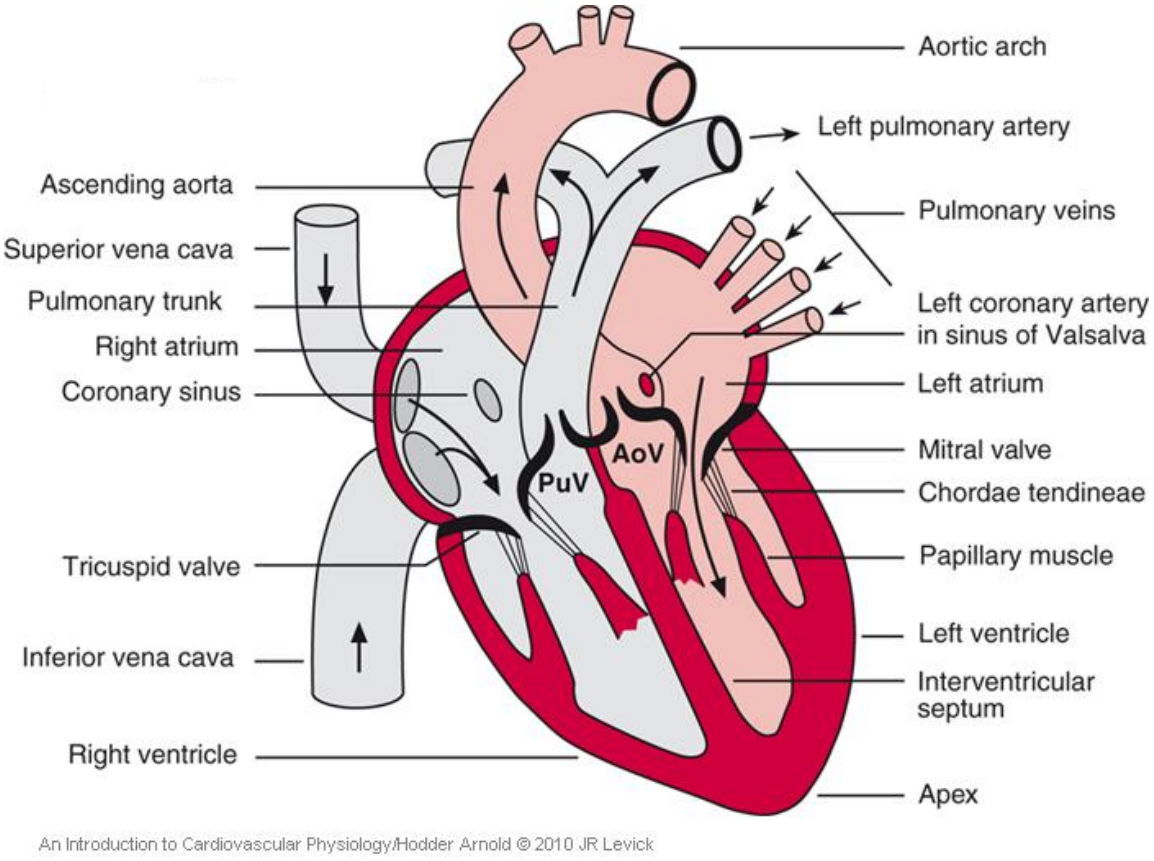

Figure 1.1: Anatomy and blood flow of the heart. The left heart and connected vessels (pink) pump oxygenated blood. The right heart and connect vessels (grey) pump deoxygenated blood. AoV and PuV are aortic and pulmonary valves, respecitvely (modified from Levick, 2010).

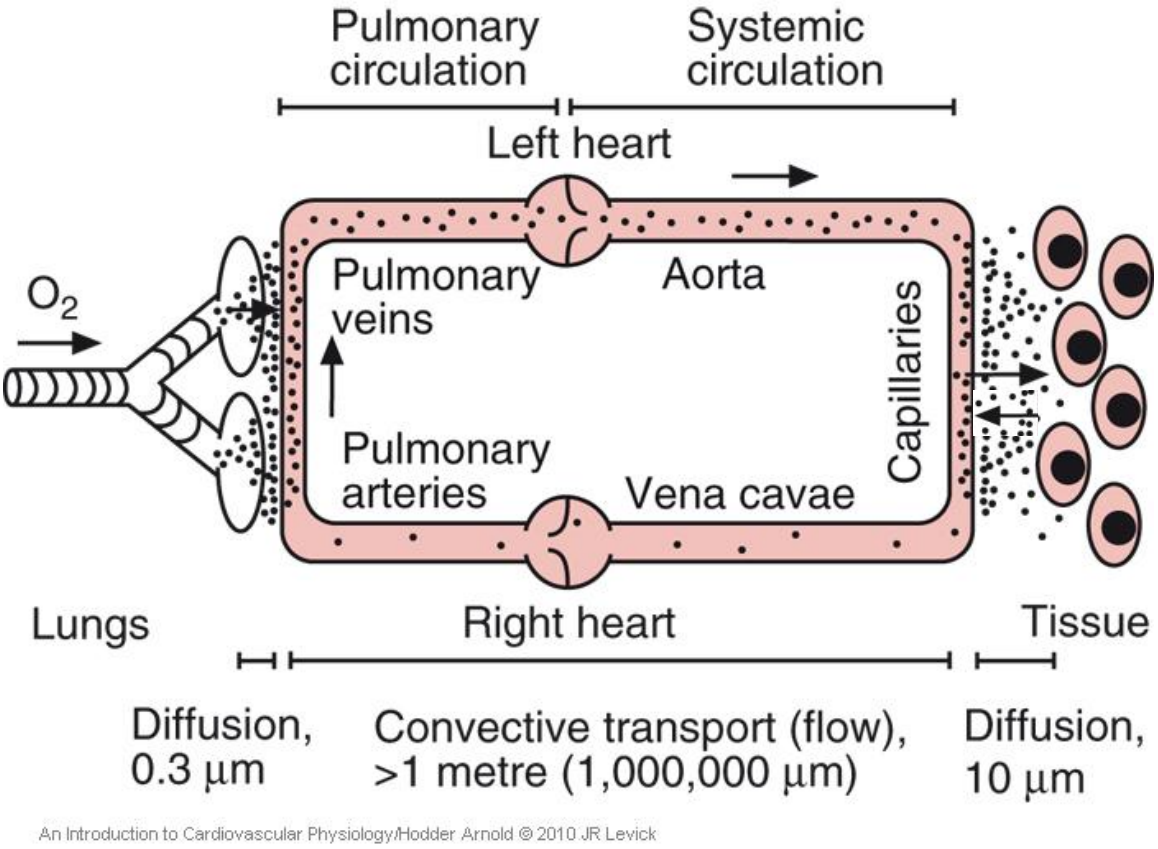

Figure 1.2: Map of human circulation and oxygen gas transport: pulmonary and systemic circulation (modified from Levick, 2010).

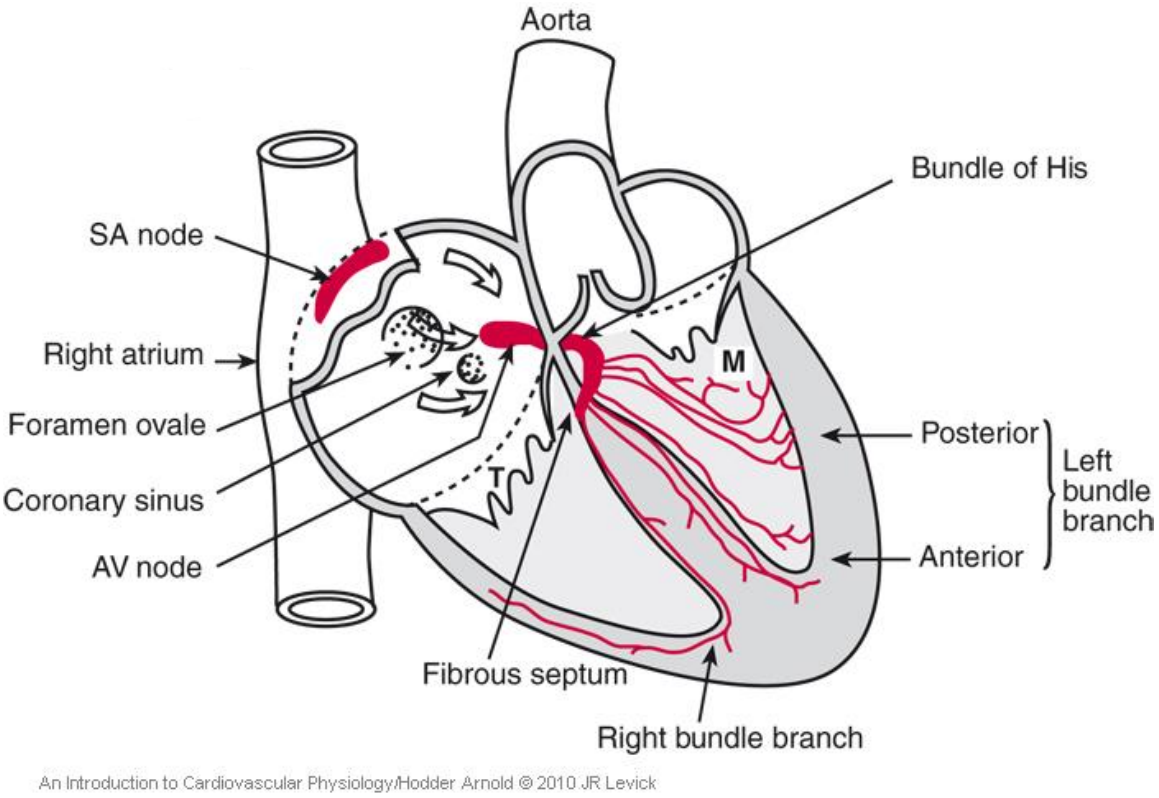

Figure 1.3: Cardiac conduction structures and pathways (modified from Levick, 2010).

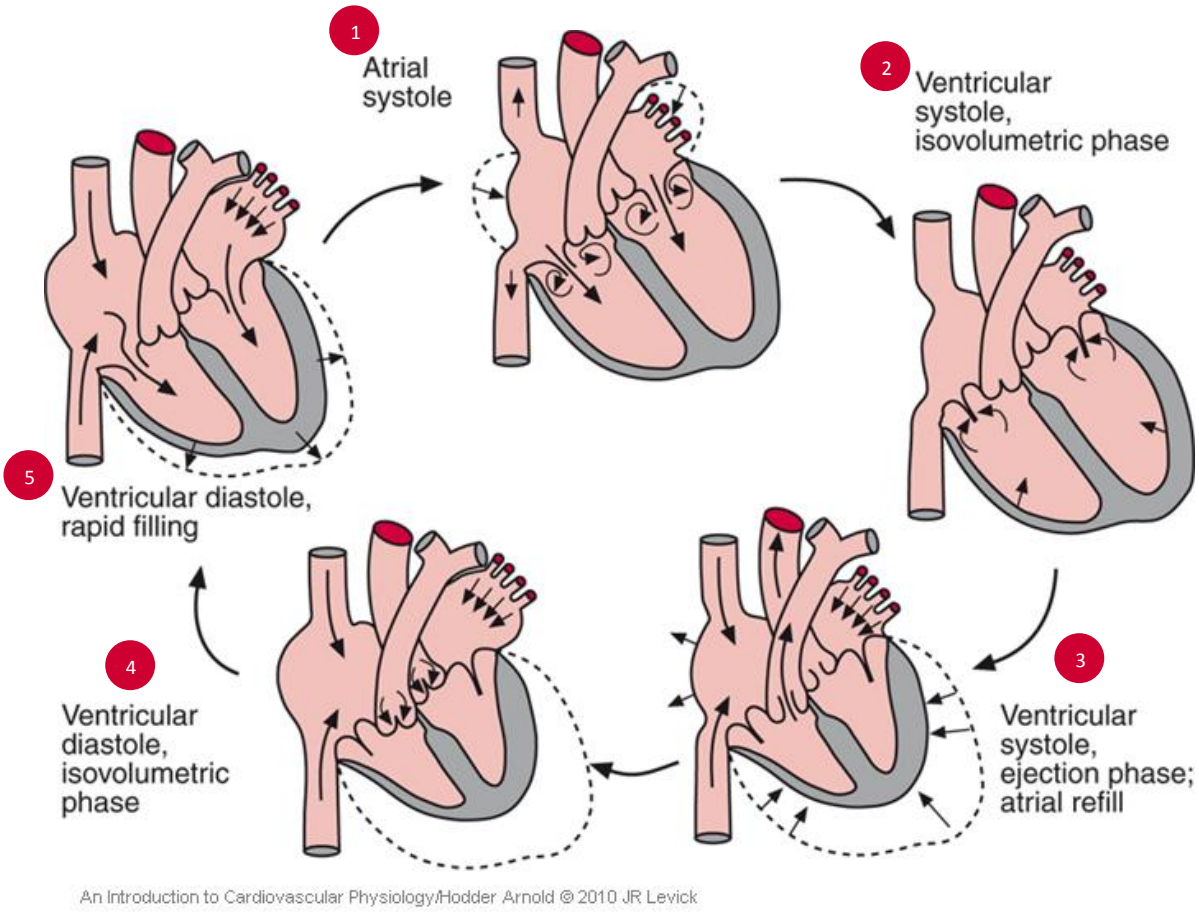

Figure 1.4: Heart valve openings and closings, and atrial and ventricular volume changes during a complete cardiac cycle in terms of ventricular and atrial systole and diastole (modified from Levick, 2010).

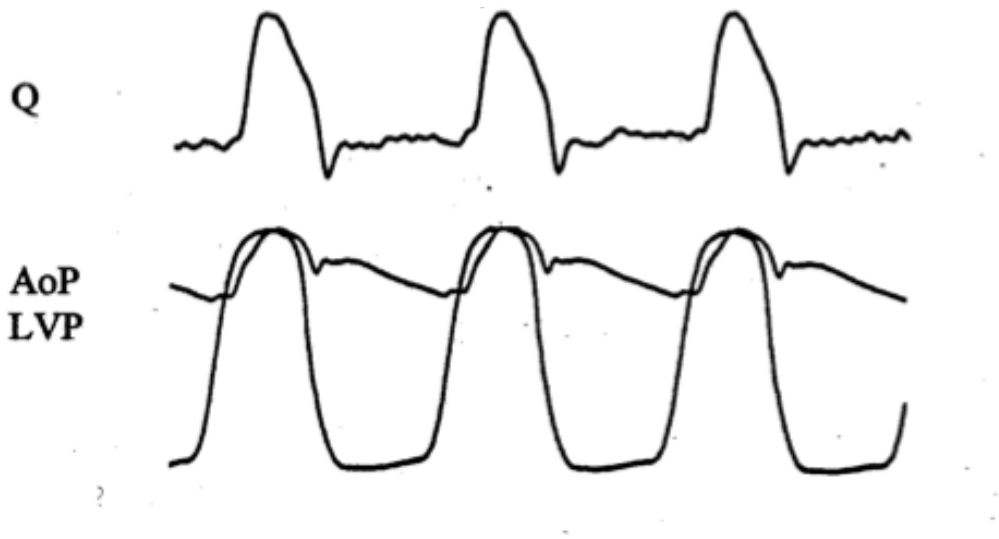

Figure 1.5: Aortic and left ventricular pressure and aortic flow waveforms over time – measured simultaneously. Left ventricular pressure (LVP), aortic pressure (AoP), and aortic flow (Q) (modified from Li, 2004).

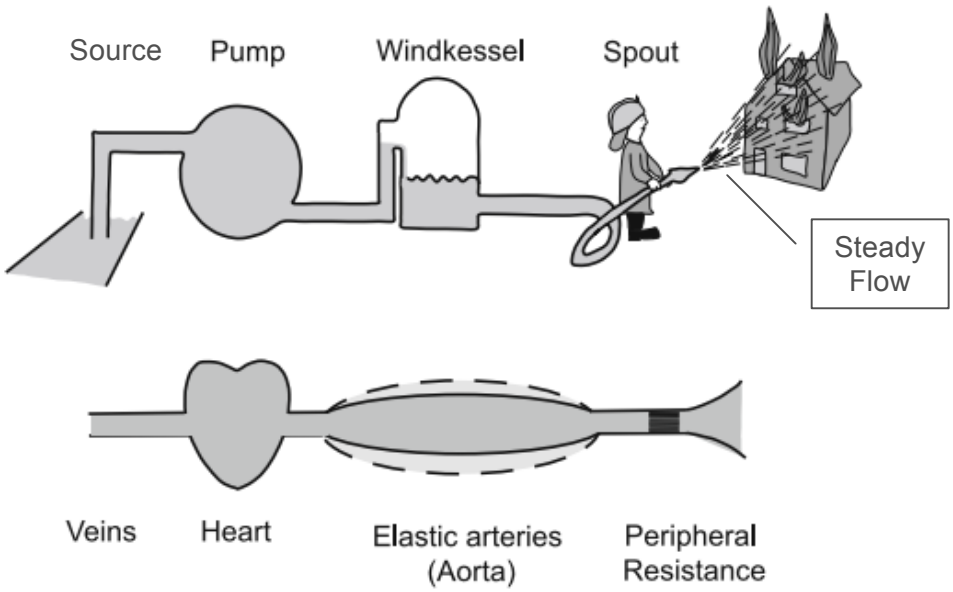

Figure 1.6: The Windkessel analogy: a reservoir represents the Windkessel component, and is key to allowing for storage of fluid for steady fluid streams out of the spout. Physically, the large arteries act as this reservoir (Windkessel) element. Arterial compliance, aortic valve openings and closings, and peripherally resistant pathways work together to provide a relatively constant peripheral flow (modified from Westerhof et al., 2009).

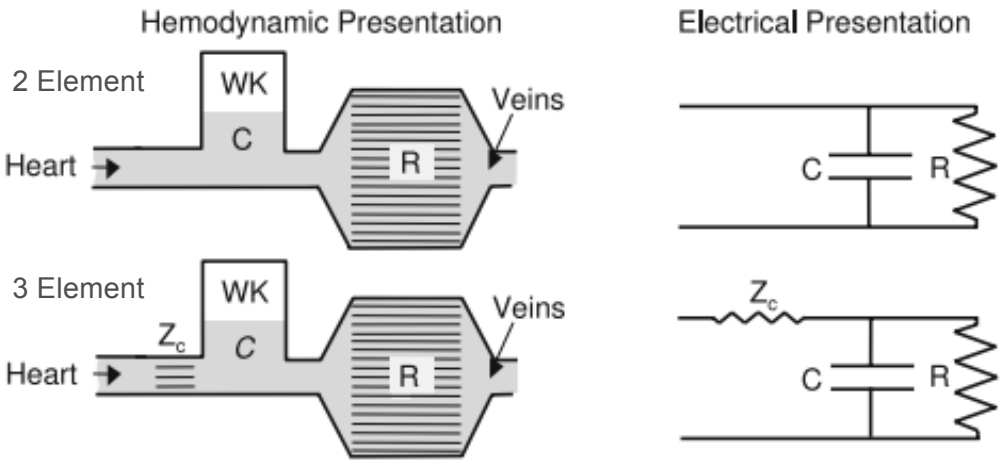

Figure 1.7: Representations of the Windkessel multi-element model presented in hemodynamic and electrical forms. Z_c is characteristic impedance of the aorta (modified from Westerhof et al., 2009).

Chapter 2. Aims and Significance of the Research

For decades cardiovascular diseases (CVDs) have been, and continue to be the leading cause of global mortality. Of the total global deaths in 2008, 30% were due to CVD. It is projected that total mortality will continue to grow from more than 17 million deaths in 2008, to 23.3 million deaths in 2030 (World Health Organization, 2011a, 2011b). High blood pressure, stroke, and heart attack constitute the main causes of CVD related deaths, with hypertension making up about 9.4 million, or 16.5% of all deaths annually (World Health Organization, 2013). Of deaths due to stroke or coronary heart disease, hypertension was found to be responsible for 51% and 45% of cases, respectively (World Health Organization, 2013). These serious effects of hypertension lead to great interest in identifying the pertinent parameters that contribute to hypertension and heart failure, to allow for the diagnoses, treatments, and preventions of the conditions.

2.1 Specific Aims

This thesis focuses on:

1. Quantifying hemodynamic changes that occur in hypertension and heart failure based on derivable model parameters. A list of these pertinent hemodynamic parameters include:

   Total arterial compliance (C)

   Total peripheral resistance (R_s)

   Stroke volume (SV)

   Cardiac output (CO)

   Heart rate (HR)

   Diastolic pressure (P_d)

   Systolic pressure (P_s)

   End-systolic pressure (P_{es})

Ejection fraction (EF)

Characteristic impedance (Z_0)

Input impedance (Z)

Left ventricle maximum elastance (Emax)

Effective arterial elastance (Ea)

Left ventricle-arterial system coupling index (k)

2. Quantifying pulse wave reflections, by resolving pulsatile pressure and flow into their forward and reflected components.
3. Interpreting hemodynamic changes under altered physiological conditions of induced hypertension and subsequent anti-hypertensive vasodilator administration.
4. Measuring heart-arterial system interactions (LVASI) by tracking stroke volume, ejection fraction, heart rate, and cardiac output in heart failure patients.
5. Constructing left ventricular pressure-volume (P-V) loops for heart failure patients with reduced or preserved ejection fraction to calculate maximum elastance, effective elastance, and the LV-AS coupling index.
6. Interpreting temporal LVASI changes and how wave reflections affect left ventricle function in heart failure by calculating arterial compliance.
7. Differentiate patients with heart failure with preserved or reduced ejection fraction based on LVASI parameters.

2.2 Significance

There is a current need for advances in diagnostics, treatment, and monitoring of cardiovascular disease such as hypertension and heart failure. With cardiovascular disease being the main cause of global mortality, understanding how peripheral resistance, compliance, and impedance of the arterial system change in disease conditions will allow doctors to better treat patients, and ultimately avoid developing heart failure. Studying the interactions of the left ventricle and arterial system will give insight into key parameters that can be used to identify at-risk patients, as well as classify heart failure patients into respective groups of reduced or preserved ejection fraction. There is a current need for a link between a universal index, or non-dimensional ratio, and pertinent cardiovascular parameters that can be used to diagnose patients with HFpEF due to the almost-asymptomatic progression of the disease in the elderly, especially in those with hypertension.

Creating a tool for clinical use that makes detecting hypertension and critical heart failure in its early stages will benefit society greatly. Though many doctors are not trained in understanding the relationship between pressure and flow in the cardiovascular system, a simple index used to measure LVASI health that can translate a plethora of patient measurements and parameters into a diagnosis will allow for better treatment and care for those at risk of hypertension and hypertensive-related heart failure. Model-based analysis is the first step in developing this diagnostic technology, and allows for investigation into significant changes and trends seen in disease cases.

Chapter 3. Methods and Analysis

3.1 Experimental Data Collection

Retrospective Animal Experimental Studies:

Data was obtained from previous experiments in six anesthetized, open-chest mongrel canines (Li et al., 1990). Rutgers IACUC (Institutional Animal Use and Care Committee) previously approved the experimental protocol (Li et al., 1990). A pressure sensor on the tip of a catheter, and a Biotronex BL-610 flow probe positioned over the aorta were used to measure simultaneous measurements of aortic pressure and flow. EKG leads were also positioned and attached to provide simultaneous lead II EKG information. The collected signals were digitized using BIOPAC software at a sampling rate of 100 hertz. The pressure transducer's and flow probe's frequency responses were uniform beyond 100 Hz and uniform within 5% up to 35 Hz, respectively. Three conditions were studied: steady-state normotensive; induced hypertension by systemic intravenous administration of methoxamine; and subsequent vasodilation by intravenous sodium nitroprusside.

The weights of the six canines ranged from 20-24 kg. The anesthetic Nembutal (pentobarbital sodium) (30 mg/kg) was given intravenously, and ventilation was through the tracheal tube with an external respirator. The ascending aorta was isolated via a left thoracotomy at the fifth intercostals space, and a cuff-type electromagnetic probe was put in placement. A dual-sensor Millar catheter-tip semiconductor pressure transducer was inserted retrograde into the femoral artery and maneuvered to the point where the proximal sensor was positioned (the same location as the flow probe).

Retrospective Human Studies:

Aortic and left ventricular pressure waveforms and echocardiogram data was obtained from previously collected medical records and procedures in 18 adult cardiovascular patients. All

patient data sets received for this study were without patient identifying information (PHI) or identification key code in accordance to HIPPA and Institutional Review Board (IRB) Authorization guidelines, and were obtained in close proximity to each other. IRB has approved the use of recorded data. The retrospective records included the use of aortic and left ventricle pressure waveforms, catheterization reports and measurements, echocardiogram reports, and medical history.

For catheterization, the risks, benefits and alternatives of procedure were explained to each patient and appropriate consent was obtained before the procedure was performed in a hospital Cath Lab under aseptic technique using Lidocaine local anesthetic, appropriate guide wire, contrast media (Amersham Visipaque), pressure transducer tip catheters (6FR Arrow Wedge Pressure; Cordis 4FR JR4), sheaths (Cordis Corporation AVANTI), and dilators. Catheters were inserted retrograde into either the left or right femoral artery and maneuvered to the aorta and left heart where contrast dyes were used to visualize flow and abnormalities. Catheter measurement equipment was zeroed before each measurement, and the mid actuary line was estimated. Pressure and simultaneous electrocardiogram measurements were recorded in the aorta and left ventricle, and continuous data was collected and electronically saved. Following the procedure, the sheath(s) was/were removed and hemostasis was obtained.

Transthoracic echocardiograms with complete 2D standard four-chamber view, M-Mode, color, and Doppler examinations were conducted for each patient using a 2-5 hertz transducer with adjusted resolution and varying phase for best visualization. M-Mode and 2D measurements and calculations were reported on the final patient report, along with time and Doppler measurements. No images or volume waveforms were provided in the patient data sets, though end systolic/diastolic volumes were reported.

LV and aortic pressure waveforms used in this work were obtained as scanned copies, which were then digitized using WebPlotDigitzer 3.6 software (Rohatgi, 2015) and imported into MATLAB 2014a (MathWorks Inc., 2014).

3.2 The Windkessel Model and Computation of Arterial System Parameters

The arterial tree was lumped into a simplified system using the 3-element Windkessel model (Figure 3.1). Compliance and total peripheral resistance were calculated from aortic pressure and flow waveform data (example waves shown in Figure 1.6).

As described in chapter 1, compliance (C) is a measure of arterial stiffness, and is defined in equation (1.2) as the ratio of change in volume over the simultaneous change in pressure measured during one period of the cardiac cycle. Total arterial compliance is the summation of compliances for the large elastic arteries and vessels. Peripheral resistance, R_s, is a measure of collective resistance to flow of fluid through the entire systemic vascular bed. As shown in equation (1.1), R_s is the average pressure divided by the average flow for a full period of the cardiac cycle. In this chapter, a deeper discussion and derivation of these equations will be covered.

The Windkessel model uses a capacitor to represent the storage properties of the large arteries, and a resistor to represent the small peripheral vessels. The terms compliance and peripheral resistance are paired to their respective components due to physiological characteristics of large arteries and small vascular beds. The pumping of the heart during systole distends the large arteries allowing them to hold a reservoir of blood, which during diastole is slowly ejected into the smaller peripheral vessels (Figure 3.2). This way the arterial stretching and contracting (mainly of the aorta) is what is thought to be largely responsible for the transition between pulsating flow from the heart to steady flow through the periphery (Li, 2004).

The Windkessel model simulates aortic stored flow with the term Q_s, which is defined as the amount of dynamically stored blood flow during each contraction:

$$Q_s = Q_i - Q_o \tag{3.1}$$

Where Q_i is the inflow to the large arteries, and Q_o is the outflow to the small peripheral vessels. The outflow to the peripheral vessels is defined as the pressure difference due to peripheral resistance (R_s) between the arterial pressure (P) and the venous pressure (P_v):

$$Q_o = (P - P_v)/R_s \tag{3.2}$$

If we assume steady flow ($Q_o = Q_i$) and a negligible P_v value, we obtain equation (1.1), shown again in (3.3):

$$R_s = \bar{P} / \bar{Q} \tag{3.3}$$

We defined compliance earlier in this chapter, but mathematically, aortic compliance is defined as the amount of change in blood volume with respect to the amount of change of pressure in the aorta, as presented in chapter one equation (1.2), and again below:

$$C = dV / dP \tag{3.4}$$

It can be shown that Q_s, which is approximately the change in aortic volume over time, is dependent on arterial compliance and change in arterial pressure over time:

$$Q_s = C\, dP / dt \tag{3.5}$$

Rearranging (3.1) to solve for Q_i we obtain:

$$Q_i = Q_s + Q_o \tag{3.6}$$

Writing an expression for arterial flow in terms of arterial compliance, using the two Windkessel parameters, C and R_s, we obtain the following equation through substitution of (3.5) and (3.2) into (3.6), and assuming a negligible P_v:

$$Q(t) = C\frac{dP}{dt} + \frac{P}{R_s} \tag{3.7}$$

Which shows the relation of arterial flow to compliance, pressure, and peripheral resistance. If all else equal, Q will increase with an increase in C, or a decrease in R_s.

During diastole, flow into the aorta is zero:

$$0 = C\frac{dP}{dt} + \frac{P}{R_s} \tag{3.8}$$

Solving for dP/P yields:

$$\frac{dP}{P} = -\frac{dt}{R_s C} \tag{3.9}$$

If we integrate both sides of (3.9) we obtain:

$$\ln P = \frac{t}{R_s C} \tag{3.10}$$

or

$$P = P_o \cdot e^{\frac{-t}{R_s C}} \tag{3.11}$$

Valid for $t = t_d$, the diastolic period (shown in Figure 3.3). This shows that aortic pressure is a function of both arterial compliance and peripheral resistance.

For the present study, direct calculations of R_s and C were done based on the graphs of the experimental canine data. For example, R_s was found by taking the ratio of average pressure over one period, and the average flow over the corresponding period. Identifying the end-systolic pressure (P_{es}), diastolic pressure (P_d), and diastolic period (t_d) from the pressure waveform, the time constant (τ) and arterial compliance (C) could be calculated. Figure 3.3 shows the locations of these values for a pressure waveform.

To solve for τ we begin with the equation for diastolic pressure:

$$P_d = P_{es} \cdot e^{\frac{-t_d}{\tau}} \tag{3.12}$$

and with all variables known, we can rearrange and solve for τ:

$$\tau = \frac{-t_d}{\ln\left(\frac{P_d}{P_{es}}\right)} \tag{3.13}$$

Conventionally, τ can also be defined in terms of R_s and C:

$$\tau = R_s C \tag{3.14}$$

Solving for compliance we obtain:

$$C = \frac{\tau}{R_s} \tag{3.15}$$

or in terms of measured aortic pressures:

$$C = \frac{t_d}{R_s \ln\left(\frac{P_{es}}{P_d}\right)} \tag{3.16}$$

The 3-element model also includes a characteristic impedance term, Z_0, which is viewed as the total arterial load to the heart, or average resistance to flow at the root of the aorta or ascending aorta. Z_0 is a function of frequency, and at high frequencies it can be approximated as the average of the input impedance, Z. Z_0 is defined as the complex ratio, by harmonic, of pressure and flow (Li, 2004). For each vascular impedance harmonic, n, there is a specific magnitude and phase component. Since pressure and flow waveforms are out of phase due to a time delay between their initiation and arrival to the same physical point, the derivation of the impedance term incorporates a phase angle within 90º (Li, 2004). Mathematically, when the pressure wave arrives ahead of the flow wave the phase is positive, and when P lags Q, the phase is negative. Note, a phase difference is synonymous with a time delay when moving between the frequency and time domains (Li, 2004). The derivation of impedance in terms of harmonic components of pressure and flow is presented below, where the harmonic frequencies are $n\omega$, and phase is ϕ_n, where n is an increasing positive integer (1, 2, 3…).

For the oscillatory pressure waveform, the following mathematic transformation from the time to frequency domain can be performed where the total wave over time, t, is the sum of the

mean blood pressure and the collective harmonic sums of varying sinusoidal waves at different harmonic frequencies and phases.

$$p(t) = \bar{p} + \sum_{n=1}^{N} p_n \sin(n\omega t + \phi_n) \tag{3.17}$$

$$\omega = 2\pi f \tag{3.18}$$

Where f is frequency in hertz, and is physically represented by the number of heart beats per second. A similar equation to (3.17) can be written for the flow wave, q(t).

Converting from the time domain to the frequency domain, and expressing P and Q in terms of magnitude and phase, the following expressions are true for the n^{th} harmonic:

$$P_n = |P_n| e^{j(\omega t + \phi_n)} \tag{3.19}$$

$$Q_n = |Q_n| e^{j(\omega t + \varphi_n)} \tag{3.20}$$

and the ratio of pressure to flow is:

$$\frac{P}{Q} = \frac{|P_n| e^{j(\omega t + \phi_n)}}{|Q_n| e^{j(\omega t + \varphi_n)}} \tag{3.21}$$

Similar to (3.19) and (3.20), vascular impedance can be written in terms of magnitude and phase for the n^{th} harmonic:

$$Z_n = |Z_n| e^{j\theta_n} \tag{3.22}$$

with the magnitude of impedance as the ratio of the amplitude of pressure and flow for the n^{th} harmonic, and phase lag, θ_n, defined as follows:

$$|Z_n| = \frac{|P_n|}{|Q_n|} \tag{3.23}$$

$$\theta_n = \phi_n - \varphi_n \tag{3.24}$$

As mentioned previously, characteristic impedance, Z_0, is a term that is incorporated into the 3-element Windkessel model and is a function of frequency, and at high frequencies it can be approximated as the average of the input impedance, Z:

$$Z(\omega) = \frac{P(\omega)}{Q(\omega)} \tag{3.25}$$

$$Z_0(\omega) \approx \overline{Z}(\omega)_{HF} \tag{3.26}$$

To calculate Z_0, the experimental data was analyzed using MATLAB 2014a (MathWorks Inc., 2014). Fast Fourier transforms (FFT) and discrete Fourier transforms (DFT) were used for analysis of the control, hypertensive, and vasodilated conditions. The Fourier analysis converted the pressure and flow waveforms from time domain to frequency domain, revealing the amplitude versus frequency data for both pressure and flow pulse waves in accordance to harmonic index. This information was used to calculate frequency-/harmonic-specific results for impedance. Results were then compared between experimental and control conditions.

Next, we analyzed the arterial system dynamics associated with pulse wave reflections. It has been shown that pressure pulse amplitude increases as the wave propagates away from the heart (McDonald, 2005). This increase is a result of wave reflections due to either geometric or structural changes in the vessel structures, like the splitting of vessels into branches or increased vascular wall stiffness (Li, 1989). This wave reflection phenomenon is also true for flow waveforms. Reflected pressure and flow waves are 180 degrees out of phase. Therefore, higher amplitude in the reflected wave will result in an increase in total pressure amplitude (P), and a decrease in total flow amplitude (Q). This implies that the reflected wave for flow (Q_r) has negative amplitude; therefore, the total flow wave (Q) has lower amplitude than the forward wave component of the flow (Q_f). Moreover, pressure and flow are simply the summation of the forward and reflected waves measured at the same site (Figure 3.4)

$$P = P_f + P_r \tag{3.27}$$

$$Q = Q_f + Q_r \tag{3.28}$$

If the characteristic impedance, $Z_{0,}$ is known (or calculated using MATLAB methods described above), the forward and reflected terms can be solved for:

$$P_f = \frac{\left(P + Q \cdot Z_0\right)}{2} \tag{3.29}$$

$$P_r = \frac{\left(P - Q \cdot Z_0\right)}{2} \tag{3.30}$$

$$Q_f = \frac{\left(Q + P/Z_0\right)}{2} \tag{3.31}$$

$$Q_r = \frac{\left(Q - P/Z_0\right)}{2} \tag{3.32}$$

Note that Z_0 can also be defined in terms of forward and reflected components, and is not dependent on wave reflection.

$$Z_0 = \frac{P_f}{Q_f} = -\frac{P_r}{Q_r} \tag{3.33}$$

The influences of reflected waves are demonstrated under varying CVS conditions, such as hypertension and vasodilation. The differences seen in these conditions are beyond what used seen in the clinical setting, and the interpretation of this data in relation to impedance is focused on particularly in this study.

3.3 Time-Varying Elastance Model of the Left Ventricle and Computation of Cardiac Parameters

The 3-element Windkessel model describes the arterial system in terms of characteristic impedance, total arterial compliance, and peripheral vascular resistance. The physical link between the heart and arterial system is found at the junction of the left ventricle and aorta. Therefore, the aortic compliance (especially during systole) influences the LV's ability to eject

blood. In order to study the left ventricle-arterial system interactions (LVASI), we need to first introduce model parameters that account for the left ventricle.

Just as the 3-element Windkessel uses lumped parameters to describe the arterial system, the left ventricle can be modeled using a lumped parameter for LV maximal elastance (Emax). Emax is represented in model-form as a time-varying compliance (Figure 3.4), which describes the heart as a mechanical pump with a pressure-sensitive varying elastance. Emax is a function of LV pressure and volume; therefore as the cardiac cycle progresses from end diastole, Emax increases with pressure increase, and decreases as pressure falls after end systole. The LV compliance is dependent on the pressure-volume relationship during systole and diastole, which is directly connected to the arterial system dynamics. During ejection, the compliance of the LV is dependent on both the contractility of the heart and the resistance to flow embedded in the arterial system.

Emax is defined as LV end systolic pressure (ESP) divided by LV end systolic volume (ESV) minus the residual volume of the LV (V_0):

$$E_{\max} = \frac{ESP}{ESV - V_0} \tag{3.34}$$

Here we assume V_0 is equal to be zero.

3.4 Analysis of Heart-Arterial System Interactions

One of the most commonly used measures of LVASI is the ratio of LV maximal elastance (Emax) to effective arterial elastance (Ea) (Chirinos, 2013; Korkhof, 2013). This ratio is termed the LVAS coupling index, k:

$$k = {Ea}/{Emax} \tag{3.35}$$

Ea is used to describe the arterial system, and is another lumped index for arterial load. Ea is used to characterize the arterial system as a whole, but does not describe individual artery

elastic properties, nor is it exclusively dependent on arterial properties. Therefore, caution is needed when using Ea as an index when describing pulsatile LV load (Chirinos, 2013).
The 3-element Windkessel, and pressure-volume analysis, can be used to derive Ea, which is shown to be a steady-state parameter that incorporates peripheral resistance (R_s), arterial compliance (C), characteristic impedance of the aorta (Z_0), and the systolic and diastolic time intervals (t_s and t_d, respectively):

$$E_a = \frac{R_s}{t_s + \tau(1 - e^{-t_d/\tau})} \tag{3.36}$$

Here τ is the exponential diastolic pressure decay time constant, given by equation (3.14) as the product of R_s and C.

The properties of the aorta play a major role in cardiac performance due to its primary location as the bridge between the heart and the rest of the vascular system. One of these influences include preserving flow waves, which contributes to the vascular load on the heart—a concept of great interest to cardiologists studying CVD and heart failure.

To study LVASI, and overall heart health, clinicians look at the heart's ability to pump an adequate amount of blood to the rest of the body. One measure of this is stroke volume (SV), or the amount of blood the heart can pump from each ventricle per beat:

$$SV = \int_0^T Q(t)dt \tag{3.37}$$

SV is the area under the flow curve over one period, T, which is defined as $T = t_s + t_d$, and is shown in Figure 3.3.

SV is not only a function of preload, or the amount of blood and pressure in each ventricle before contraction, but also the heart's ability to contract and the amount of tension in the ventricle wall during ejection, called afterload. A common measure of cardiac performance is the evaluation of the ejection fraction (EF) of the LV, which is defined as the ratio of total ejected volume, SV, to the total resting volume, end diastolic volume (EDV):

$$EF = SV / EDV \tag{3.38}$$

EF defines the diagnostic classification of heart failure into two main groups: heart failure with preserved ejection fraction (HFpEF) or heart failure with reduced ejection fraction (HFrEF). Clinically these classes are based on cutoff values for ejection fraction and range from EF = 45-50%, where patients with an EF lower than the cutoff are diagnosed with HFrEF, and those at or above the cutoff are said to have HFpEF. This study uses an EF cutoff value of 49%. One of the aims of this study is to classify HFpEF patients from HFrEF patients based on LVASI parameters.

In conjunction with EF, clinicians use cardiac output (CO) as an indication of left ventricular health and performance. Cardiac output is the product of heart rate (HR) and stroke volume:

$$CO = SV \times HR \tag{3.39}$$

Where HR is defined as:

$$HR = 1 / T \tag{3.40}$$

Therefore, SV, EF, and HR can all be calculated from a set of flow and pressure waves, and can used to assess cardiac performance.

Keeping LVASI the focus, we can give a new definition for arterial compliance, C. Based on equation (3.4) we see that C can be defined as the change in volume over the change in pressure. Therefore, C can be estimated based on LVASI parameters SV and pulse pressure (PP):

$$C \approx SV / PP \tag{3.41}$$

Here SV is the difference of EDV and ESV, and PP is the difference of arterial systolic and diastolic pressure.

Given the definition for SV, another relation for Ea can be established. Generally, Ea is approximated by the ratio of end-systolic pressure (ESP) and SV:

$$E_a \approx \frac{ESP}{SV} \tag{3.42}$$

Or using mean arterial pressure (MAP) to approximate LV ESP, Ea can be estimated as:

$$E_a = \frac{MAP}{SV} \tag{3.43}$$

The approximation shown in equation (3.43), however, is only acceptable under normal physiological states and non-vasoactive conditions, and should be avoided if possible (Chirinos, 2013; Li, 2000).

Ea can also be approximated based on R_s, HR, and CO. If R_s is defined as:

$$R_s = \frac{MAP}{CO} \tag{3.44}$$

Note: the formal definition for R_s is given in equation (3.3)

then:

$$E_a \approx \frac{R_s}{T} \tag{3.45}$$

This relation for Ea is a function of mean forward ascending aortic flow and coronary flow, per minute. The use of Ea as a measure of arterial functionality is limited, and though it can be insightful on a basic level, it should not be used as a pure index of arterial load. However, its usefulness has been proven when used to define the coupling index, k, to evaluate LVASI and systolic dysfunction (Chirinos, 2013).

Both Ea and Emax can be obtained in the LV pressure-volume plane. In this study, Ea and Emax were obtained using several methods depending on the available clinical measurements. For eleven patients, available clinical information was given for all needed parameters; for seven patients, further calculations were needed to estimate LV EDV based on given LV ESV and SV measurements:

$$\text{EDV} = \text{ESV} + \text{SV} \tag{3.46}$$

For the human-based portion of this study, aortic and left ventricular pressure waveforms from hospital catheterizations, measurements from echocardiograms, and cardiac signals from electrocardiograms (EKG) were available. Without flow waveforms, a continuous function for

LV volume over time was unknown. To remedy the lack of continuous volume over time information, simulated LV pressure-volume (P-V) loops were created based on four key points (ESV, ESP, EDV, and EDP) and using a fixed time step equal to 0.025 seconds. LV P-V loops are constructed by plotting corresponding pressure versus volume values for each discrete time point over one cardiac period. A typical P-V loop is shown in Figure 3.5 below. P-V loops are useful in studying LVASI because the slope of the line that intersects through V_0 and the end-systolic point (ES) gives Emax; and the absolute value of the slope of the line that passes through the ES and ED (end-diastolic) points defines Ea (shown in Figure 3.5). This way, knowing the four points for left ventricular ESV, EDV, ESP, and EDP (and assuming V_0 is approximately zero), Emax and Ea can be derived. This will ultimately give the coupling index, k.

Timings for LV volume changes were determined based on simultaneous EKG measurements on LV pressure waveforms (Figure 3.6). For example, the end of EDV occurs when the aortic valve opens, which correlates with the end of the S wave on an EKG; and ESV period ends when the atrial-ventricular (AV) valve opens, which occurs at the end of the T wave on an EKG. Through this the corresponding time points could be found and used in constructing simulated LV volume curves, and ultimately construct simulated LV P-V loops. The process of calculating Ea and Emax based on P-V loop slopes provides a visual tool for understanding otherwise purely mathematic calculations. Visualizing changes and relationships in LVASI gives further insight into the coupled relationship based on the elastic-dynamic properties of the arterial and left ventricular systems. The overall goal is to analyze the changes that occur in the matching of the arterial system and the left heart in patients with HFpEF or HFrEF. Identifying these changes will give insight into which physical properties may be contributing to disease, and which characteristics can be used to distinguish between these two patient groups.

Statistical analysis will be performed for human clinical studies using MATLAB 2014a statistics toolbox (MathWorks Inc., 2014) and will include linear regression analysis, mean and standard deviation, and t-test using significance at $p < 0.05$.

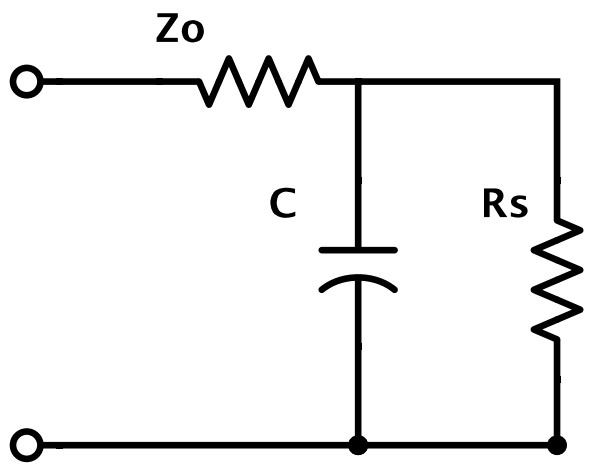

Figure 3.1: Three-element Windkessel model, with Z_0 as characteristic impedance, C as total arterial compliance, and R_s as total peripheral resistance.

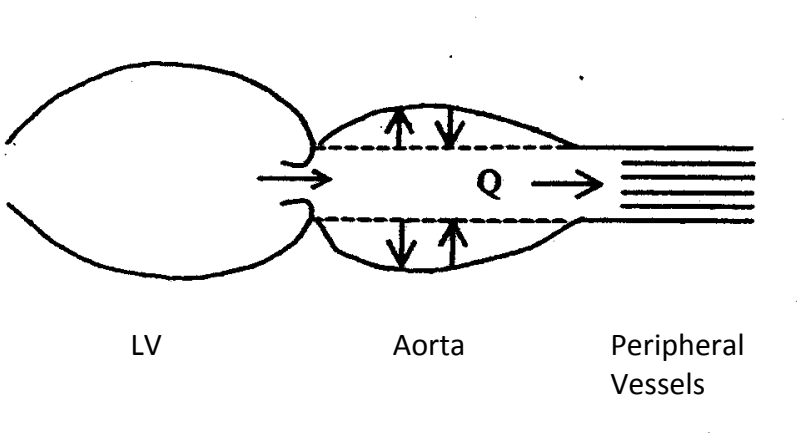

Figure 3.2: Schematic of blood flow (Q) from the left ventricle (LV) through the systemic circulation with respect to the 3-element Windkessel model. The blood is ejected into an elastic vessel (aorta) that stores flow during systole (solid line) and releases flow into the rigid peripheral vessels by elastic recoil during diastole (dotted line) (modified from Li, 2004).

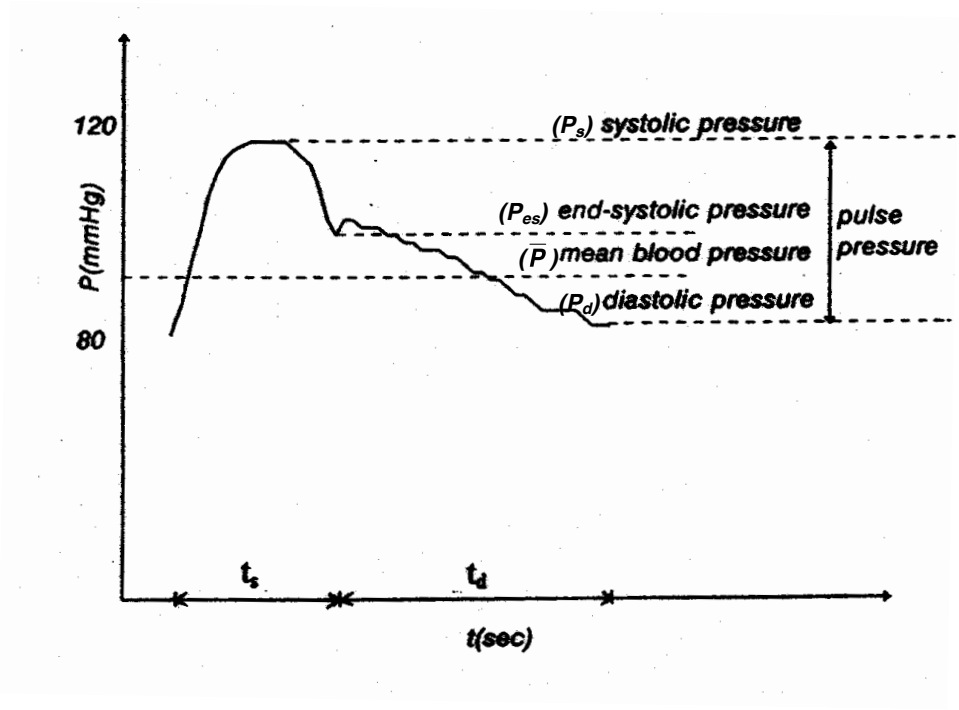

Figure 3.3: Example of an aortic pressure waveform over one heartbeat showing the locations and common values for the systolic, diastolic, end-systolic, and mean blood pressures. The diastolic period (t_d) and systolic period (t_s) are also shown (modified from Li, 2004).

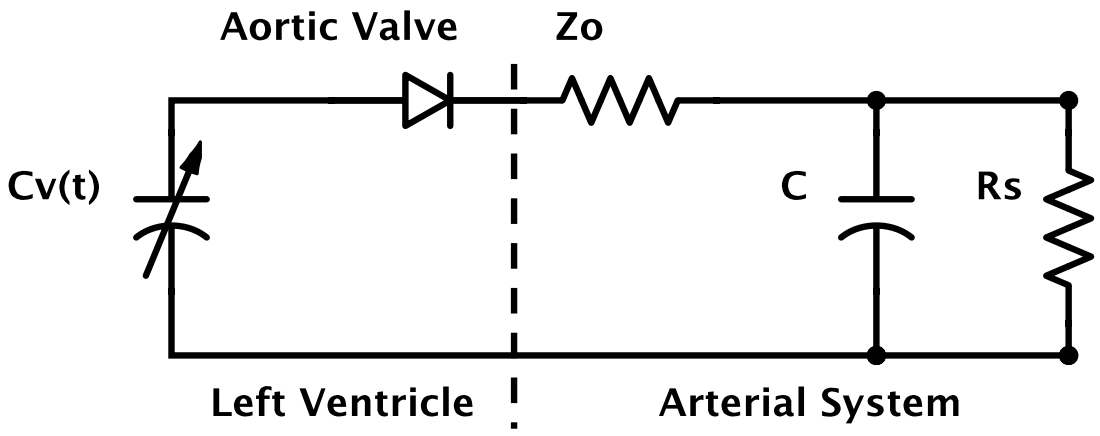

Figure 3.4: Left ventricle-arterial system coupling. The LV is represented by a time-varying compliance Cv(t) and the arterial system is represented by a 3-element Windkessel with Z_0 as characteristic impedance, C as total arterial compliance, and R_s as total peripheral resistance.

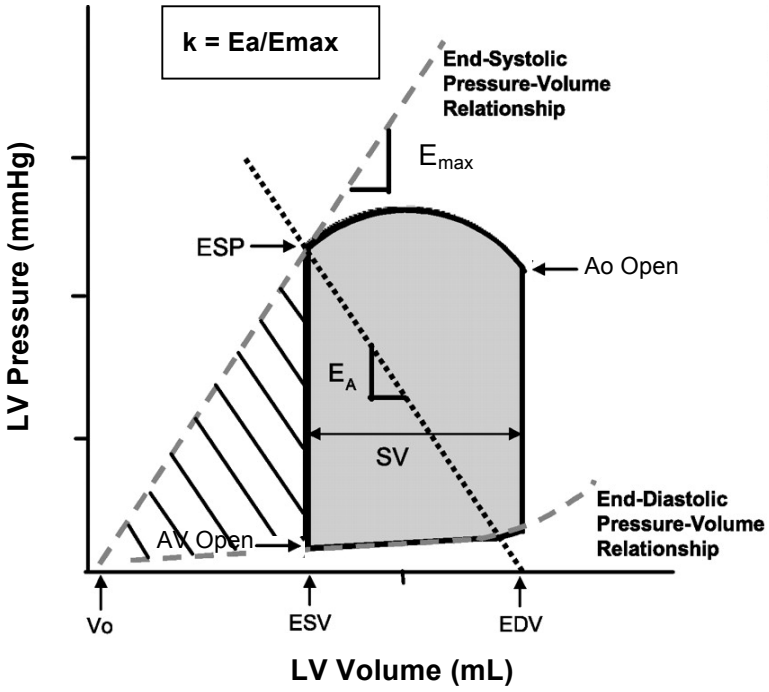

Figure 3.5: Example of a left ventricle pressure-volume loop (LV P-V loop). Note the dashed line for the end-systolic pressure-volume relation (ESPVR), which passes through the end-systolic point and the residual volume (V_0) intercept. The slope of the ESPVR gives the LV maximal elastance (E_{max}). The effective arterial elastance (E_A) is derived from the slope of the line joining the end-diastolic volume (EDV) and the end-systolic pressure (ESP) points. The width of the loop represents the stroke volume (SV), and the hatched area is the LV potential energy (PE). (Taken and adapted from, (modified from Chantler et al., 2008)).

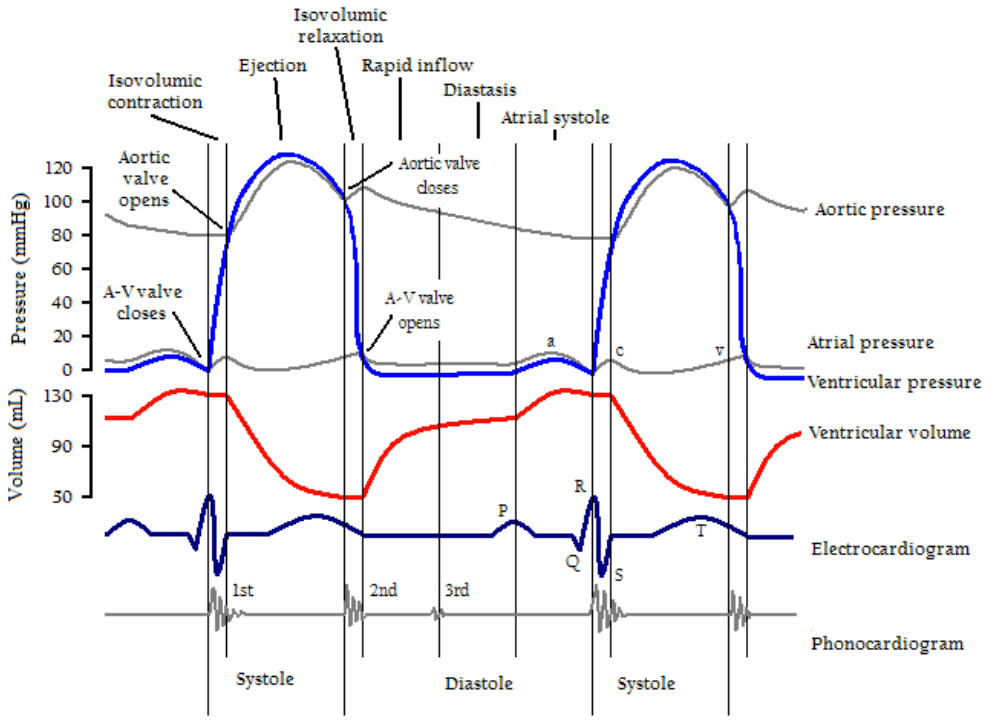

Figure 3.6: Cardiac cycle measurements for two heart beats. LV volume changes were determined based on EKG wave timing and corresponding LV pressure waveforms (Chang, 2011).

Chapter 4. Results

4.1 Retrospective Animal Experimental Studies

4.1.1 Model Based Analysis

From collected experimental data for control, hypertensive, and vasodilated conditions, pulsatile pressure and flow waveforms were digitized and graphed. It is seen that in comparison to the normal control condition, the systolic pressure in hypertension is significantly higher at about 200 mmHg compared to 105 mmHg (Fig. 4.1.1 and 4.1.2). It is also seen that there is a small decrease in mean flow between hypertensive and control conditions: 13.24 ml/second versus 20.28 ml/second, respectively. For the vasodilated condition, the pressure is below control conditions (61 mmHg versus 90 mmHg), with a slight increase in mean flow (33.11 ml/second versus 20.28 ml/second). The cardiac period, T, for hypertension is about equal to the control (0.45 seconds compared to 0.43 seconds), whereas the vasodilated T decreases to 0.36 seconds. These and other pertinent hemodynamic parameters are tabulated in Table 4.1.1.

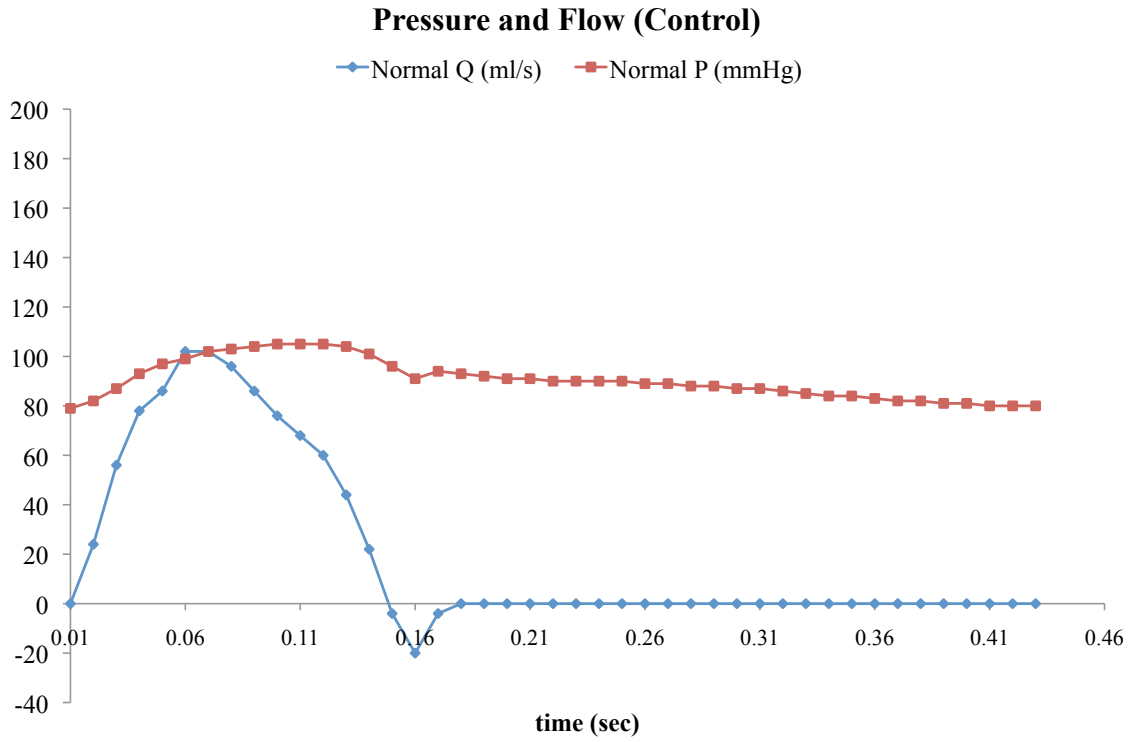

Figure 4.1.1: Experimental pressure and flow waveforms for normal healthy conditions over one cardiac cycle. Data collected at 100 Hz.

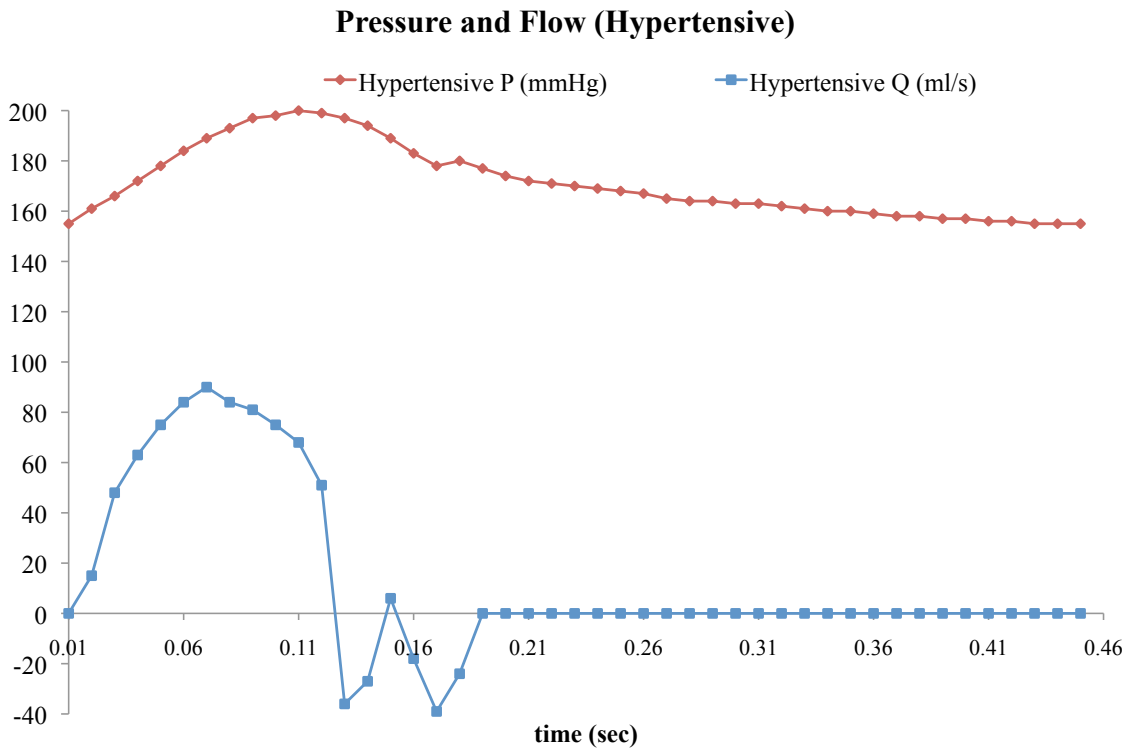

Figure 4.1.2: Experimental pressure and flow waveforms for hypertensive conditions over one cardiac cycle. Data collected at 100 Hz.

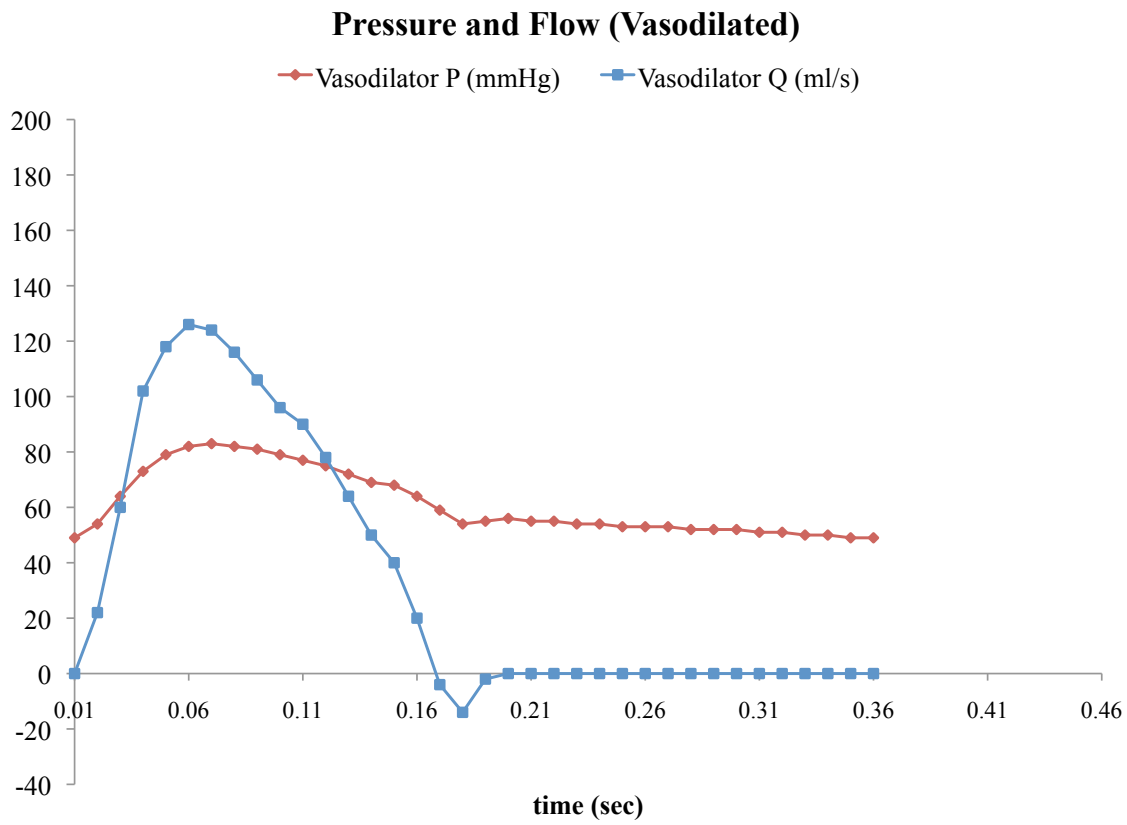

Figure 4.1.3: Experimental pressure and flow waveforms for vasodilated conditions over one cardiac cycle. Data collected at 100 Hz.

From the pressure and flow waveforms, values for mean pressure and flow as well as R_s were calculated. Values for P_s, P_d, P_{es}, t_s, t_d, and T were located by hand for each pressure wave (example estimation graph shown in Fig. 3.3). Compliance was calculated, as well as the time constant τ. Values such as HR, SV, CO, and EF are also included, and were calculated for each condition. Results are shown in Table 4.1.1.

As expected, mean pressure increases for hypertension and decreases in vasodilation (as stated above). As well, the opposite is seen for mean flow with a decrease in hypertension and increase in vasodilation. Peripheral resistance increases with increased pressure, up from 4.461 mmHg-sec/ml to12.93 mmHg-sec/ml, and decreased with dilation to1.852 mmHg-sec/ml. These changes in R_s correspond with greatly reduced compliance in hypertension, down from 0.423 ml/mmHg to 0.156 ml/mmHg, and significantly increased compliance in dilation to 0.763 ml/mmHg.

Under the pressure-overload conditions in hypertension, heart rate, stroke volume, end diastolic volume, and cardiac output all decrease relative to normal health control conditions. The opposite is seen for vasodilated conditions, with an increase relative to the control for heart rate, stroke volume, end diastolic volume, and cardiac output. Ejection fraction was assumed to be 0.6 for all conditions.

Table 4.1.1: Measured and calculated hemodynamic parameters for experimental pressure and flow waveforms, as well as calculated cardiac parameters (HR, SV, EDV, CO).

		Control	Hypertension	Vasodilator
Calculated	$\bar{P}$ (mmHg)	90.47	171.3	61.33
	$\bar{Q}$ (ml/sec)	20.28	13.24	33.11
	R_s (mmHg/ml/s)	4.461	12.93	1.852
Measured	P_s (mmHg)	105	200	83.0
	P_d (mmHg)	79.0	155	61.3
	P_{es} (mmHg)	91.0	178	54.0
	t_s (sec)	0.163	0.170	0.180
	t_d (sec)	0.267	0.280	0.180
	T (sec)	0.430	0.450	0.360
Calculated	**τ** (sec)	1.89	2.02	1.40
	C (ml/mmHg)	0.423	0.156	0.763
	Z_0 (mmHg/ml/s)	0.1686	0.1871	0.2683
	HR (bpm)	139.5	133.3	166.7
	SV (ml)	8.72	5.96	11.9
	EDV (ml)	14.53	9.933	19.83
	CO (ml/min)	1216	794.5	1984
Cst.	**EF** (%)	60	60	60

4.1.2 Frequency Domain Fourier Analysis

Canine experimental data was analyzed by fast Fourier transforms (FFT) for control, hypertensive, and vasodilated conditions. The first ten harmonics, excluding the characteristic 0-order harmonic, are included in the pressure-flow analyses for each condition.

In the healthy control condition, pressure magnitude maximum occurs in the first harmonic with a value of about 4.8 mmHg, whereas the maximum for flow magnitude is 18.75 ml/sec. Both flow and pressure magnitudes quickly decrease, and by the fourth harmonic the values remain low and waver between about 0.2 and 0.5 mmHg for pressure, and 1 and 2.5 ml/sec for flow. The phase angle plots for pressure and flow demonstrate the time delay between the two waves, with pressure lagging flow. The unequal magnitudes and uneven switching between positive and negative angles between the two waves support this result of wave propagation delay.

Similar trends are seen in the hypertensive case. Here, when compared to the control situation, the first harmonic maximum magnitude value is higher at about 8.9 mmHg, and the flow maximum magnitude value is lower at about 14.5 ml/sec. Similarly, by the fourth harmonic the values for pressure and flow magnitude remain low and near values similar to those seen in the control condition, though the trend is not as drastic in the flow magnitude results, as there is seen a slight increase starting at harmonic five with 1.0 ml/sec, reaching about 2.5 ml/sec by harmonic ten. The phase analysis reveals the same trends in wave propagation delay, with pressure lagging behind flow.

The vasodilated FFT results show the pressure and flow maximum values for the first harmonic being about 7 mmHg and 27.5 ml/sec, respectively. These values are both an increase relative to the control, and a decrease in pressure and increase in flow relative to the hypertension values. Magnitude in pressure gradually approaches zero from the fourth to tenth harmonics, and the flow values rise for the fourth, but then fall to about zero by the tenth. The phase analysis shows very similar results between the pressure and flow waves, in both magnitude and sign.

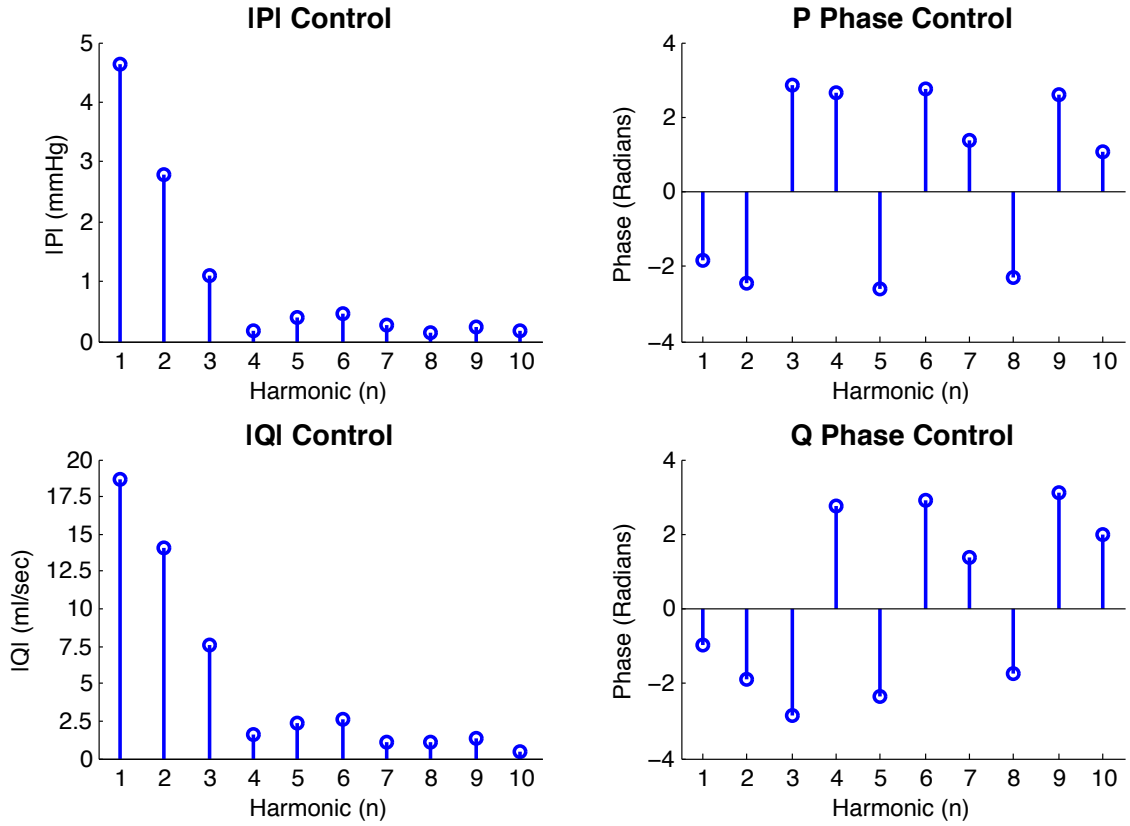

Figure 4.1.4: Fast Fourier Transforms (FFT) of pressure and flow waveforms (Control condition).

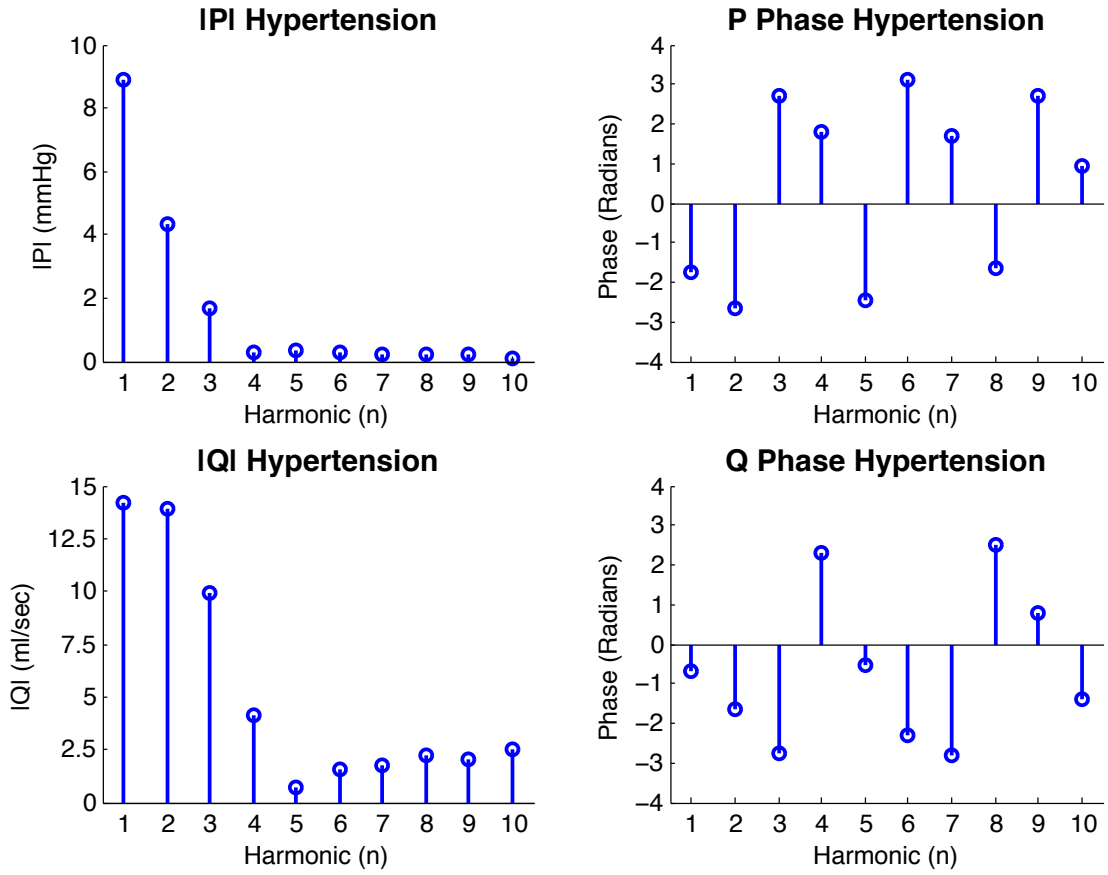

Figure 4.1.5: Fast Fourier Transforms (FFT) of pressure and flow waveforms (Hypertensive condition).

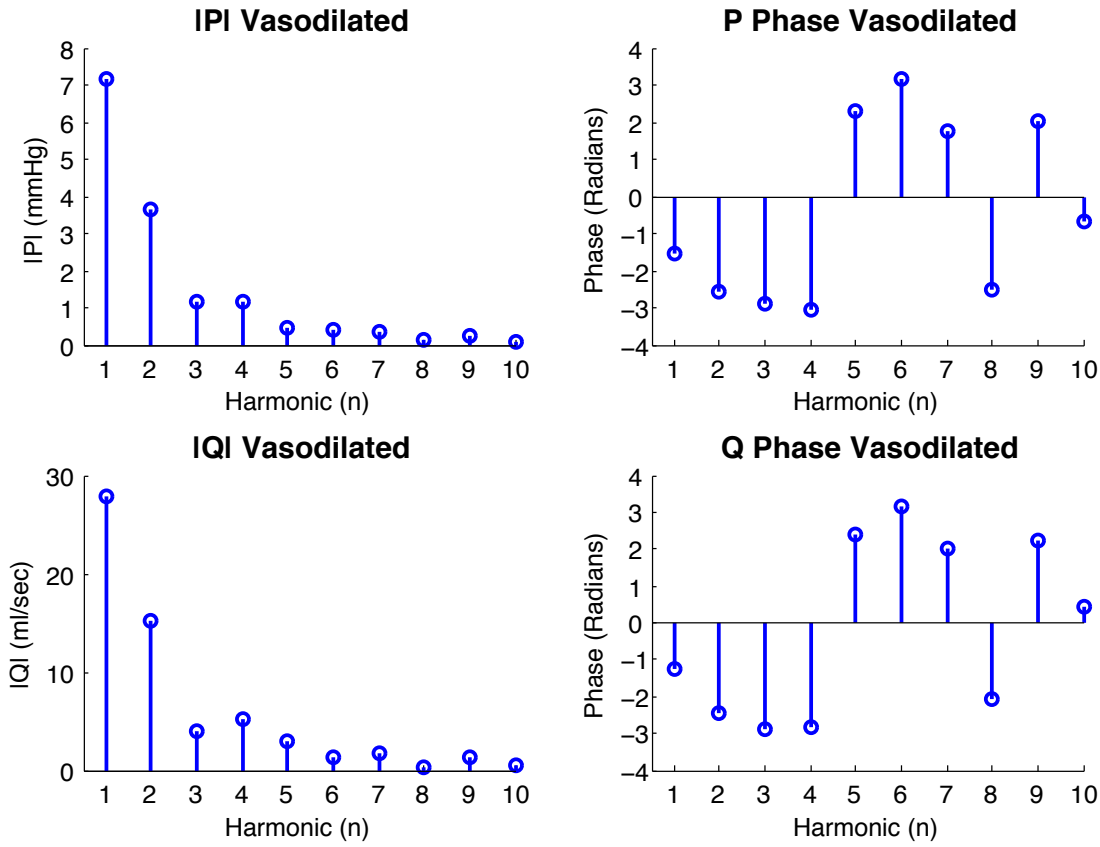

Figure 4.1.6: Fast Fourier Transforms (FFT) of pressure and flow waveforms (Vasodilated condition).

Once the |P| and |Q| data for each condition was calculated, as shown above, |Z| was evaluated. Peripheral resistance, R_s, is equal to the 0^{th} order harmonic of impedance magnitude. For the hypertensive case, R_s increases from 4.46 mmHg-sec/ml to 12.9 mmHg-sec/ml. The opposite trend is seen in the vasodilated case, with a decrease in peripheral resistance to 1.85 mmHg-sec/ml. Note that after about the third harmonic, the magnitude of impedance is relatively constant, and oscillates about a certain value. This value is assumed to be the characteristic impedance, Z_0, and is significantly less than the values for R_s. In the control, hypertensive, and vasodilated cases, Z_0 is about 0.1686 mmHg-sec/ml, 0.1871 mmHg-sec/ml, and 0.2683 mmHg-sec/ml, respectively.

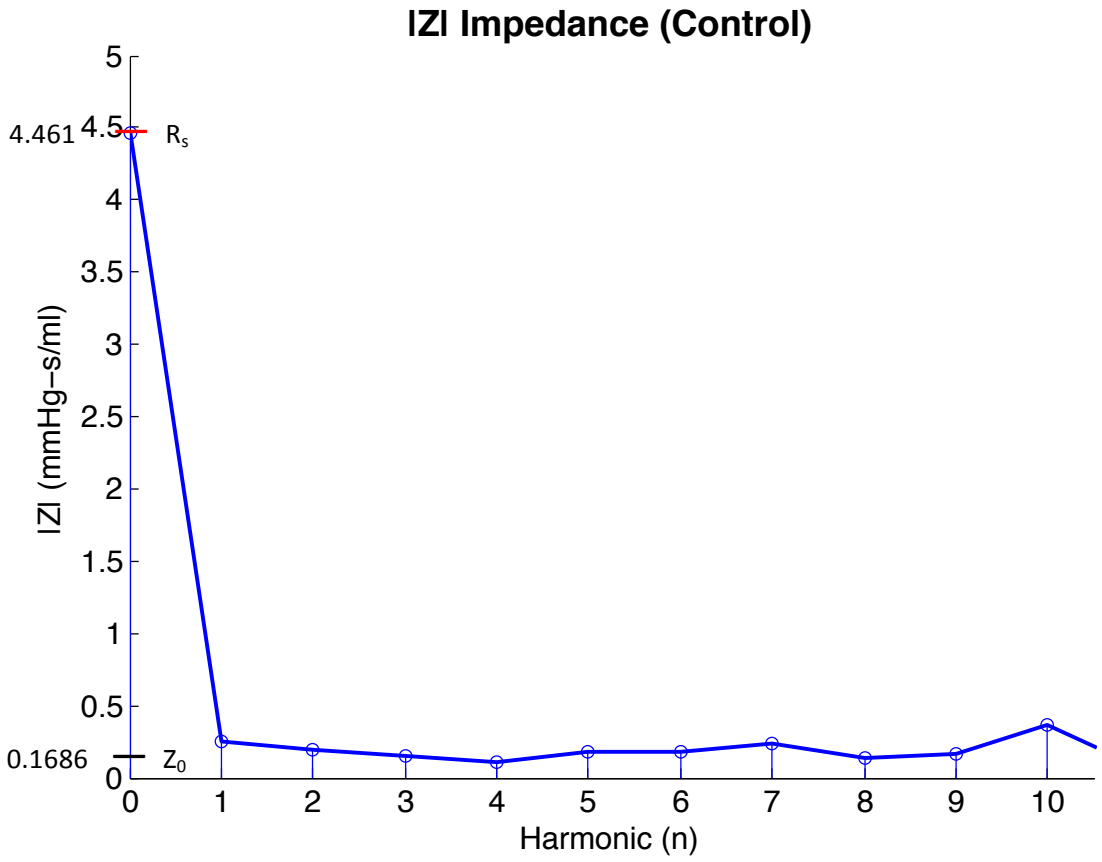

Figure 4.1.7: Magnitude of input impedance (Z) using Fast Fourier Transformations (FFT) of pressure and flow waveforms (Control condition). Peripheral resistance (R_s) and characteristic impedance (Z_0) are shown.

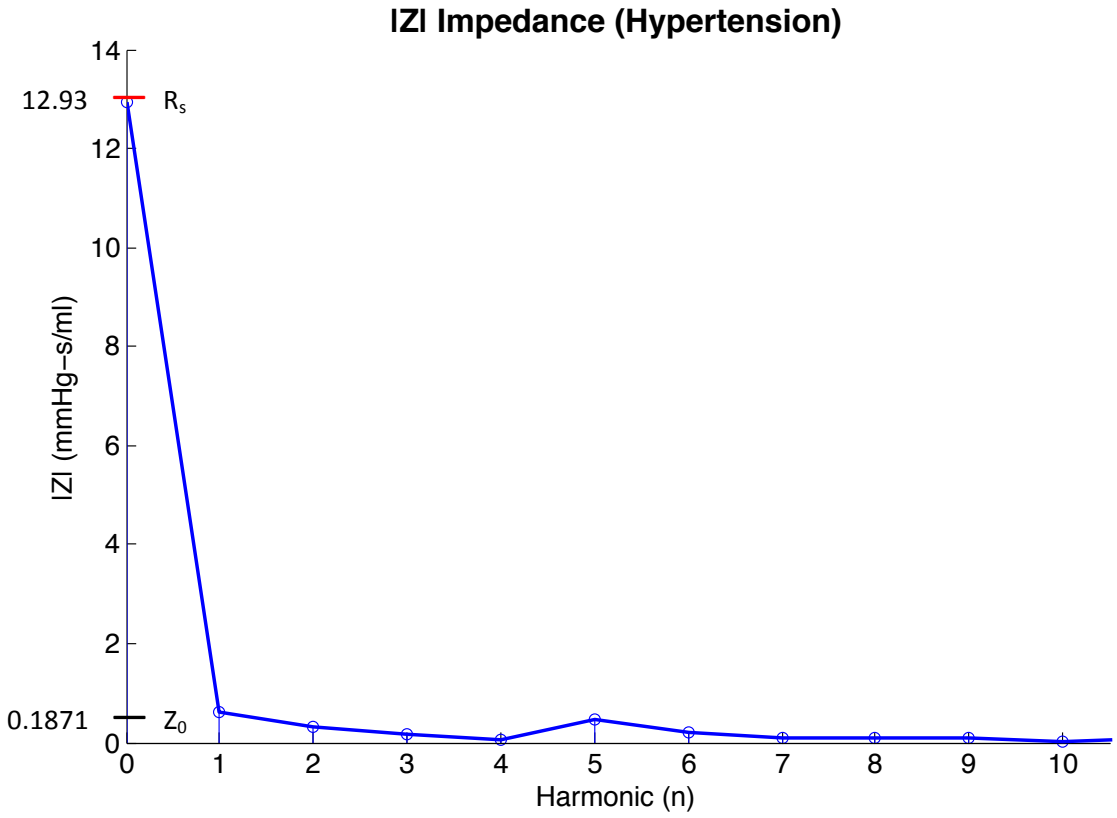

Figure 4.1.8: Magnitude of input impedance (Z) using Fast Fourier Transformations (FFT) of pressure and flow waveforms (Hypertensive condition). Peripheral resistance (R_s) and characteristic impedance (Z_0) are shown.

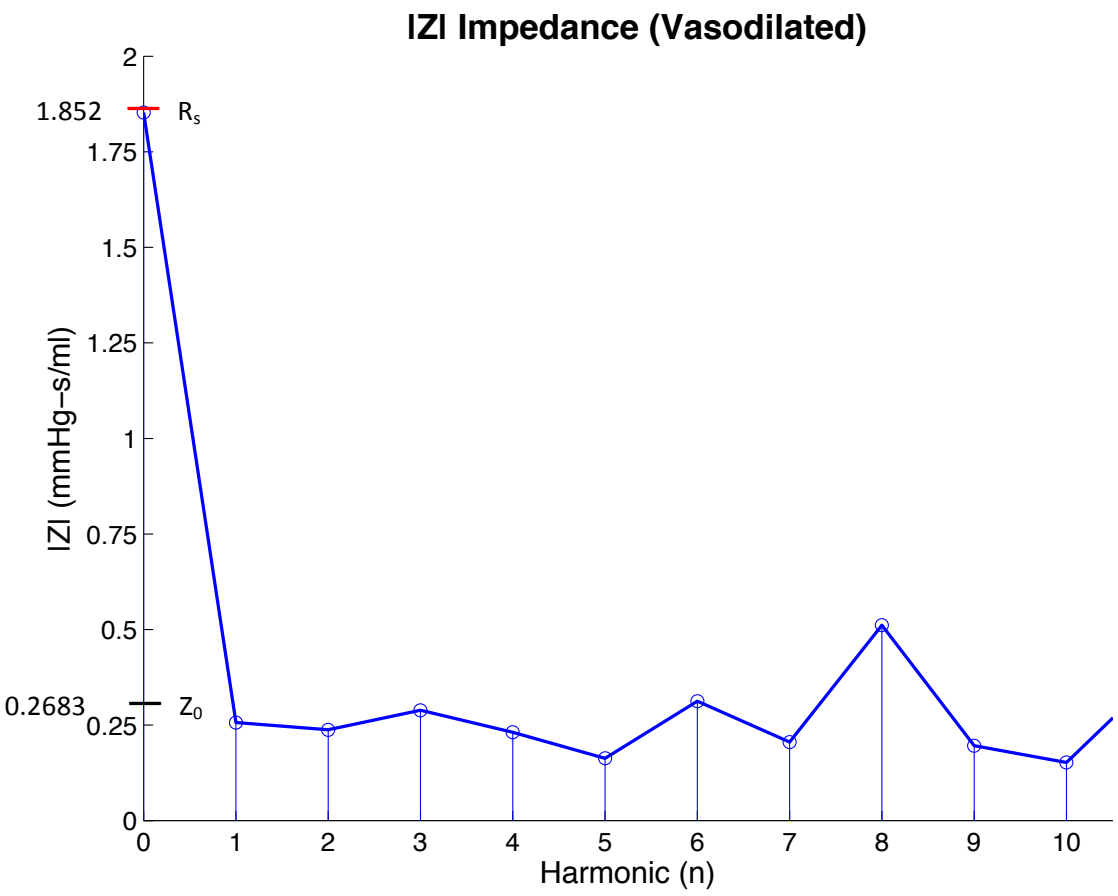

Figure 4.1.9: Magnitude of input impedance (Z) using Fast Fourier Transformations (FFT) of pressure and flow waveforms (Vasodilated condition). Peripheral resistance (R_s) and characteristic impedance (Z_0) are shown.

4.1.3 Pulse Wave Reflections

Pressure and flow pulse waves were quantified by resolving each into their forward and reflected components. It should be noted that the waves have been normalized to the initial flow and pressure values. This was done for each test condition, and the same overall trends are seen among them: For pressure, the forward and reflected waves do not exceed the total final pressure wave curve, and both forward and reflected waves have positive amplitudes. For flow, the forward wave remains above the total flow wave curve, while the reflected wave has a negative amplitude for the majority of the time due to the out of phase nature of the wave propagations.

For pressure, when compared to the control condition, hypertension demonstrated an overall increase in mean pressure for both forward and reflected waves, however wave shape differs from the control. There is a decreased influence of the forward wave and increased positive shape in the reflected wave. For the vasodilated case, there is an overall decrease in mean pressure in both waves, with an increase in forward wave influence and shape, almost to the point of the two waves (total and forward) matching exactly, and a large decrease in reflected contribution. Through this analysis it is seen that in vasodilated conditions there is very little influence of reflected waves on the total pressure waveform.

Flow analysis for hypertension reveals an overall decrease in amplitude for both forward and reflected waves. It is difficult to compare wave shape changes between the hypertensive and control conditions due to the abnormal spike seen in the flow wave for the high pressure case, but there is a large negative influence from the reflected wave and a drastic decrease in positive amplitude influence from the forward wave. For the vasodilated condition, similar affects are seen in flow as were shown for pressure: the forward portion dominates the total flow wave, and the reflected portion hardly contributes. Interestingly, the total mean flow decreases in hypertension, but there is an increase in forward and reflected magnitudes, and an increase in forward flow wave in vasodilation and drastic decrease in reflected amplitude, with an overall increase seen in mean total flow for vasodilation.

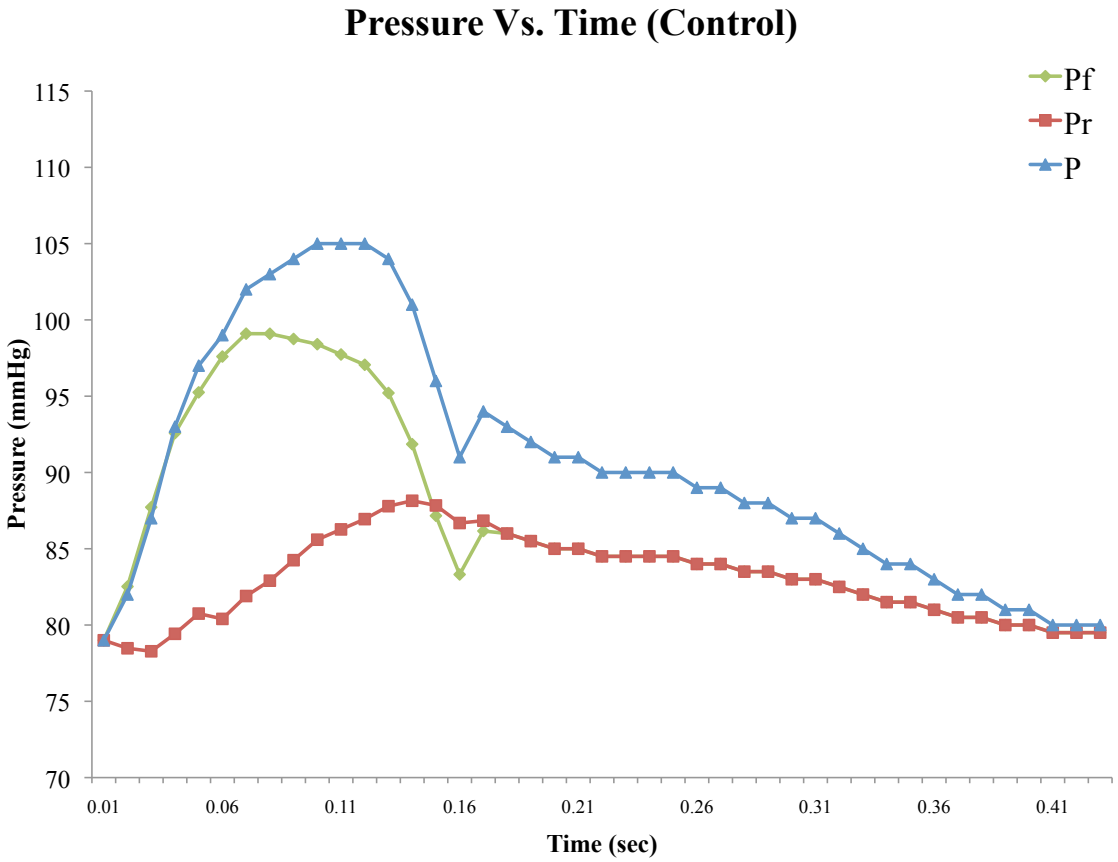

Figure 4.1.10: Pulse wave reflections for pressure over one cardiac period, resolved into forward and reflected waves; showing the summation of these waves is equal to the total pressure waveform. (Healthy, control conditions).

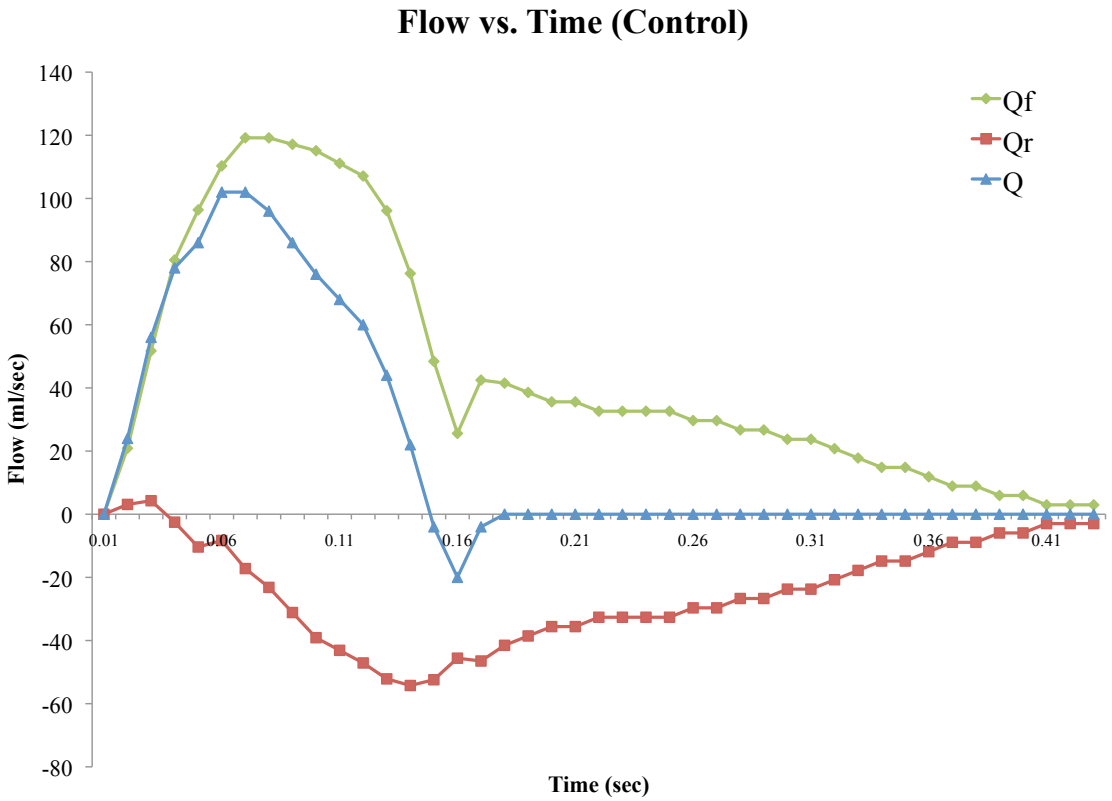

Figure 4.1.11: Pulse wave reflections for flow over one cardiac period, resolved into forward and reflected waves; showing the summation of these waves is equal to the total flow waveform. (Healthy, control conditions).

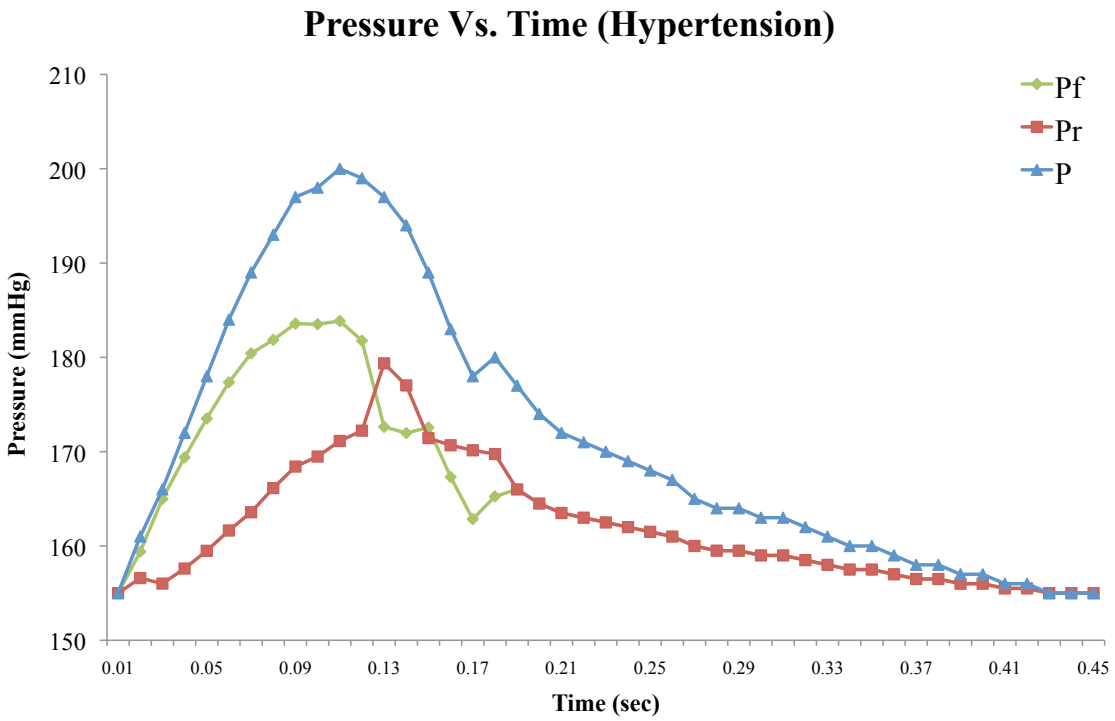

Figure 4.1.12: Pulse wave reflections for pressure over one cardiac period, resolved into forward and reflected waves; showing the summation of these waves is equal to the total pressure waveform. (Induced hypertensive conditions).

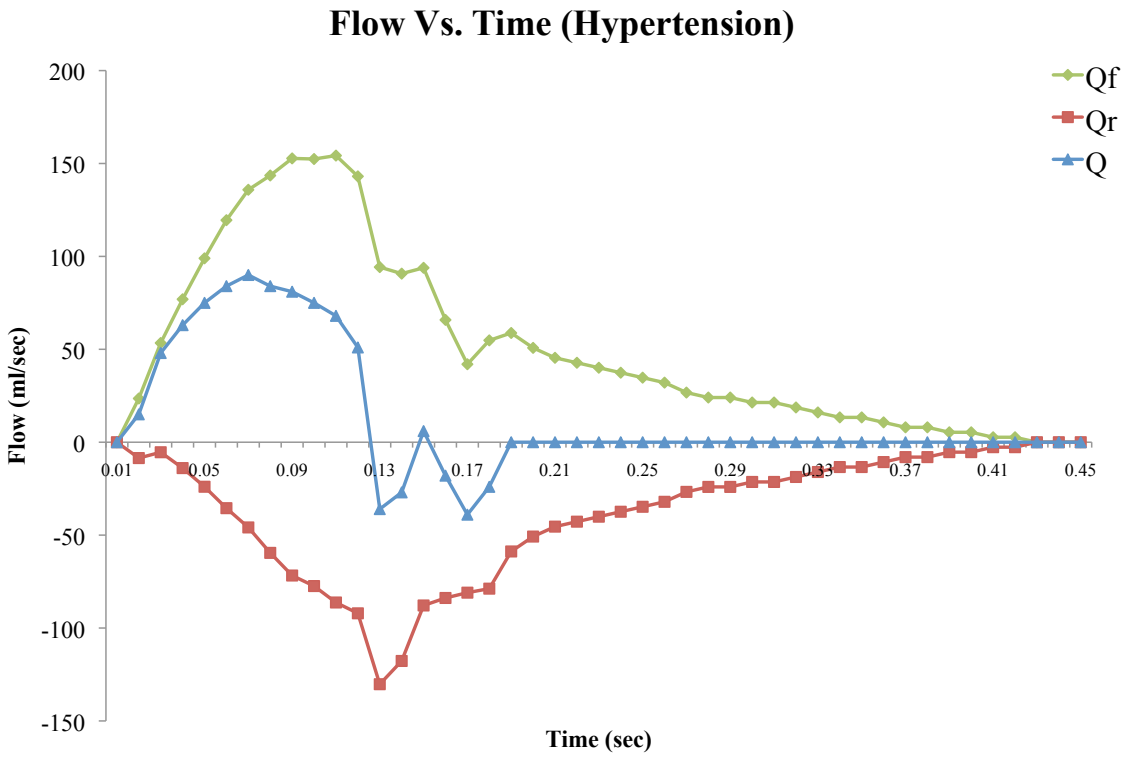

Figure 4.1.13: Pulse wave reflections for flow over one cardiac period, resolved into forward and reflected waves; showing the summation of these waves is equal to the total flow waveform. (Induced hypertensive conditions).

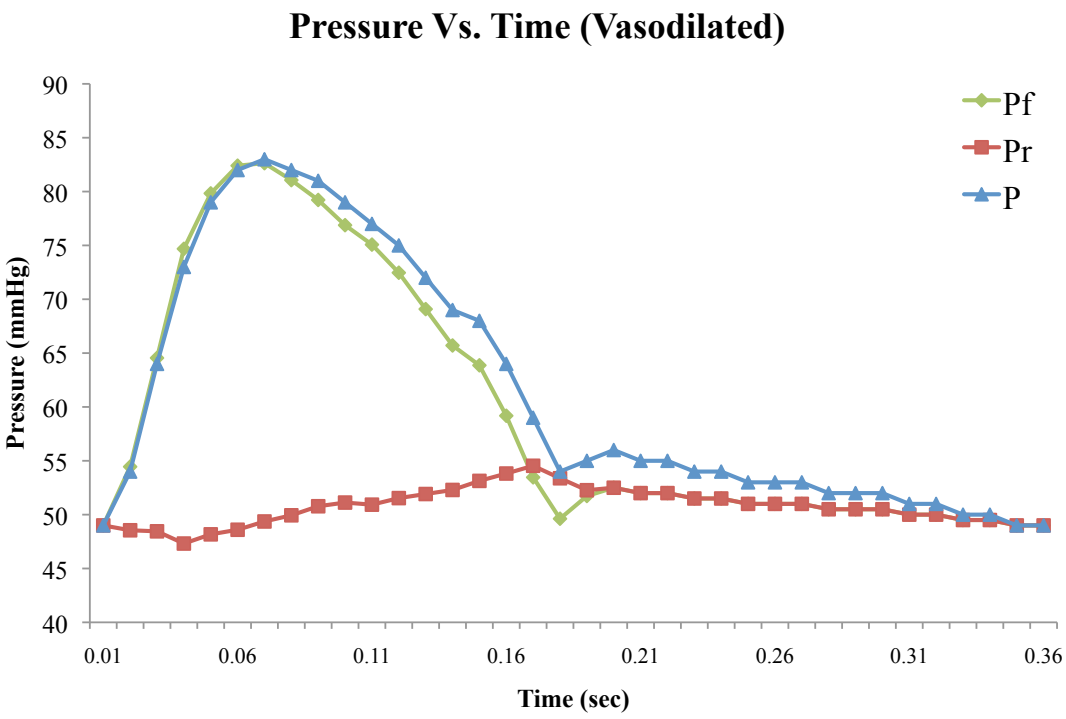

Figure 4.1.14: Pulse wave reflections for pressure over one cardiac period, resolved into forward and reflected waves; showing the summation of these waves is equal to the total pressure waveform. (Vasodilated conditions).

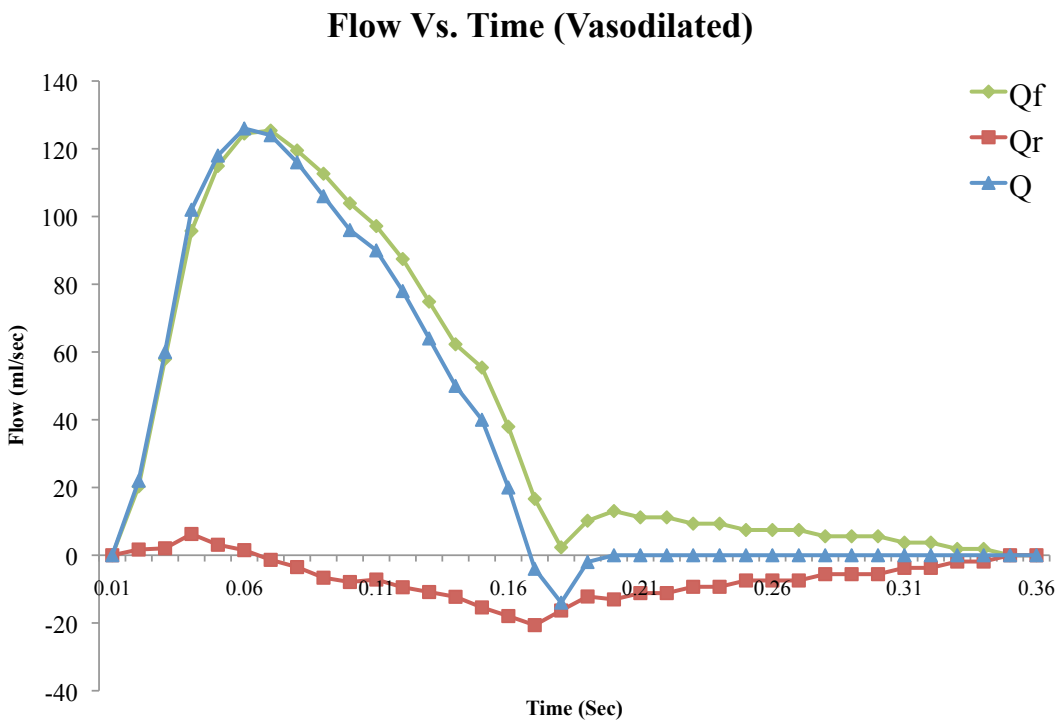

Figure 4.1.15: Pulse wave reflections for flow over one cardiac period, resolved into forward and reflected waves; showing the summation of these waves is equal to the total flow waveform. (Vasodilated conditions).

4.2 Retrospective Human Studies

4.2.1 Left Ventricular Pressure-Volume Loop Analysis

Based on collected clinical waveforms for left ventricular pressure, LV pressure-volume (PV) loops were constructed for 18 patients with either preserved or reduced heart failure (pEF cutoff was 49%). From each constructed PV loop, Ea, Emax, and k were calculated as described in chapter 3. Simulated volume over time was constructed and used to create each loop, and is shown below each corresponding pressure waveform. Data over several periods was used to calculate Ps and Pd; however, only one period was selected to create PV loops (shown in figures below).

(a)

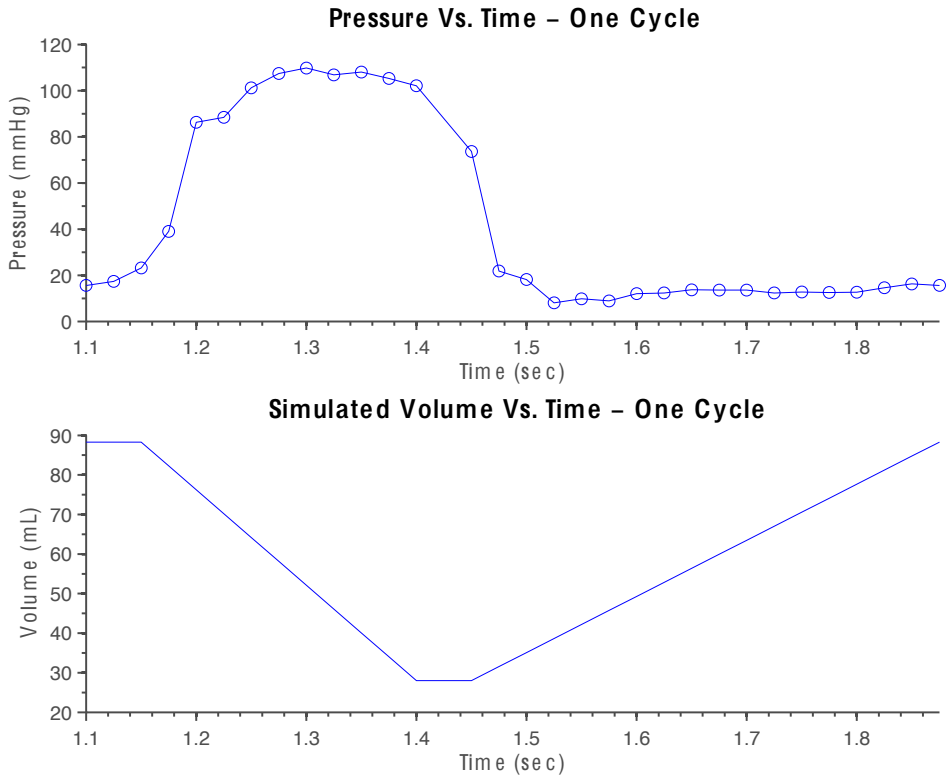

(b)

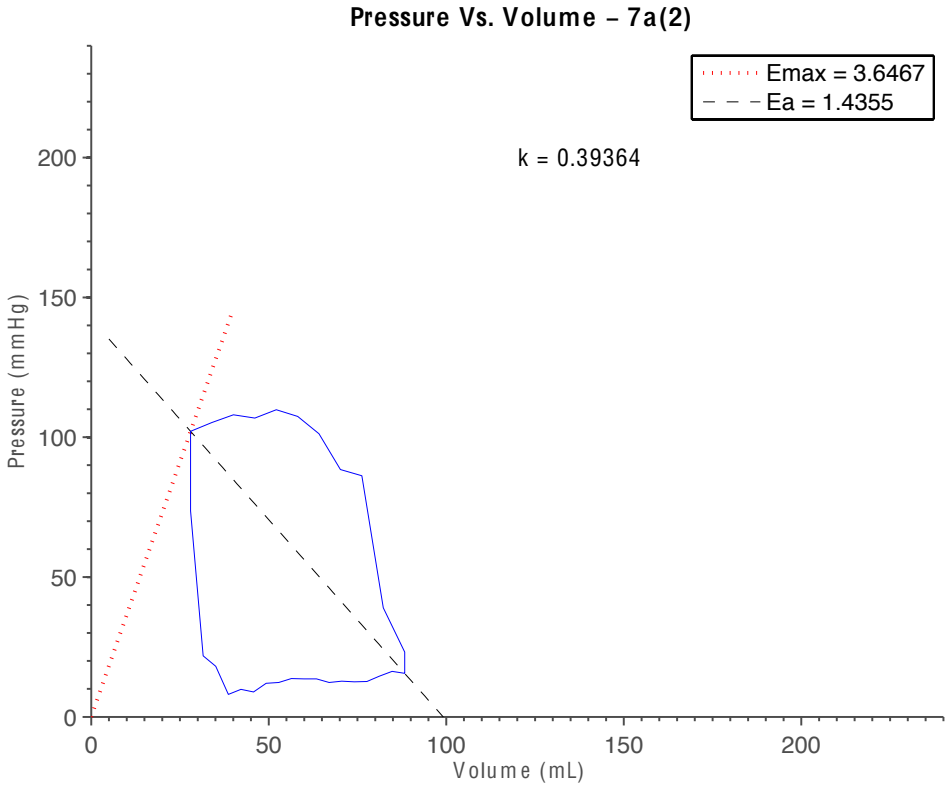

Figure 4.2.1: Patient 7a-2 (EF = 55%). *(a)* Pressure and simulated volume over time for one cardiac period. *(b)* LV Pressure-Volume loop, $V_0 = 0$ (assumed).

(a)

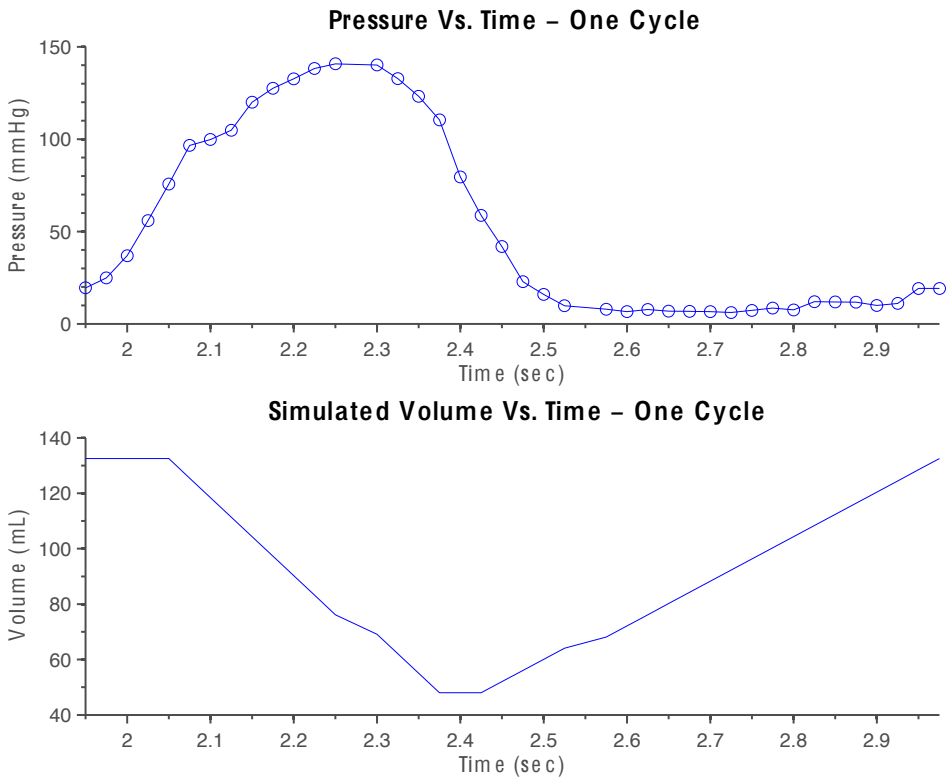

(b)

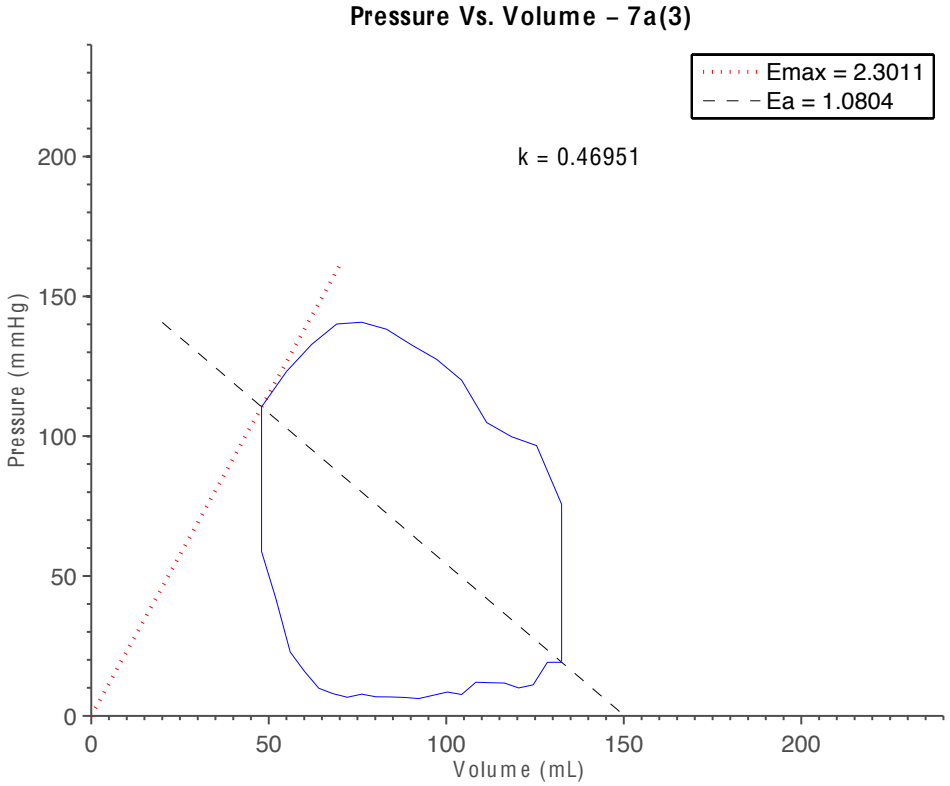

Figure 4.2.2: Patient 7a-3 (EF = 30%). *(a)* Pressure and simulated volume over time for one cardiac period. *(b)* LV Pressure-Volume loop, $V_0 = 0$ (assumed).

(a)

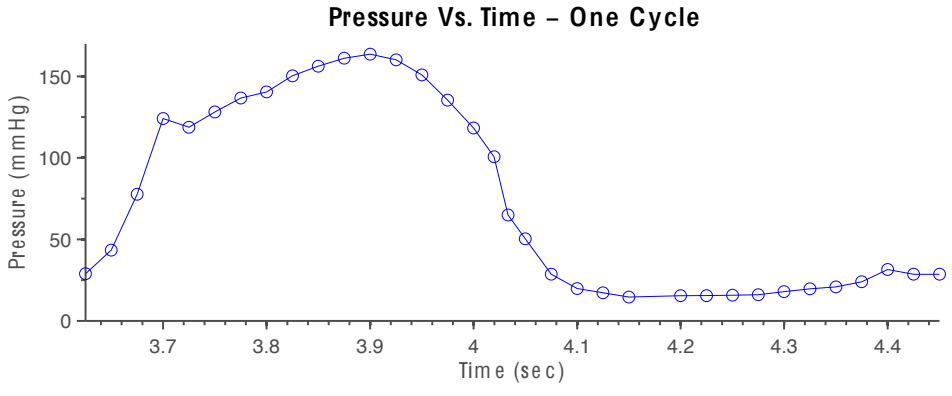

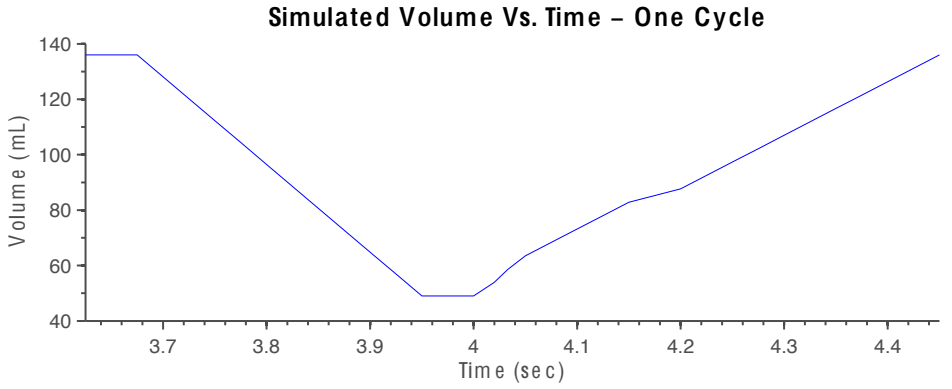

(b)

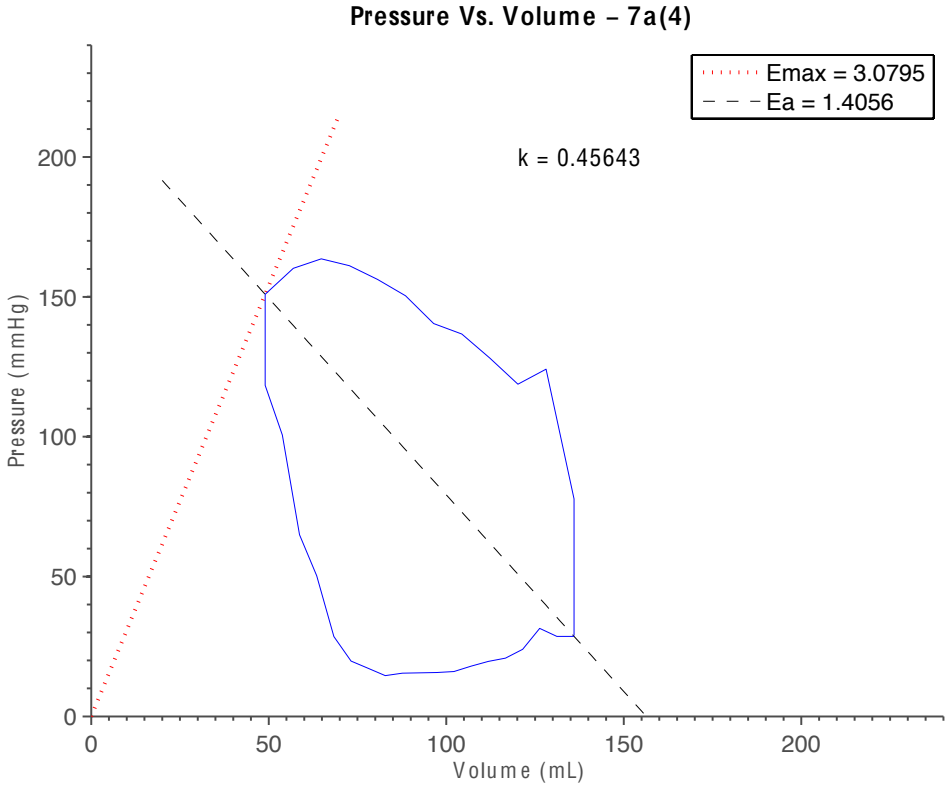

Figure 4.2.3: Patient 7a-4 (EF = 25%). *(a)* Pressure and simulated volume over time for one cardiac period. *(b)* LV Pressure-Volume loop, $V_0 = 0$ (assumed).

(a)

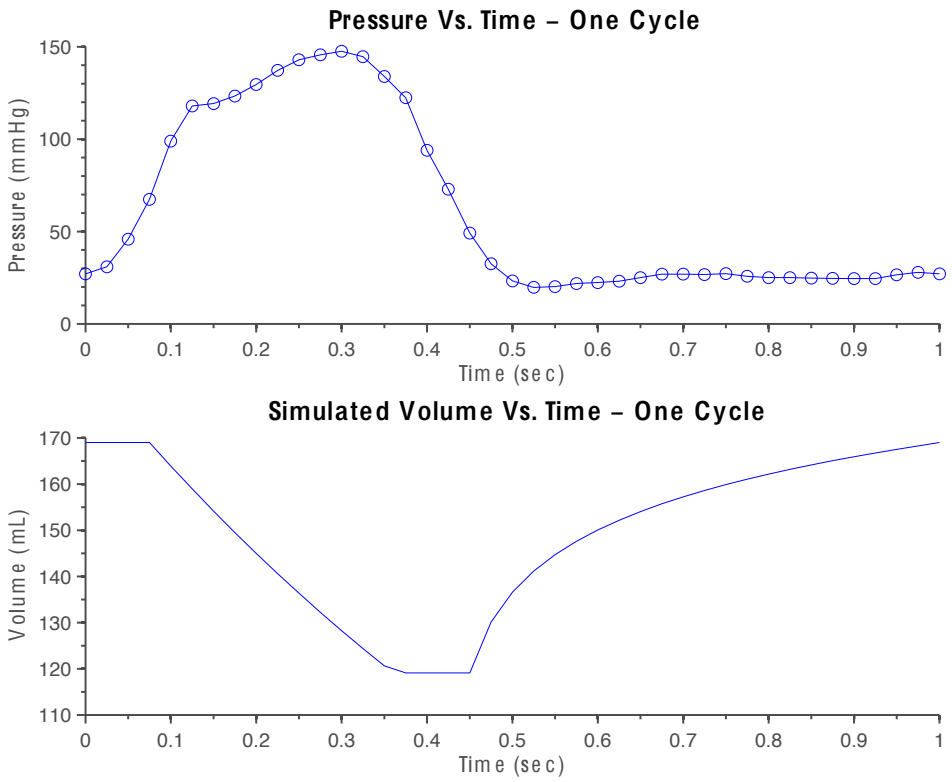

(b)

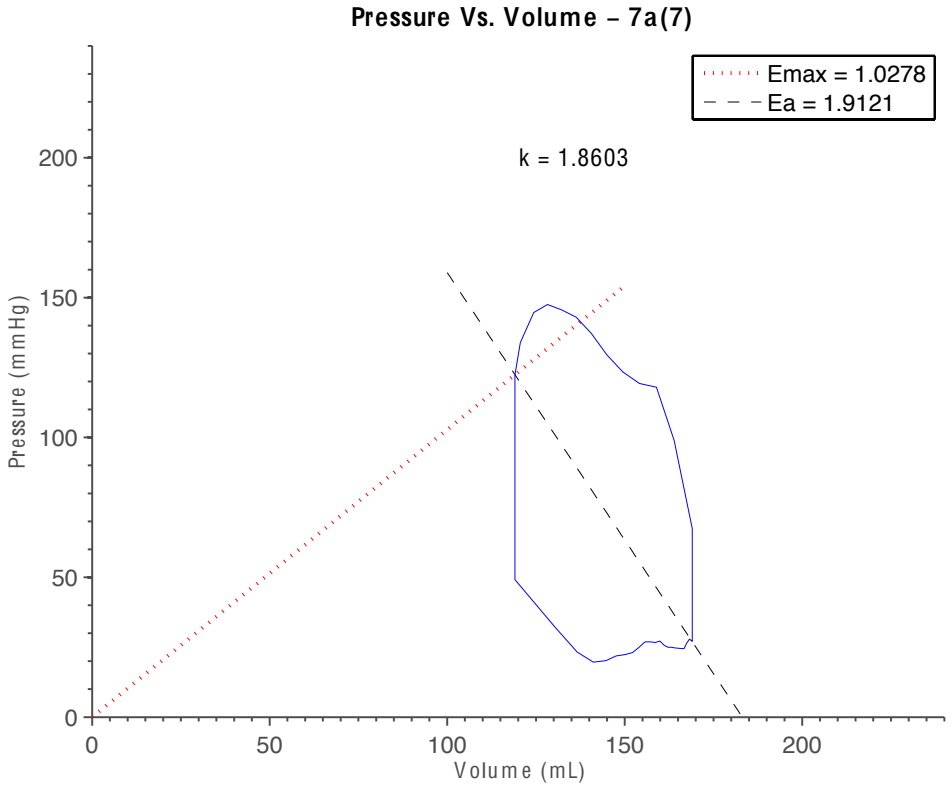

Figure 4.2.4: Patient 7a-7 (EF = 30.2%). *(a)* Pressure and simulated volume over time for one cardiac period. *(b)* LV Pressure-Volume loop, $V_0 = 0$ (assumed).

(a)

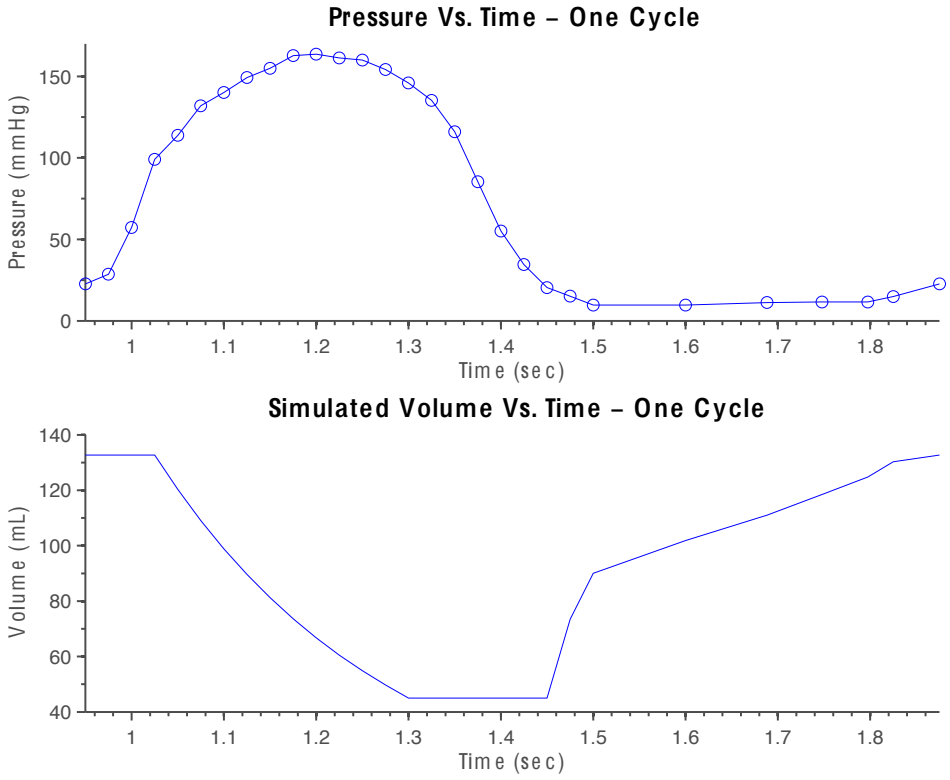

(b)

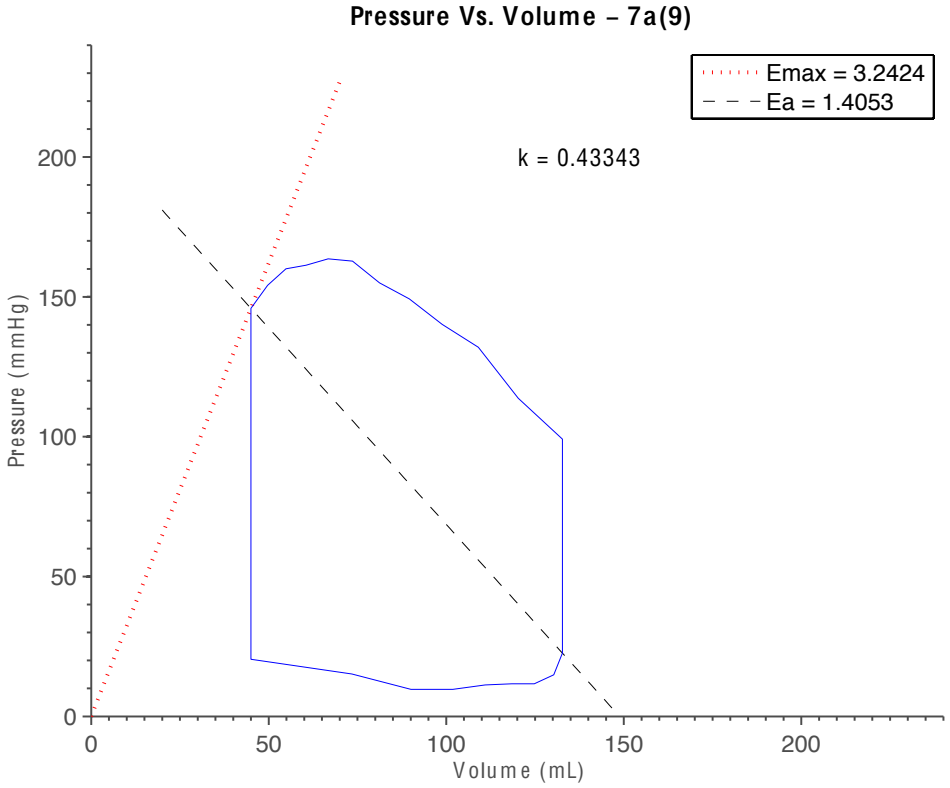

Figure 4.2.5: Patient 7a-9 (EF = 60%). *(a)* Pressure and simulated volume over time for one cardiac period. *(b)* LV Pressure-Volume loop, $V_0 = 0$ (assumed).

(a)

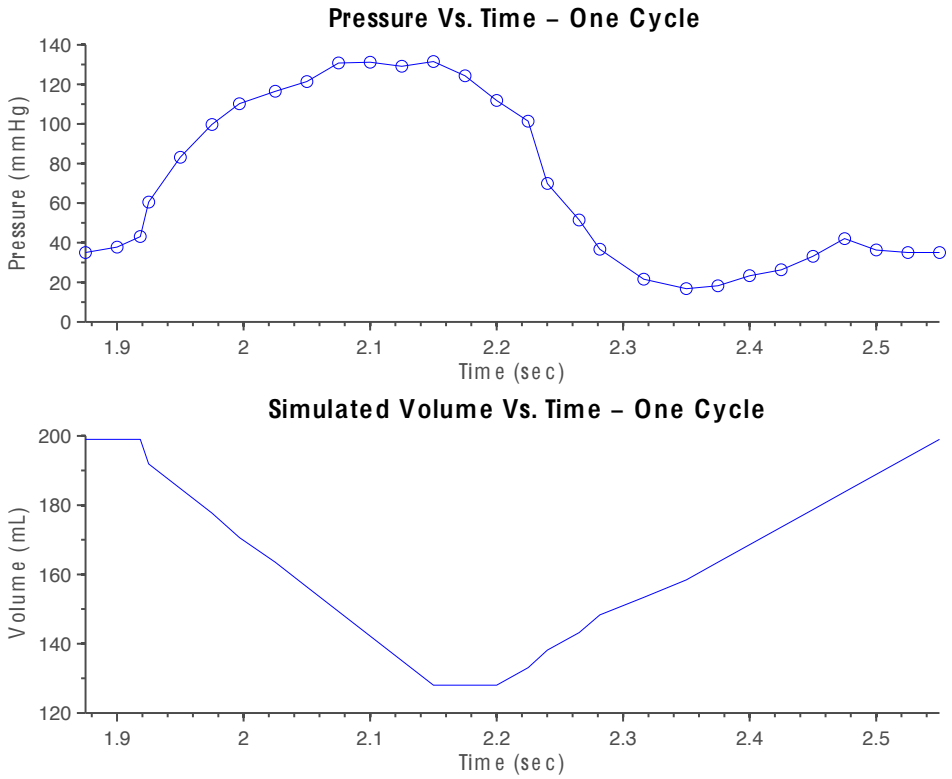

(b)

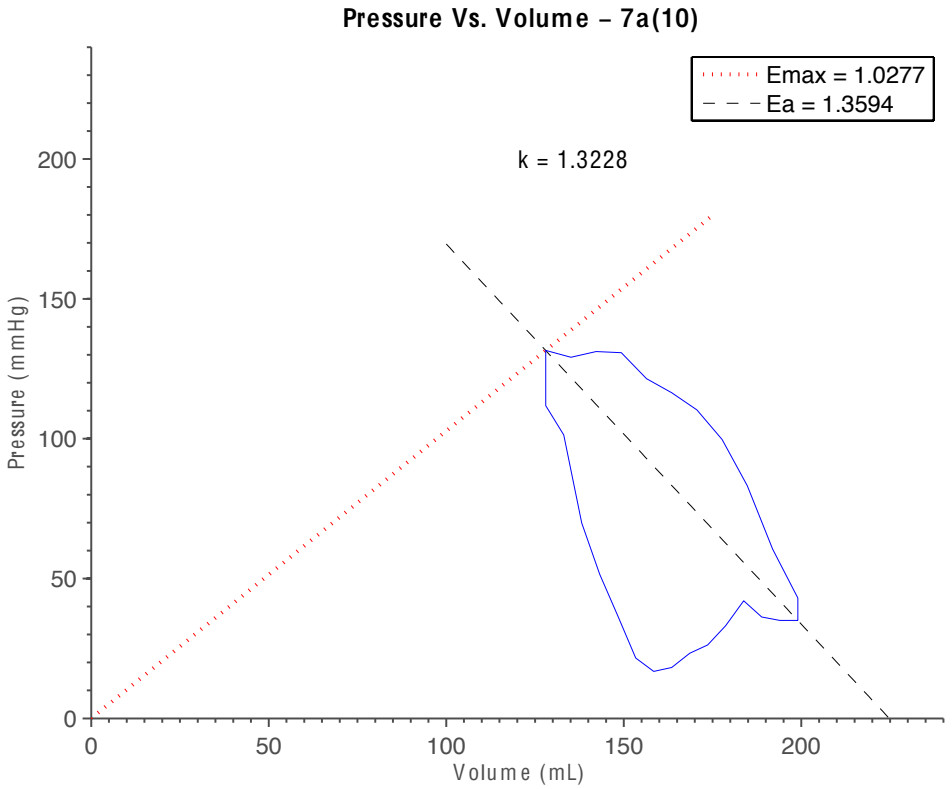

Figure 4.2.6: Patient 7a-10 (EF = 35.7%). *(a)* Pressure and simulated volume over time for one cardiac period. *(b)* LV Pressure-Volume loop, $V_0 = 0$ (assumed).

(a)

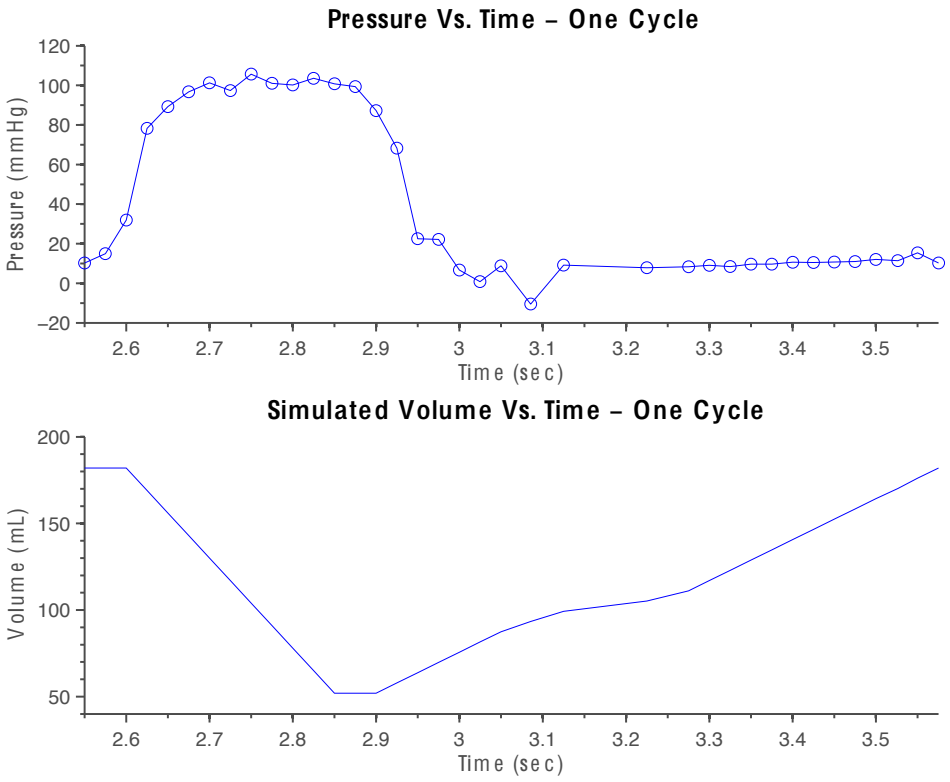

(b)

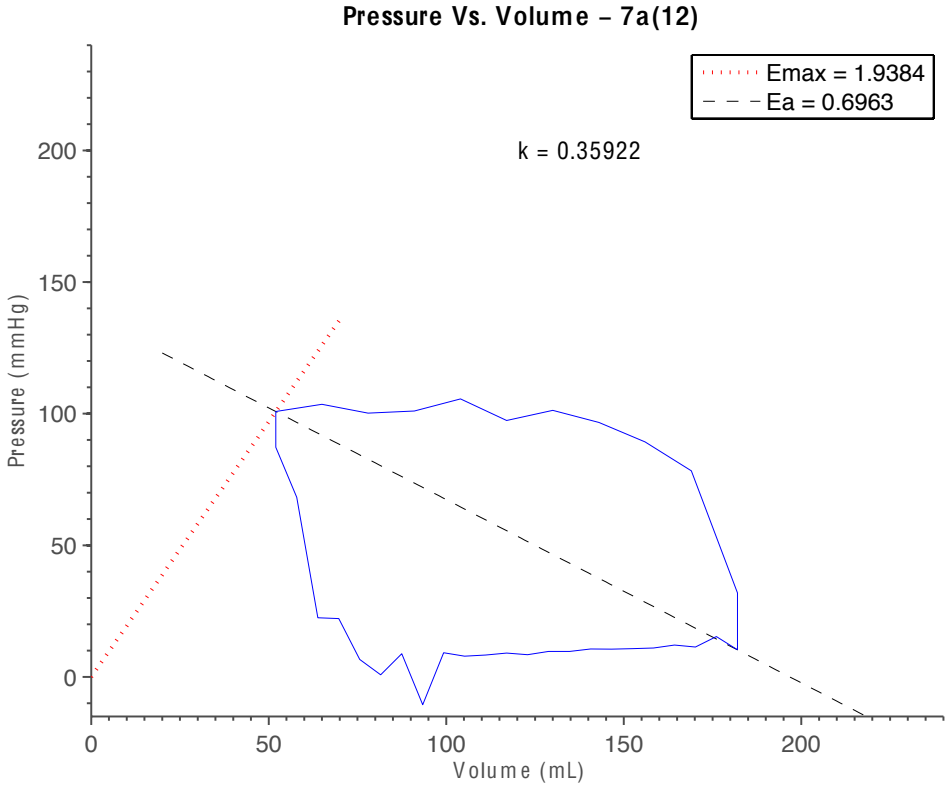

Figure 4.2.7: Patient 7a-12 (EF = 55%). *(a)* Pressure and simulated volume over time for one cardiac period. *(b)* LV Pressure-Volume loop, $V_0 = 0$ (assumed).

(a)

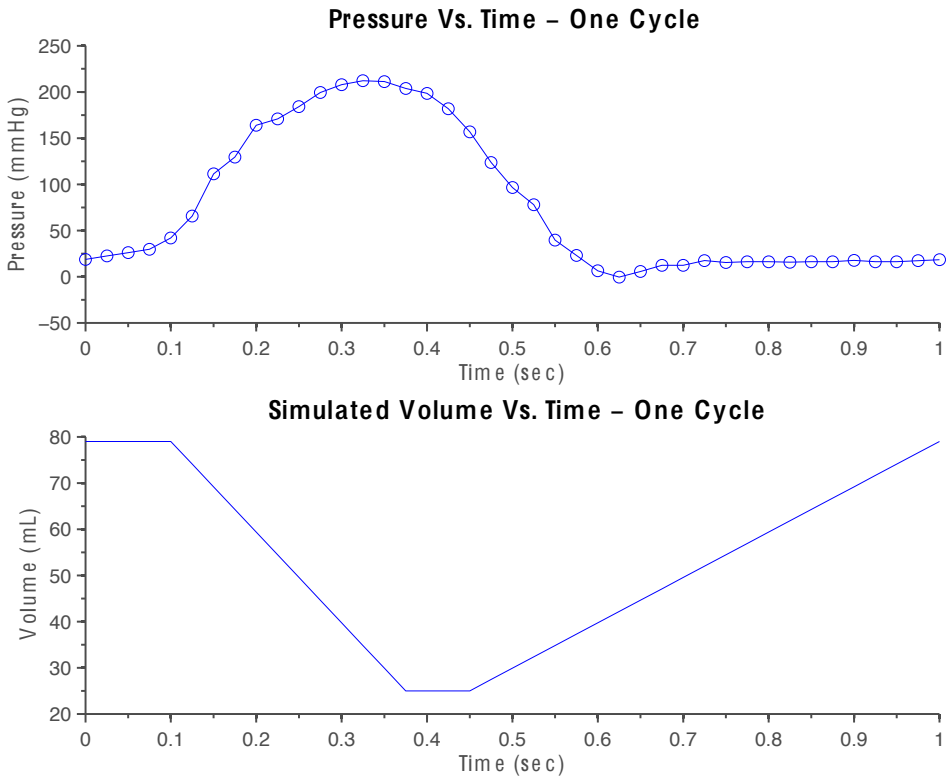

(b)

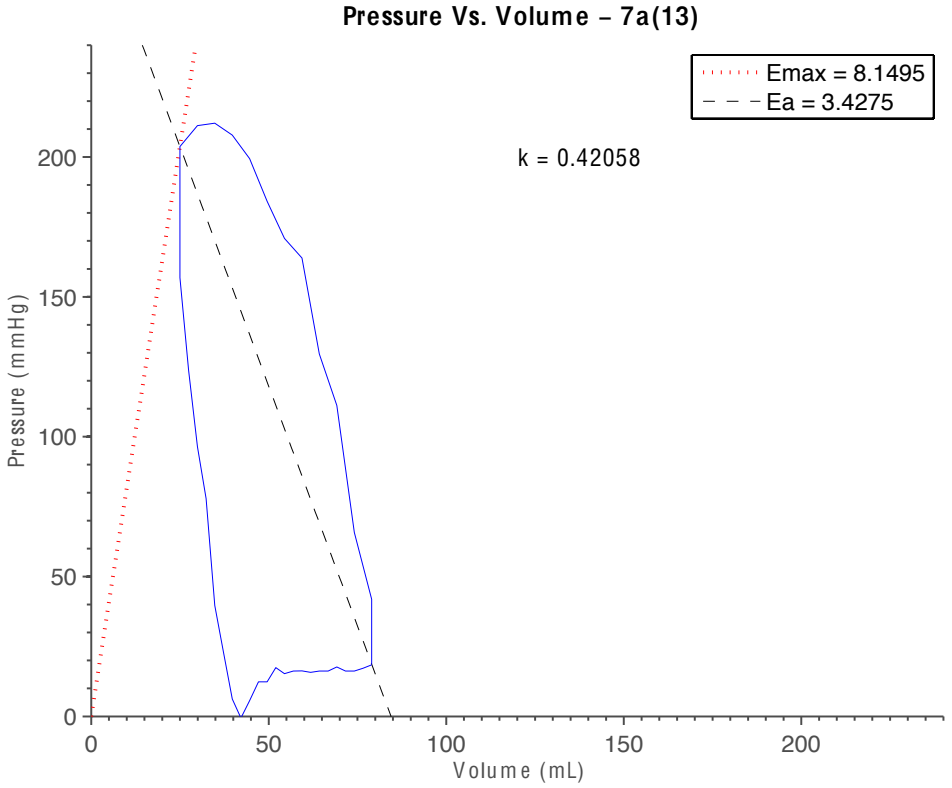

Figure 4.2.8: Patient 7a-13 (EF = 68.4%). *(a)* Pressure and simulated volume over time for one cardiac period. *(b)* LV Pressure-Volume loop, $V_0 = 0$ (assumed).

(a)

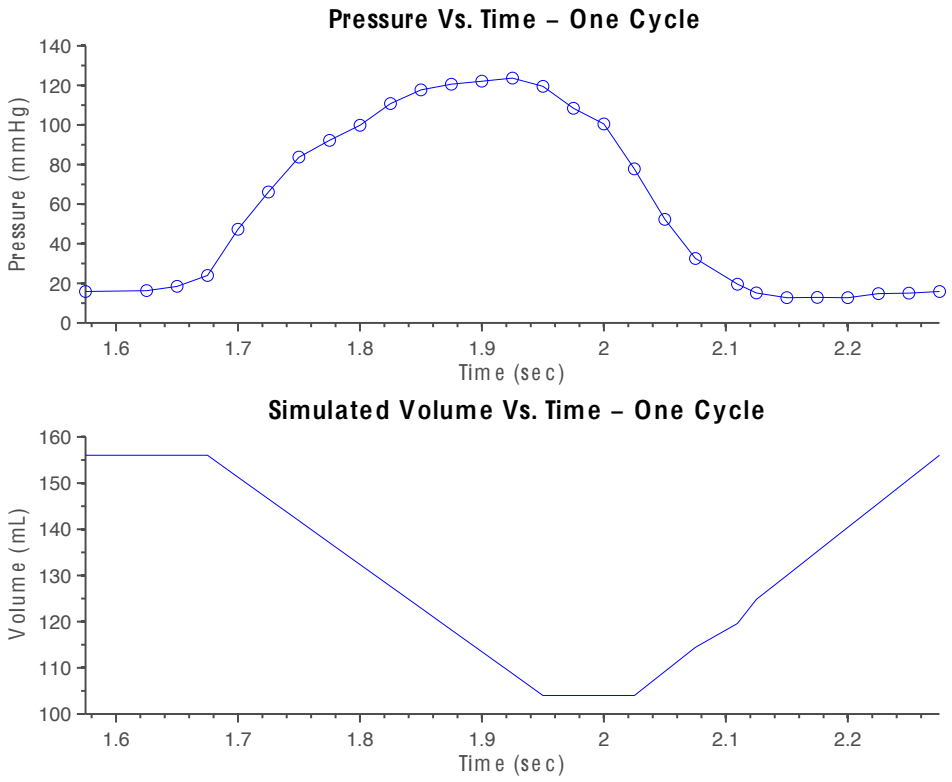

(b)

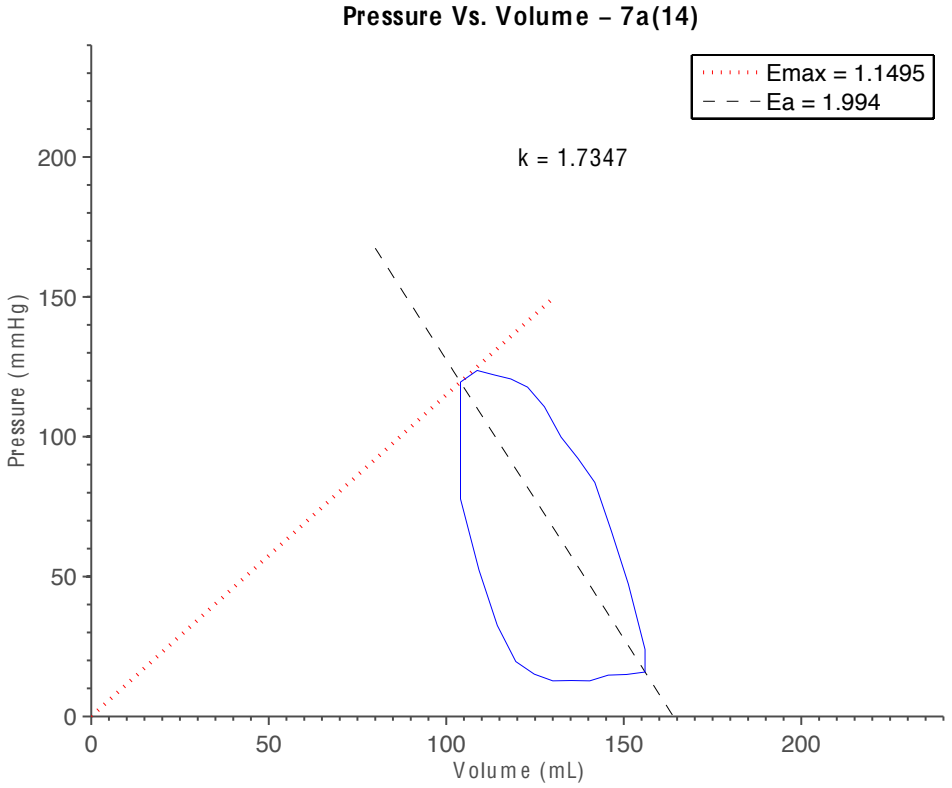

Figure 4.2.9: Patient 7a-14 (EF = 33.3%). *(a)* Pressure and simulated volume over time for one cardiac period. *(b)* LV Pressure-Volume loop, $V_0 = 0$ (assumed).

(a)

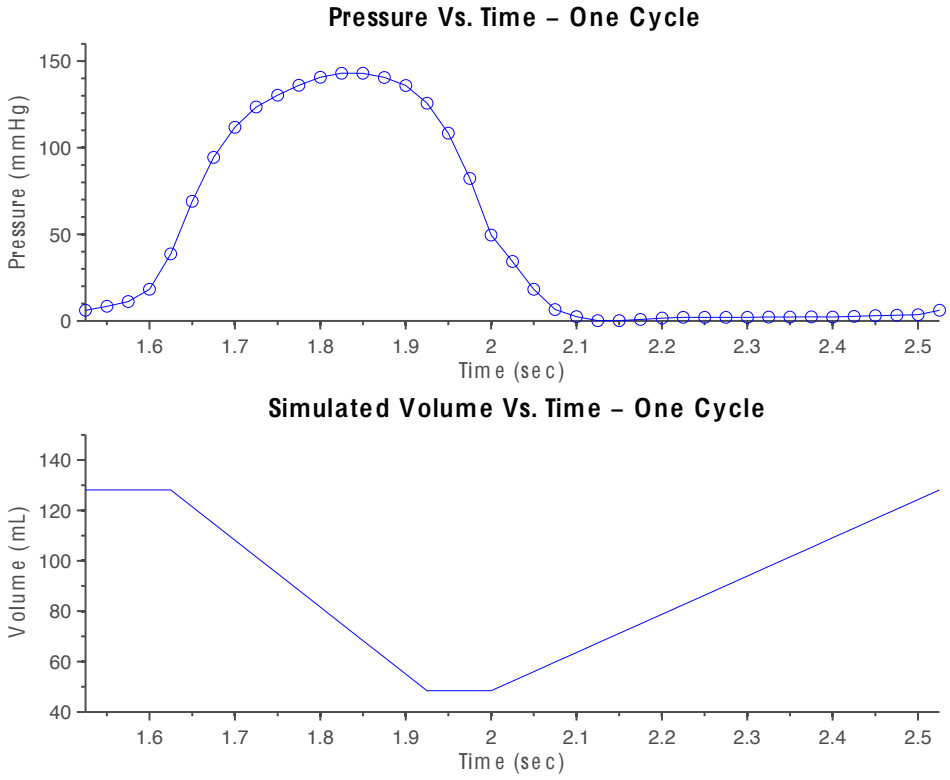

(b)

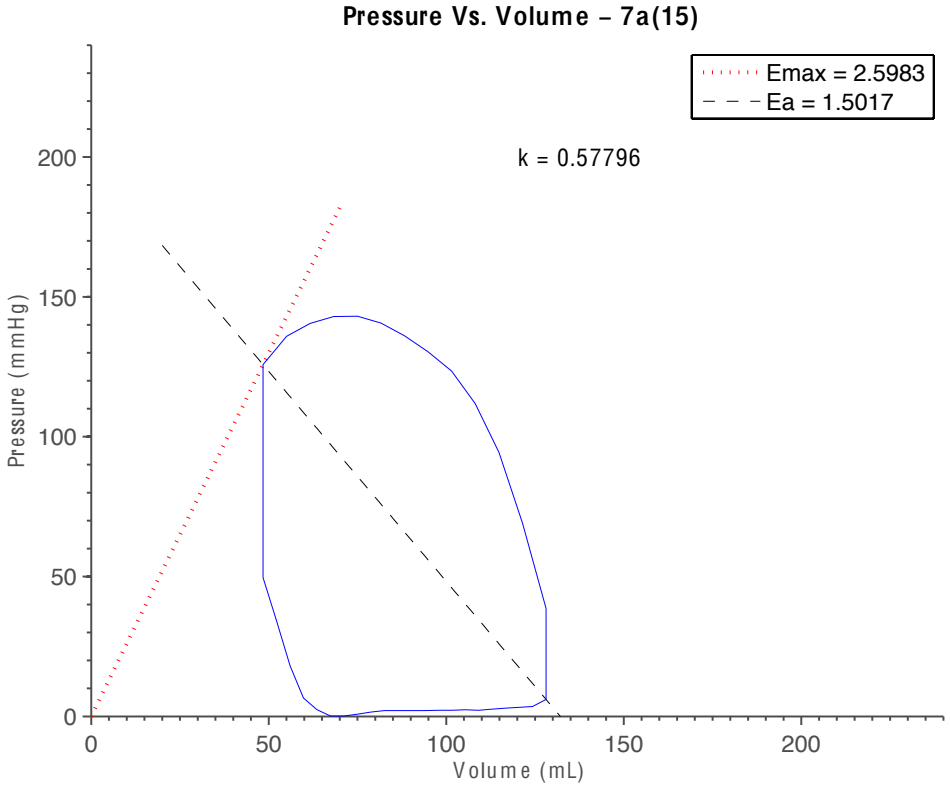

Figure 4.2.10: Patient 7a-15 (EF = 60%). *(a)* Pressure and simulated volume over time for one cardiac period. *(b)* LV Pressure-Volume loop, $V_0 = 0$ (assumed).

(a)

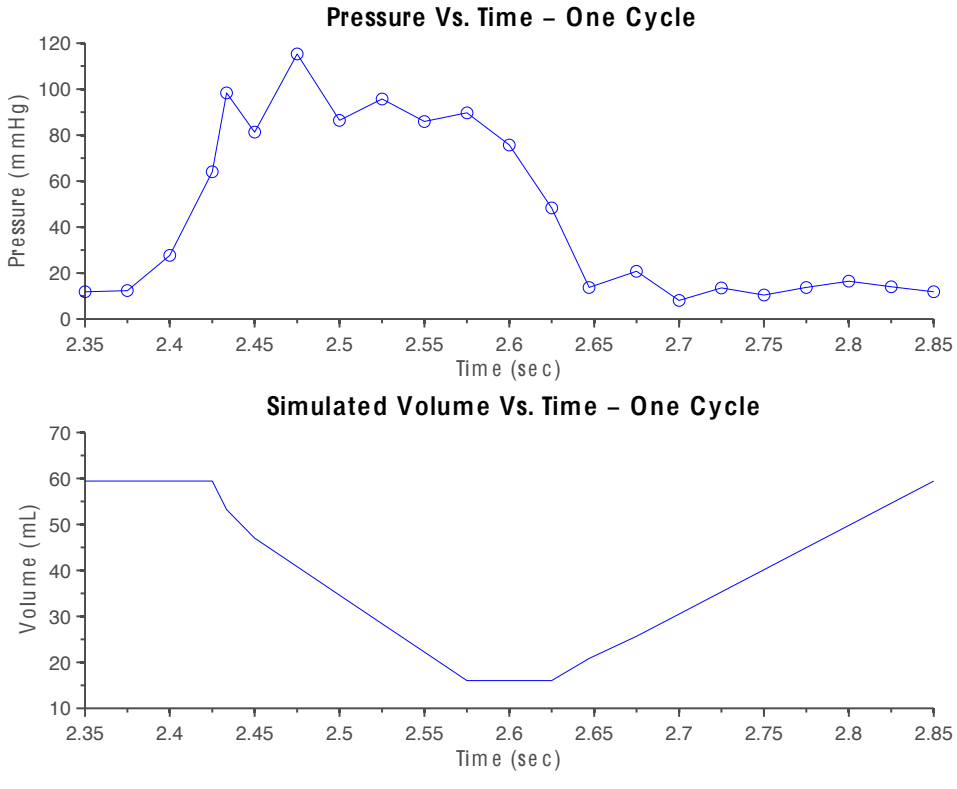

(b)

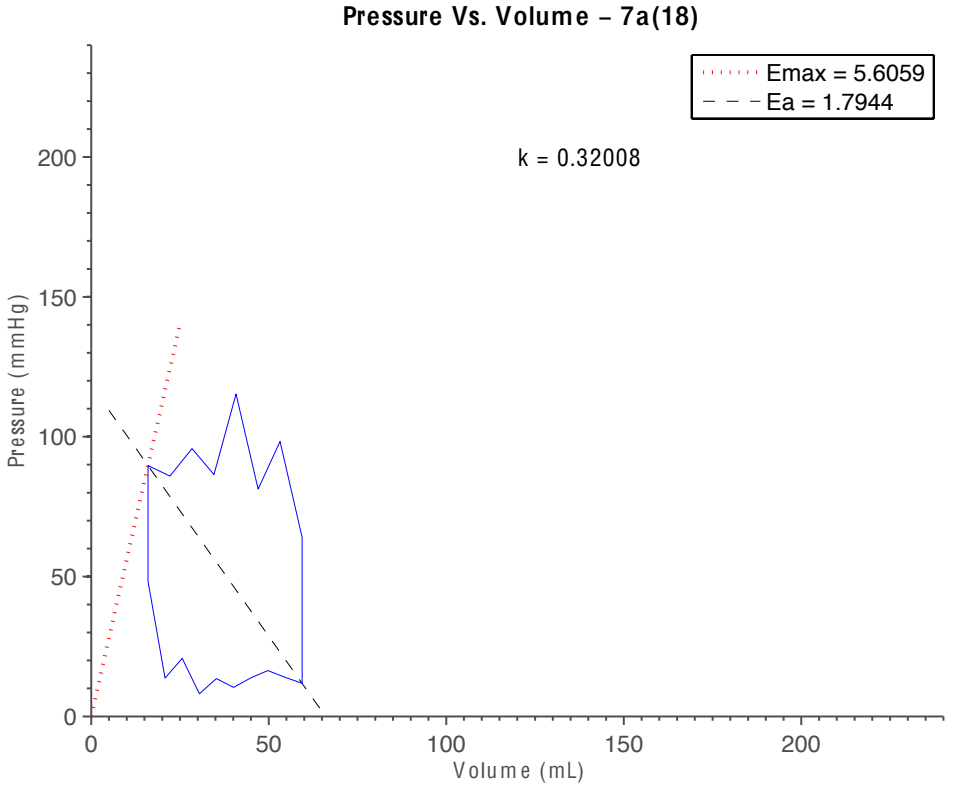

Figure 4.2.11: Patient 7a-18 (EF = 75%). *(a)* Pressure and simulated volume over time for one cardiac period. *(b)* LV Pressure-Volume loop, $V_0 = 0$ (assumed).

(a)

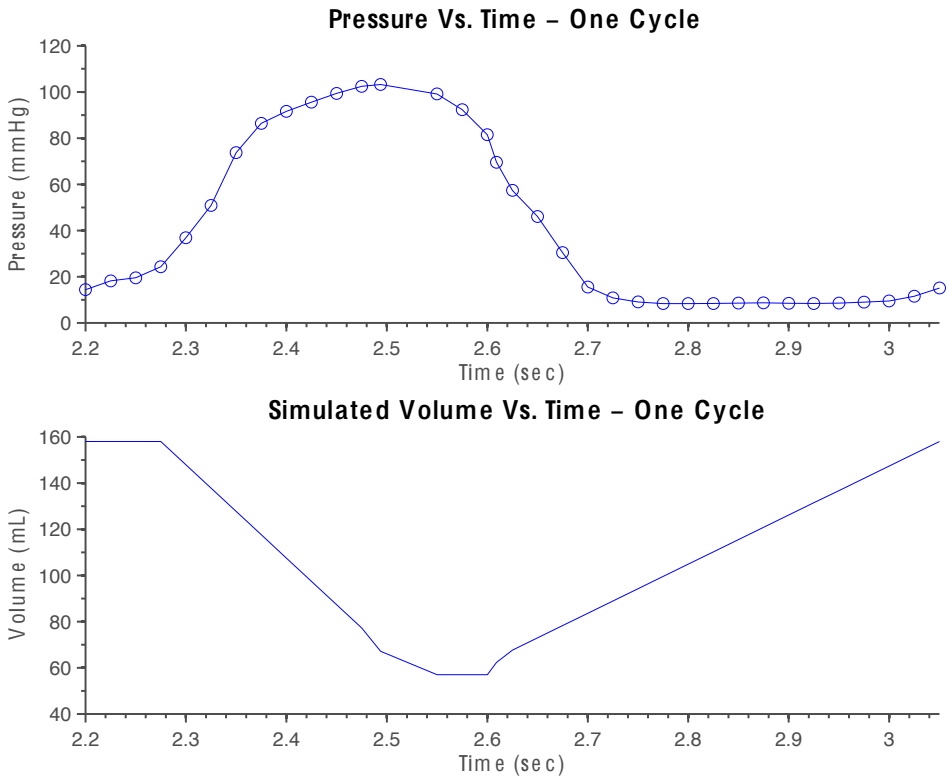

(b)

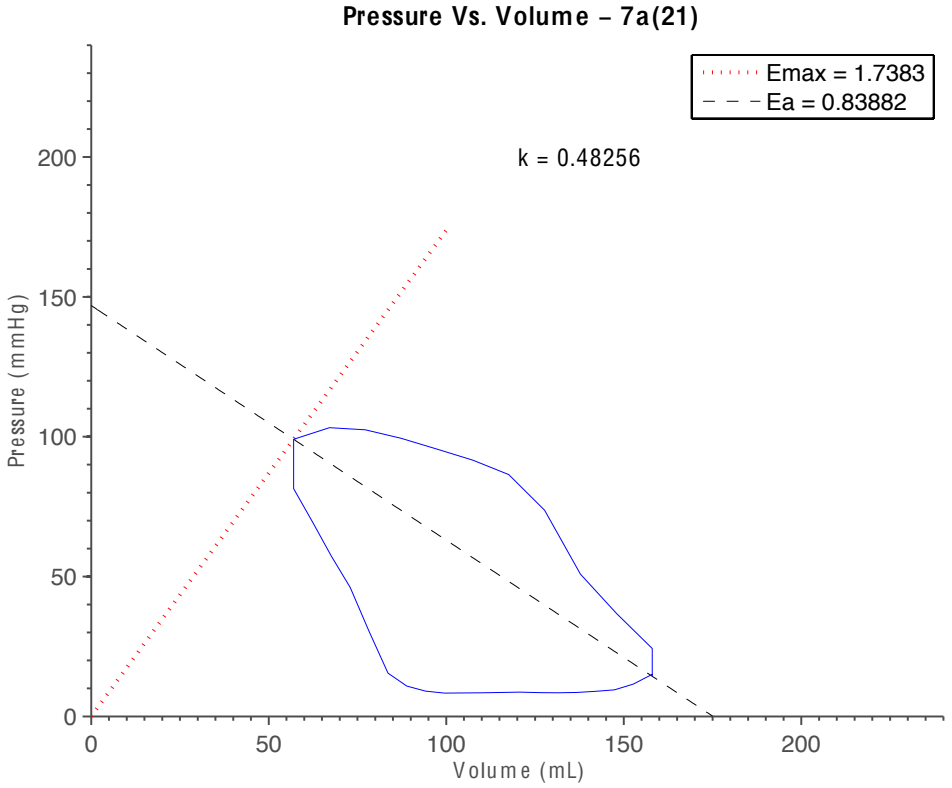

Figure 4.2.12: Patient 7a-21 (EF = 66.7%). *(a)* Pressure and simulated volume over time for one cardiac period. *(b)* LV Pressure-Volume loop, $V_0 = 0$ (assumed).

(a)

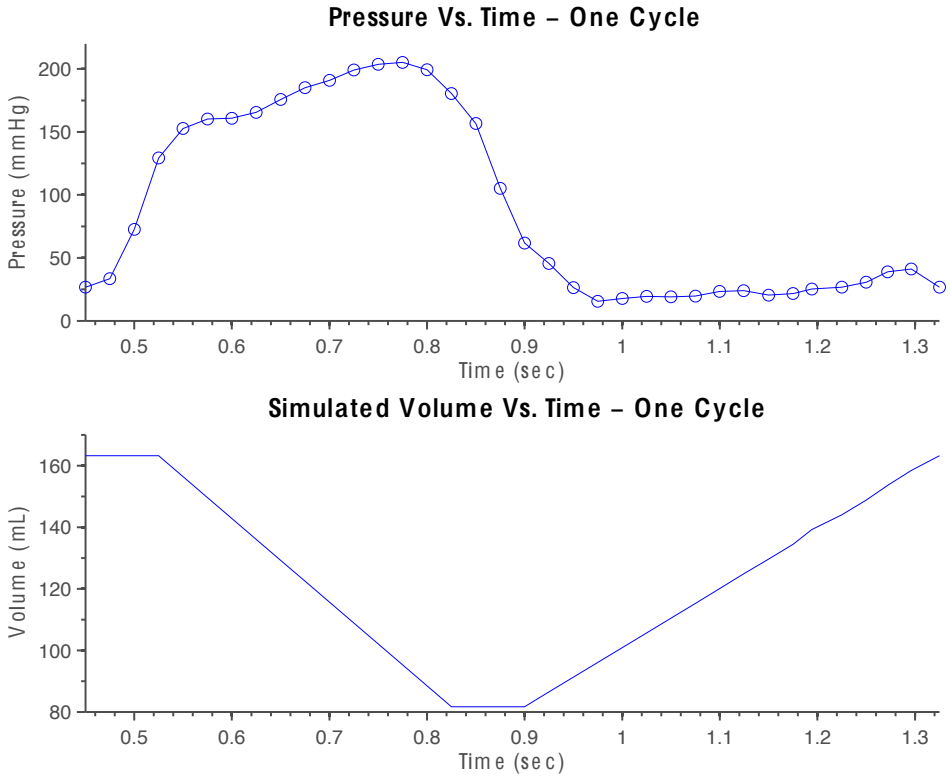

(b)

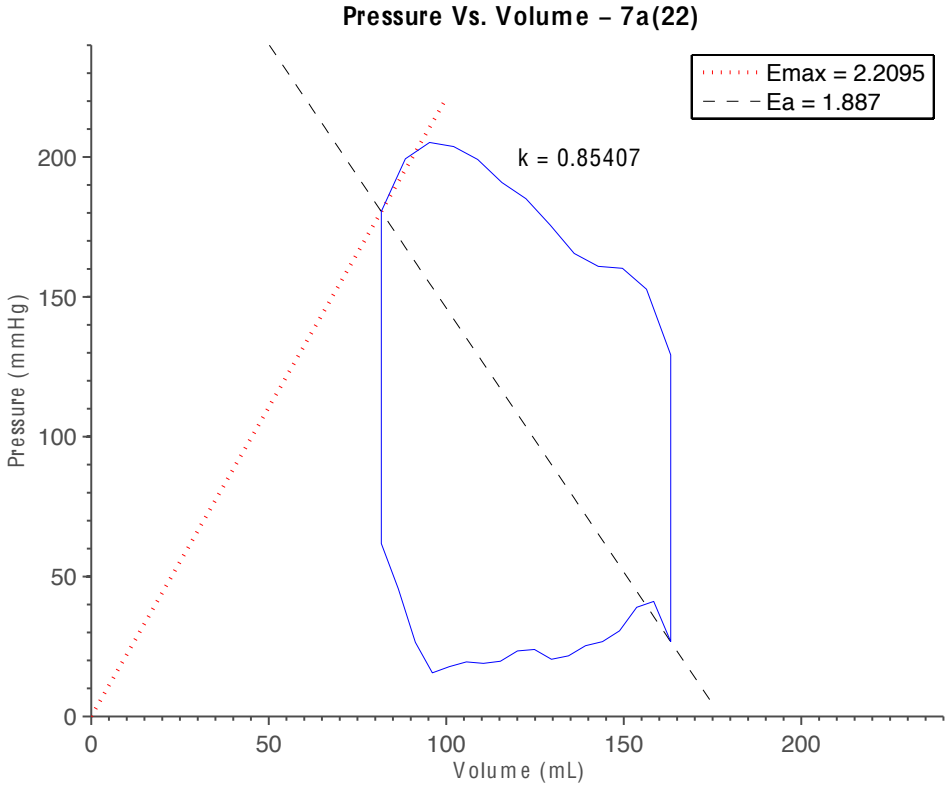

Figure 4.2.13: Patient 7a-22 (EF = 50%). *(a)* Pressure and simulated volume over time for one cardiac period. *(b)* LV Pressure-Volume loop, $V_0 = 0$ (assumed).

(a)

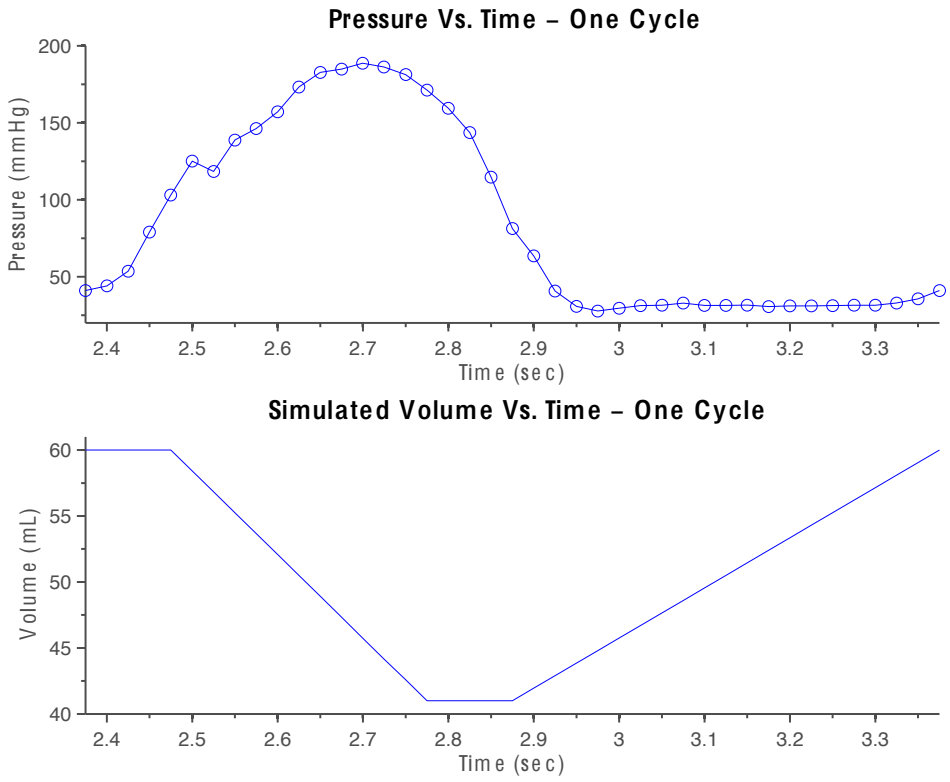

(b)

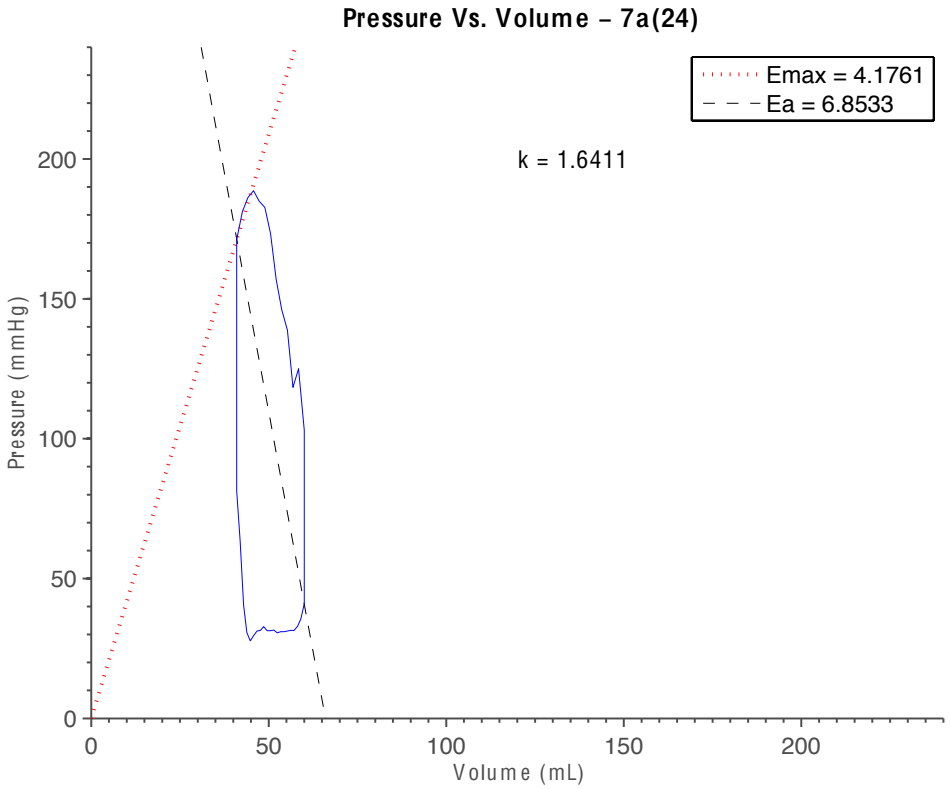

Figure 4.2.14: Patient 7a-24 (EF = 31.7 *(a)* Pressure and simulated volume over time for one cardiac period. *(b)* LV Pressure-Volume loop, $V_0 = 0$ (assumed).

(a)

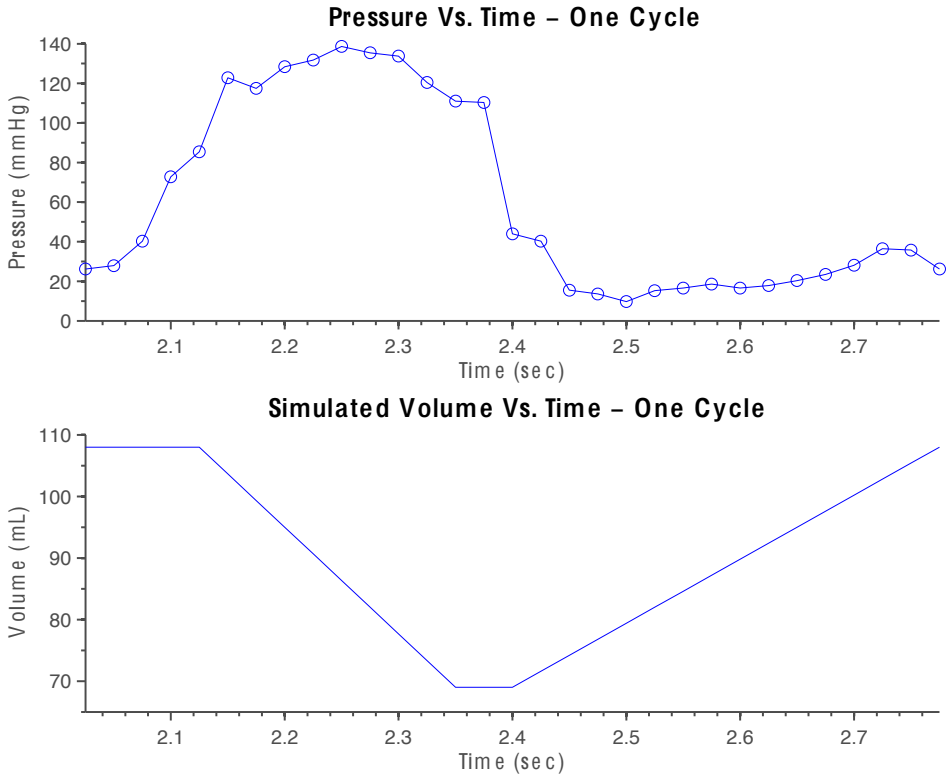

(b)

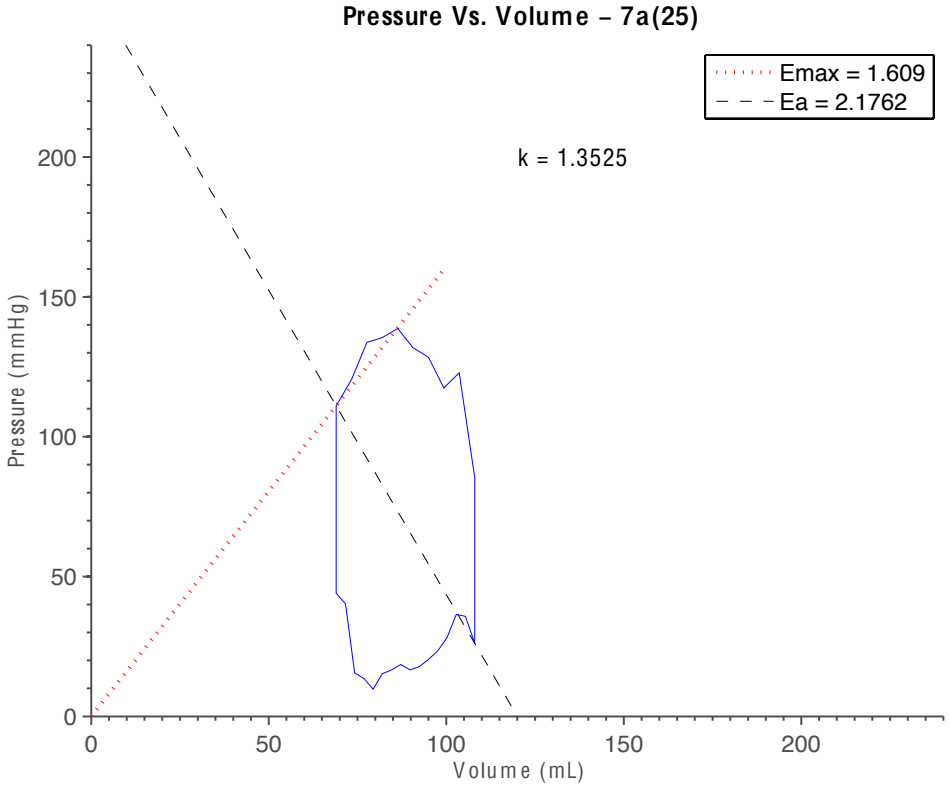

Figure 4.2.15: Patient 7a-25 (EF = 36.1%). *(a)* Pressure and simulated volume over time for one cardiac period. *(b)* LV Pressure-Volume loop, $V_0 = 0$ (assumed).

(a)

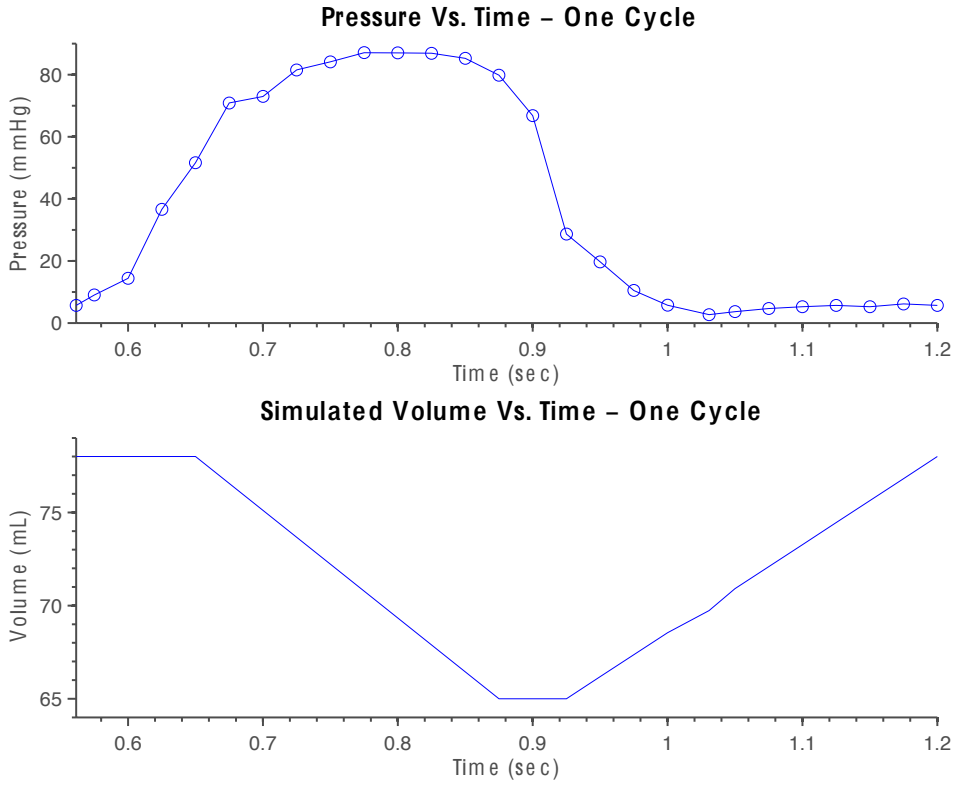

(b)

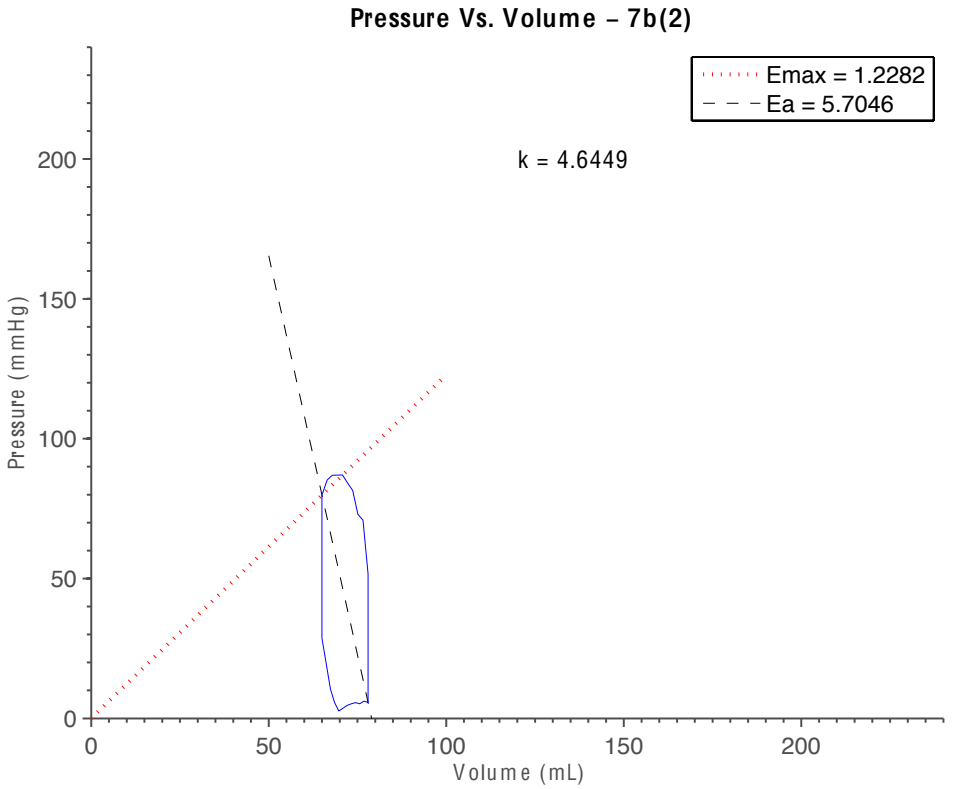

Figure 4.2.16: Patient 7b-2 (EF = 16.7%). *(a)* Pressure and simulated volume over time for one cardiac period. *(b)* LV Pressure-Volume loop, $V_0 = 0$ (assumed).

(a)

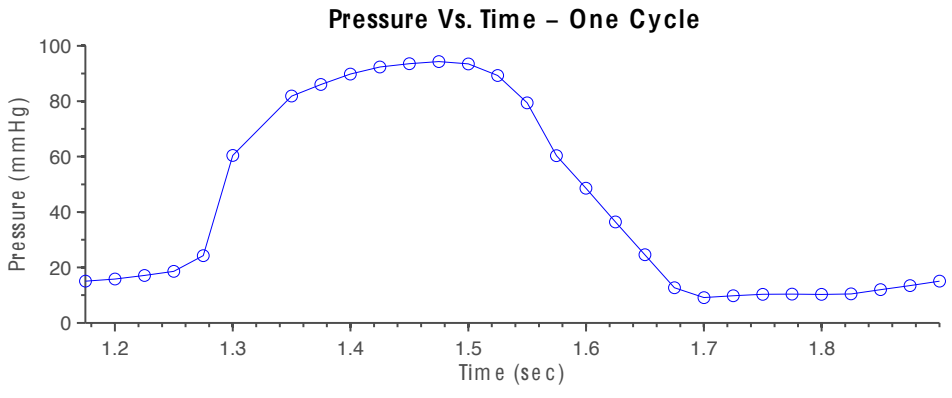

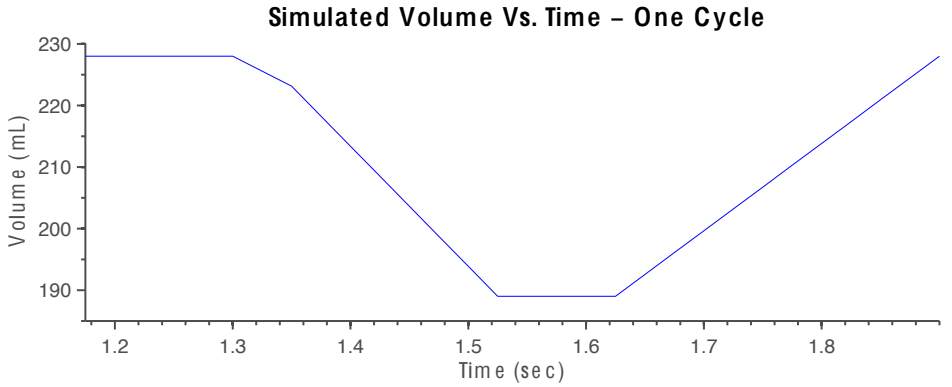

(b)

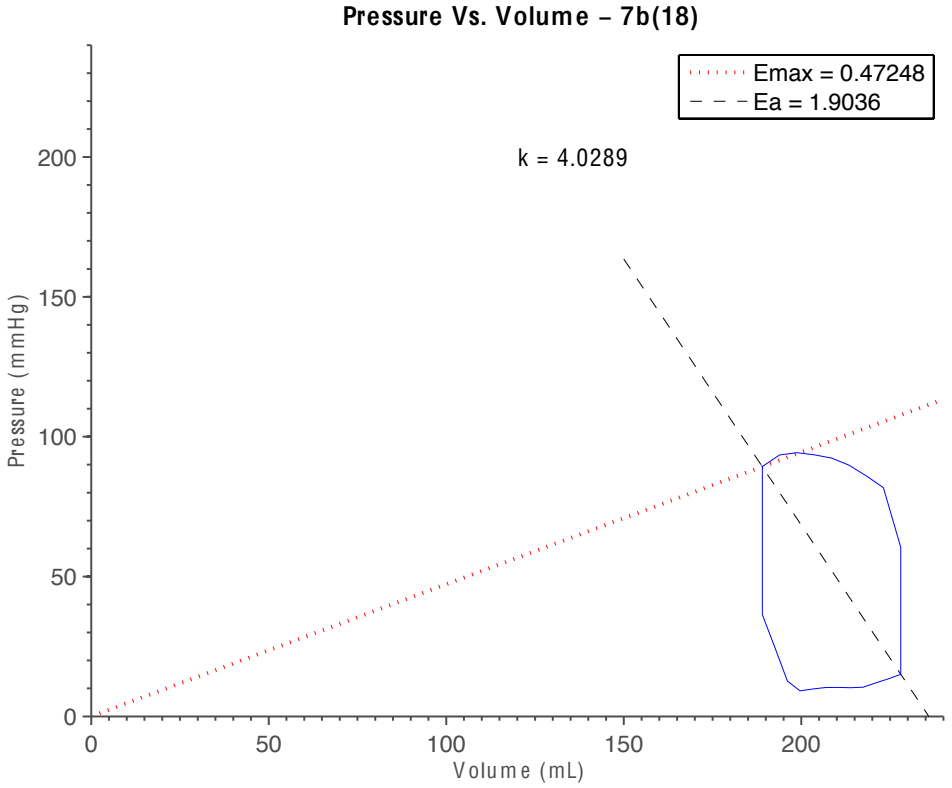

Figure 4.2.17: Patient 7b-18 (EF = 17.1%). *(a)* Pressure and simulated volume over time for one cardiac period. *(b)* LV Pressure-Volume loop, $V_0 = 0$ (assumed).

(a)

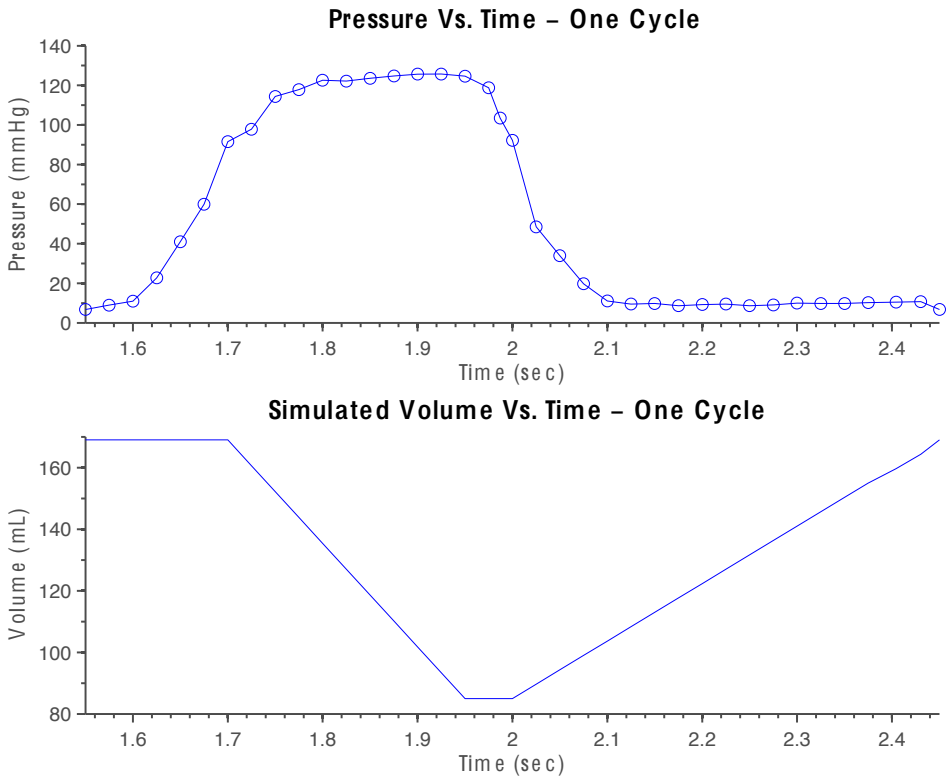

(b)

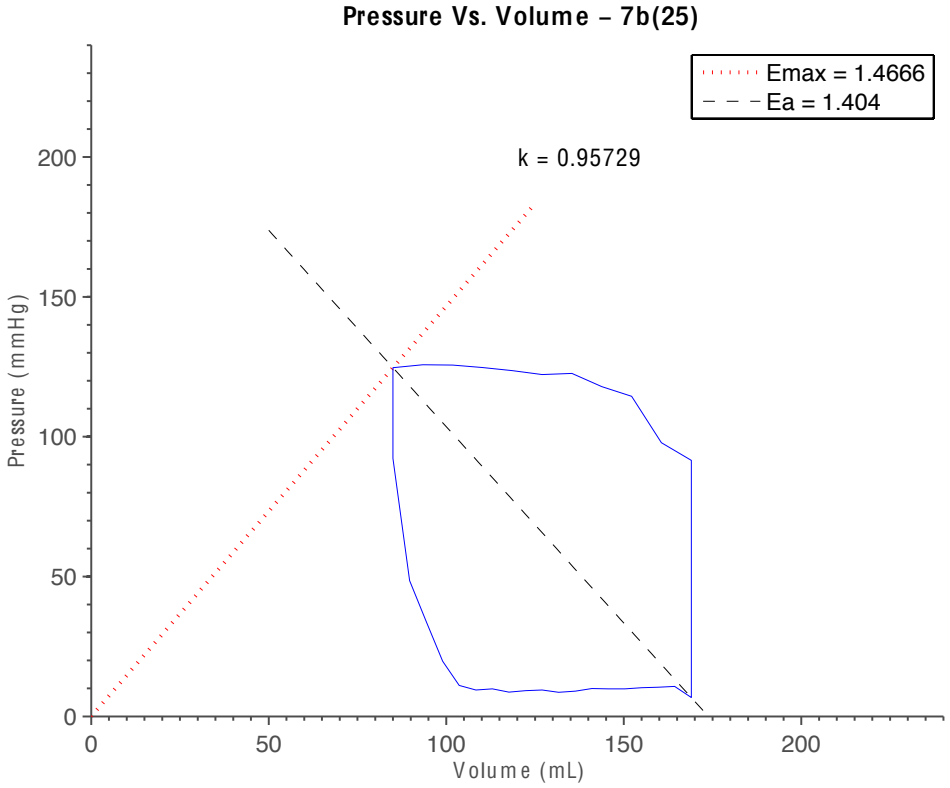

Figure 4.2.18: Patient 7b-25 (EF = 49.7%). *(a)* Pressure and simulated volume over time for one cardiac period. *(b)* LV Pressure-Volume loop, $V_0 = 0$ (assumed).

4.2.2 Coupled LV-AS Parameter Analysis

Parameter interactions were investigated by comparing effective arterial elastance (Ea), maximal elastance of the LV (Emax), arterial compliance (C), and the coupling index (k). Plots for EF versus k, k versus Ea, and k versus C were constructed. Trends are shown on each plot below, along with corresponding R-squared values. Equations for each best-fit line are shown in the figure captions. Tables 4.2.1, 4.2.2, and 4.2.3 report the measured hemodynamic parameters, computed LV-AS parameters for heart failure patients, and statistical analysis results for significant difference between groups and parameters.

Figure 4.2.19 shows the grouping of HFpEF and HFrEF patients along the EF axis. The overall trend for the relationship of EF to k is best modeled logarithmically. As k increases EF drops off exponentially. Amongst their respective groups, HFpEF patients fall in a more linear trend, as the logarithmic plot is more linear for smaller k values.

For k versus Ea, shown in Figure 4.2.20, HFrEF patients fall in a positive proportion between Ea and k (as Ea increases k increases) which is shown in the definition of k = Ea/Emax. For the HFpEF group, Ea and k show less of proportionality —Ea acts independent of k, and k remains constant and at a low value for changes in Ea.

Similar results are seen in k versus C (Figure 4.2.21). For HFpEF patients, k remains constant and at a low value for wide range of C values, but for HFrEF patients a smaller range of C values results in an entire range of k values.

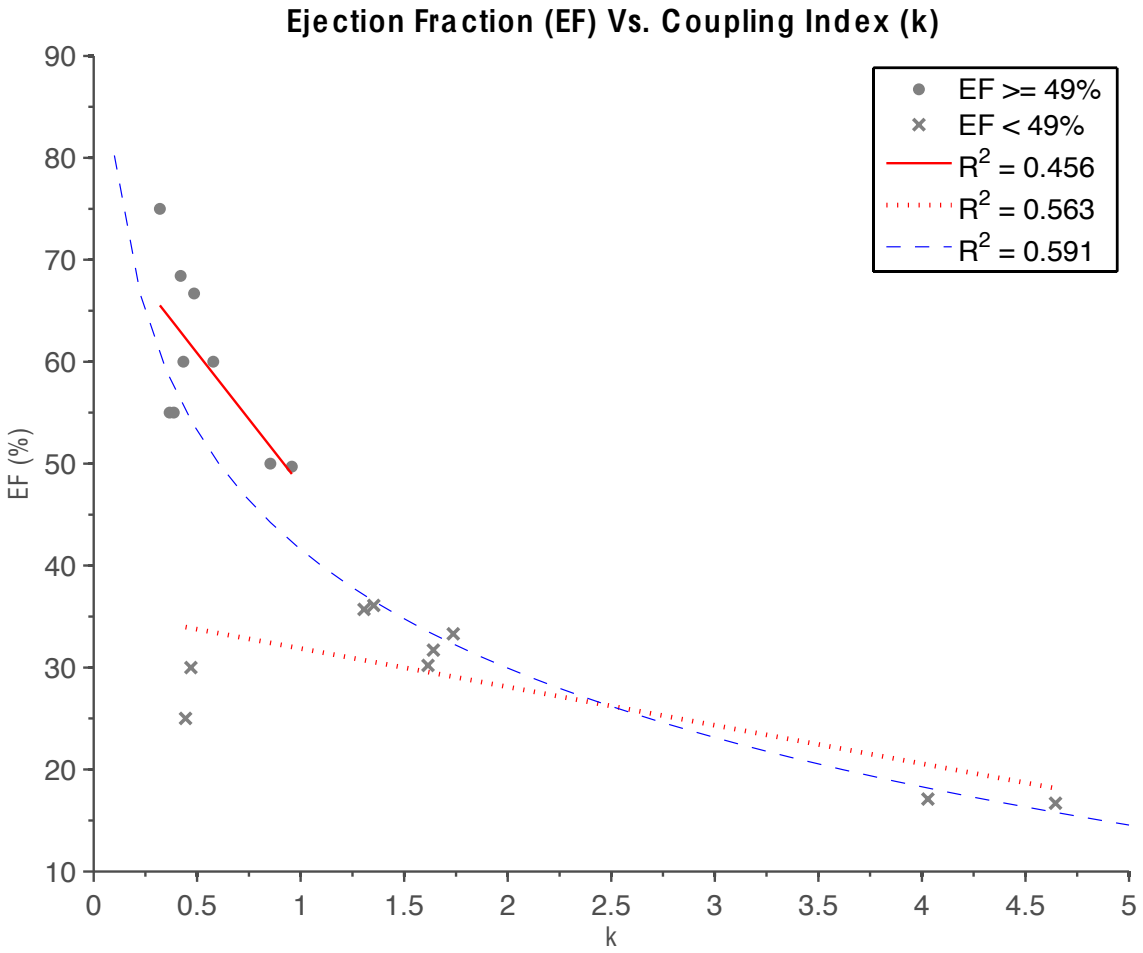

Figure 4.2.19: Ejection Fraction vs. Coupling Index. HFpEF classified as EF greater than or equal to 49%. Linear best-fit for HFpEF (solid red): $y = -26x + 74$; $R^2 = 0.456$

Linear best-fit for HFrEF (dotted red): $y = -4x + 36$; $R^2 = 0.563$

Logarithmic best-fit for all data (dashed blue): $y = -17\log(x) + 42$; $R^2 = 0.591$

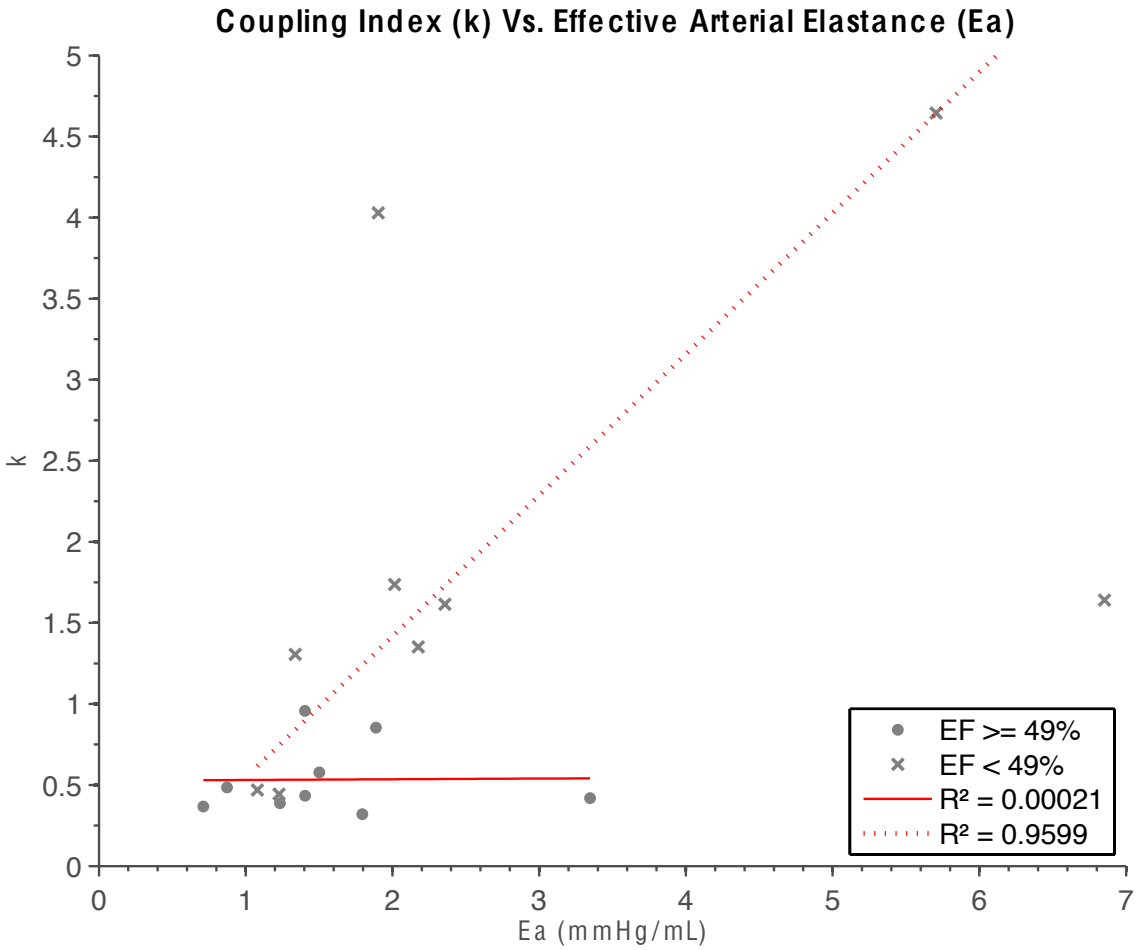

Figure 4.2.20: Coupling Index vs. Effective Arterial Elastance. HFpEF classified as EF greater than or equal to 49%. Linear best-fit for HFpEF (solid red): y = 0.0043x + 0.53; R^2 = 0.00021 Linear best-fit for HFrEF (dotted red, excluded points at Ea = 6.85, 1.90): y = 0.87x - 0.32; R^2 = 0.9599

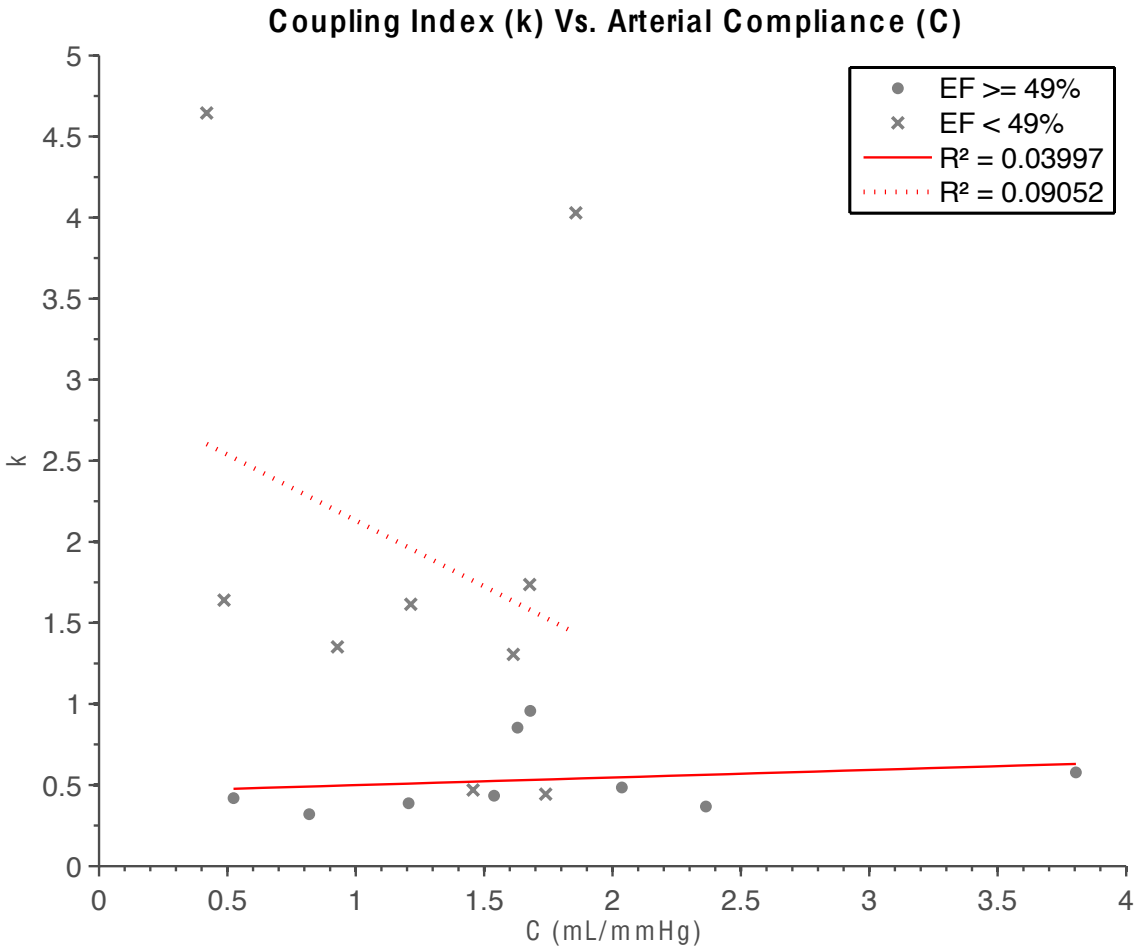

Figure 4.2.21: Coupling Index vs. Arterial Compliance. HFpEF classified as EF greater than or equal to 49%. Linear best-fit for HFpEF (solid red): $y = 0.047x + 0.45$; $R^2 = 0.03997$

Linear best-fit for HFrEF (dotted red): $y = -0.81x + 2.9$; $R^2 = 0.09052$

Table 4.2.1: Measured Hemodynamic Variables of Heart Failure Patients.
EDV calculations method or combination of methods is specified; if values were not reported from echocardiogram, EDV was calculated by adding ESV and SV (F stands for Ficks). Ao (aortic), HR (heart rate), CO (cardiac output), SV (stroke volume), EDV (end-diastolic volume), ESV (end-systolic volume).

Patient #	M/F	Age	Height (in)	Weight (lbs)	BSA (m^2)	LV Ps/Pd (mmHg)	Ao Ps/Pd (mmHg)	Ps/Pd (mmHg)	HR (bpm)	CO (L/min)	SV (ml)	EDV (ml)	ESV (ml)
7a-2	M	73	70	212	2.10	108/4	99/60	124/74	74	4.16 (Ficks) 4.9 (Thermal) 3.9 (LVOT)	60.3 (Ficks)	88.3 (sp4+F)	12.1 (Teich) 28 (sp4-el)
7a-3	M	77	70	191	2.04	141/7	138/70	133/75	73	4.73 (Ficks) 5.21 (LVOT)	84.5 (Ficks)	132.5 (sp4+F)	62.7 (Teich) 48 (sp4-el)
7a-4	M	68	68	235	2.19	163/6	189/104	160/110	76	6.61 (Ficks) 15.3 (LVOT)	87 (Ficks)	136 (sp4+F)	99.3 (Teich) 49 (sp4-el)
7a-7	M	59	69	225	2.20	151/21	153/97	126/84	78	4.23 (Ficks) 7.01 (LVOT)	51 (MODsp4)	169 (MODsp4)	118 (MOD-sp4) 153.7 (Teich) 85 (sp4-el)
7a-9	F	75	68	205	2.00	161/2	129/54	131/74	60	5.26 (Ficks) 3.2 (Thermal) 4.0 (LVOT)	87.7 (Ficks)	132.7 (sp4+F)	28.9 (Teich) 45 (sp4-el)
7a-10	F	47	69	385	2.73	129/6	121/75	124/80	88	4.92 (Ficks)	71 (MODsp4)	199 (MODsp4)	142.6 (Teich) 128 (MODsp4)
7a-12	M	48	70	332	2.59	125/3	119/70	122/67	56	7.28 (Ficks)	130 (Ficks)	182 (sp4+F)	65.2 (Teich) 52 (sp4-el)
7a-13	F	84	62	113	1.50	212/1	185/54	182/79	58	4.26 (Ficks) 4.6 (LVOT)	54 (MODsp4)	79 (MODsp4)	35.3 (Teich) 25 (MODsp4) 73 (sp4-el)
7a-14	M	69	72	237	2.30	121/7	114/75	111/80	109	4.89 (Ficks) 5.4 (LVOT)	52 (MODsp4)	156 (MODsp4)	109.1 (Teich) 104 (MODsp4)
7a-15	M	75	70	243	2.30	144/1	122/59	97/76	126	4.86 (Ficks) 4 (LVOT)	79.7 (Ficks)	128.1 (F+T)	48.4 (Teich)
7a-18	M	67	72	240	2.30	115/2	103/65	99/46	70	3.04 (Ficks) 4.8 (LVOT)	43.4 (Ficks)	59.4 (sp4+F)	16 (sp4-el)
7a-21	M	67	72	197	2.10	103/6	104/72	145/89	93	4.1 (Ficks) 4.2 (LVOT)	114 (MODsp4)	158 (MOD-sp2) 171 (MOD-sp4)	57 (MODsp4) 89 (sp4-el)
7a-22	M	40	71	185	2.00	218/16	220/111	136/86	112	8.4 (Ficks)	81.5 (MODsp4)	163.2 (MODsp4) 162.6 (sp4-el)	62.2 (Teich) 81.7 (MODsp4) 81.3 (sp4-el)
7a-24	M	60	65	200	2.00	180/26	186/97	126/87	70	4.07 (Ficks) 3.9 (LVOT)	19 (MODsp4)	60 (Modsp4)	66.9 (Teich) 41 (MODsp4) 28 (sp4-el)
7a-25	M	57	70	219	2.20	138/4	136/76	129/87	69	5.86 (Ficks) 4.5 (LVOT)	39 (MODsp4)	108 (MODsp4)	69 (MODsp4) 52 (sp4-el)
7b-2	F	32	63	160	1.80	87/1	85/59	114/83	87	3.68 (Ficks) 5 (LVOT)	13 (MODsp4)	78 (MODsp4)	147.7 (Teich) 65 (MODsp4)
7b-18	M	45	67	158	1.80	108/6	111/74	106/85	83	5.1 (Ficks)	39 (MODsp4)	228 (MODsp4)	140.7 (Teich) 189 (MODsp4)
7b-25	M	44	70	205	2.1	115/1	121/79	121/71	72	9.25 (Ficks)	84 (MODsp4)	169 (MODsp4)	78 (Teich) 85 (MODsp4)

Table 4.2.2: Computed Left Ventricle and Arterial System Parameters of Heart Failure Patients. EF (ejection fraction), Emax (LV maximum elastance), Ea (effective arterial elastance), Rs (arterial peripheral resistance), C (arterial compliance), k (coupling index, Ea/Emax).

Patient #	EF (%)	Emax (mmHg/ml)	Ea (mmHg/ml)	Rs (mmHg/ml/s)	C (ml/mmHg)	k
7a-2	55	3.1840	1.2347	1.0011	1.2060	0.3878
7a-3	30	2.3011	1.0804	0.8880	1.4569	0.4695
7a-4	25	2.7626	1.2271	0.9688	1.7400	0.4442
7a-7	30.2	1.4596	2.3577	1.8136	1.2143	1.6153
7a-9	60	3.2423	1.4053	1.4053	1.5386	0.4334
7a-10	35.7	1.0247	1.3383	0.9125	1.6136	1.3061
7a-12	55	1.9384	0.7112	0.7620	2.3636	0.3669
7a-13	68.4	7.9755	3.3470	3.4624	0.5243	0.4197
7a-14	33.3	1.1599	2.0150	1.1092	1.6774	1.7372
7a-15	60	2.5983	1.5017	0.7151	3.8048	0.5780
7a-18	75	5.6061	1.7944	1.5381	0.8189	0.3201
7a-21	66.7	1.7977	0.8724	0.5628	2.0357	0.4853
7a-22	50	2.2094	1.8870	1.0109	1.6300	0.8541
7a-24	31.7	4.1760	6.8533	5.8743	0.4872	1.6411
7a-25	36.1	1.6090	2.1762	1.8923	0.9286	1.3525
7b-2	16.7	1.2281	5.7046	3.9342	0.4194	4.6449
7b-18	17.1	0.4725	1.9036	1.3761	1.8571	4.0289
7b-25	49.7	1.4666	1.4040	1.1700	1.6800	0.9573

Table 4.2.3: T-test Results for Computed Left Ventricle and Arterial System Parameters of Heart Failure Patients. Ea* excludes two values indicated on Figure 4.2.20.
$p < 0.05$ shows statistical significance.

Data Series	Groups	Mean	Standard Error	p-value
EF vs. k	*HFpEF*	59.978	3.775	3.12E-07
	HFrEF	28.422	3.775	
k vs. Ea*	*HFpEF*	0.5336	0.4750	0.0336
	HFrEF	1.6528	0.4750	
k vs. C	*HFpEF*	0.5336	0.4925	0.0127
	HFrEF	1.9156	0.4925	

Chapter 5. Discussion and Suggestions for Future Research

While there have been many studies with experimental animal studies and human studies, few have looked at combining modeling studies with the analysis of the interaction of the heart and the arterial system with respect to heart failure. This thesis provides one of the first such studies.

5.1 Combining Animal Experiments with Model-based Characterization of the Arterial System Load to the Heart

The three-element Windkessel model in the present study was effective in estimating the arterial system's load on the heart through calculation of arterial compliance, peripheral resistance, and aortic characteristic impedance in three physiological conditions (normal, hypertensive, and vasodilator-treated) in canines. This lumped model analysis allows the complex network of abundant arteries and veins to be simplified for rapid analysis through simple mathematics, without large compensations in accuracy and application. As mentioned in chapter 3, the Windkessel model describes the reservoir properties of large arteries in terms of arterial compliance, and the perfusion to small resistive vessels in terms of peripheral resistance. This is allows for both compliance and resistance components to be quantified in clinical applications, and provides a simple and fast diagnostic tool to detect disease such as hypertension and early signs of heart failure.

Previous work has been done on validating the Windkessel model for its estimates for arterial system performance (Westerhof et al., 2009). The three-element model is accurate in estimating overall wave shape, and at low frequencies, there is a small error in the calculation of impedance. This model also makes an overestimation for compliance because of an assumption that compliance is constant, rather than pressure dependent. However, a wide number of studies

support and continue to implement the three-element Windkessel since compliance overestimation is not drastic, and generally, linearity is preferred over nonlinearity (Fogliardi et al., 1996; Westerhof et al., 2009). A more accurate model for the pressure-dependent arterial compliance behavior has been accounted for in a nonlinear system presented by Li et al. (1990), in which arterial compliance is shown to vary throughout the cardiac cycle.

As a general description of the arterial system in terms of three parameters that are viable measures of heart health, the three-element Windkessel is adequate in providing insight into many areas of analysis, such as those shown in this study. We have shown the application of the Windkessel in estimating compliance, peripheral resistance, and impedance. As well as being instrumental in interpretation of hemodynamics, pressure-flow relationships at the entrance of the arterial system, and pulse wave analysis in forward and reflected waves.

However, some limitations exist. For example, this model is unable to examine pressure-flow interactions within individual vessels, i.e. distal pressures are skewed, as well as the need for direct and accurate measurement of the pressure and flow in the proximal aorta. Due to the lumped parameters used in the model, it is unable to give insight into effects of local hemodynamics on individual parts such as only the aorta, or only the vascular bed. Wave transmission mechanisms and wave propagation cannot be studied, and the assumption that pulse wave velocity is infinite can be limiting in some cases. However, the model is very useful in studying the ventricle-artery interactions of the circulatory system, and gives a deeper insight into arterial-heart conditions in terms of three distinct parameters.

It was shown in the current work that the frequency dependence of impedance is linked to forward and reflected waves in pressure and flow — the lower the frequency the greater the wave reflections. As wave frequency increases, out-of-phase cancellations occur more often, which reduces the number of backward reflected waves. This is seen for harmonics above the third, and results in the aorta's characteristic impedance becoming dominant in determining total input impedance. As the amount of wave reflections increase (i.e. at low and intermediate frequencies),

the amount of energy required of the heart to pump increases (Li, 1989). Through the understanding of external work of the heart, it can be seen that at low frequencies the input impedance is equal to the peripheral resistance. As shown in Figures 4.1.7 through 4.1.9, R_s is much larger than the impedances at higher frequencies (estimated to be approximated by Z_0). Due to this, the heart has to pump against a much greater load at lower frequencies, and through the following equation for external work (EW), it is seen that as mean aortic pressure, P_{Aomean}, increases, EW of the heart also increases:

$$EW \approx P_{Aomean} \times SV \tag{5.1}$$

The changes in P_{Aomean} due to increased input impedance are significantly greater than those decreases in SV seen in hypertension (Li, 1989). Therefore, it is insightful to understand the role frequency plays in pulse wave reflection for pressure and flow, and the implications this has on input impedance and the energy requirements of the heart.

The impedance results presented for this study reflect the findings of previous investigators, and support the claim that as peripheral resistance increases and compliance decreases, as is the case for hypertension, the characteristic impedance plays a more dominating role in input impedance. This is further supported by the demonstrated increase in wave reflections (Figures 4.1.8, 4.1.12, and 4.1.13). The opposite dynamic is seen in vasodilation (Figures 4.1.9, 4.1.14, and 4.1.15), and intuitively makes sense since it counteracts high-pressure dynamics. The response seen in vasodilation helps combat increased resistance and decreased compliance by ultimately lowering input impedance. These general and specific hemodynamic responses are to be expected, and have also been found by previous investigators (Berger et al., 1996; Li, 2000, 2004; O'Rourke and Avolio, 1980; Westerhof et al., 1971).

The concept of frequency-dependent impedance ties in many aspects investigated in this study. For example, the increased load on the heart seen in hypertension is attributed to many interconnected factors all studied: increased cardiac cycle period (decreased frequency), which as just discussed, results in greater contribution of reflected waves (supported by the forward and

reflected wave components shown in Figures 4.1.12 and 4.1.13), as well as an increase in peripheral resistance and decrease in compliance. With a decrease in heart rate and mean flow, comes a decrease in stroke volume and cardiac output also seen in hypertension. These interconnected relationships are a general trend throughout physiology, and it is by investigating the derived arterial system parameters presented in the current work that practitioners may be able to better diagnose and monitor disease onset and progression.

The same interconnected trends are seen for vasodilation, but to the opposite direction. Looking at the frequency domain Fourier analysis of pressure and flow for the vasodilated condition (Figure 4.1.6), it is seen that there are similar phase plots for P and Q. Examining the graphs for forward and reflected waves (Figures 4.1.14 and 4.1.15) helps reveal a probable cause: a drastic, almost nonexistent, influence of reflected waves. Normally, pressure waves lag flow waves, but under vasodilated conditions, it appears that this is not the case, and even though all the required changes that must occur to counteract the high-pressure condition are present, there may be a deeper mechanism behind the seen hemodynamic changes in terms of wave reflections. The validity of the forward and reflected wave analysis performed in this study is supported by recent work of Li et al. (2010).

Many anti-hypertensive drugs are vasodilators, and generally work well in controlling mean arterial pressure. This form of treatment is normally the first line of defense against high blood pressure (Li, 2000). The results in this study demonstrate the hemodynamic changes that occur under both hypertensive and vasodilated conditions. The overall trend of the vasodilated results is a decrease in mean pressure, peripheral resistance, and impedance, along with an increase in mean flow, compliance, stroke volume, and cardiac output. These changes would be beneficial to a patient with hypertension, as they are all opposite of those under high-pressure situations, and would act to stabilize values back to normal healthy levels.

Hypertension causes artery stiffening (decreased compliance), which then is tied into a plethora of hemodynamic and cardiac system changes, as discussed previously, but one

interesting aspect of the disease is that hypertension-related heart failure has been shown to preserve the ejection fraction of the left ventricle. Heart failure occurs when ejection fraction is less than 30%. Heart failure with preserved ejection fraction (HF_pEF) is currently a highly debated topic among investigators as to the leading causes. It is currently believed that there are abnormalities in the left ventricle's ability to relax fully during diastole, and not caused by increased ventricle stiffness (Udelson, 2011). As shown in this study, hypertension induces decreased compliance and increased peripheral resistance, which normally leads to a thickening of the LV wall (Levick, 2010). Wall tension in the left ventricle in hypertension can be understood more accurately by evaluating the cylindrical wall stresses defined by Laplace's Law and the Lamé equation. Laplace's Law states that wall stress (T) is equal to pressure (P) times the vessel's radius of curvature (r); while Lamé's equation has T equal to the product of P and r, divided by wall thickness, h:

$$\textit{Laplace's Law:} \qquad T = P \times r \tag{5.2}$$

$$\textit{Lamé:} \qquad T = (P \times r)/h \tag{5.3}$$

In hypertension, ejection fraction is preserved, and for wall tension to remain constant in accordance to Lamé, as P increases the wall thickness, h, must also increase to normalize wall tension. This is indeed what is seen in real life hypertensive cases with reduced SV as well as EDV. Compared to heart failure with reduced ejection fraction (HF_rEF), which demonstrates failure of the left ventricle to pump blood to the rest of the body, with a decrease in SV, HF_pEF is more a defect in diastolic function of the LV, where as HF_rEF is a defect in systolic function of the LV.

5.2 Heart Failure with Preserved or Reduced Ejection Fraction and Heart-Arterial System Interaction in Human Studies

The clinical studies investigated in the present research focused on LV-AS interactions. This thesis identified critical parameters to characterize the heart and the arterial system. These

parameters included Ea, Emax, arterial compliance, C, and the LV-AS coupling index, k. The goal was to examine the effectiveness of these parameters in separating patients with HFpEF from those with HFrEF. The coupling of the arterial system dynamics to the heart, particularly the left ventricle-aortic interface, was studied through the examination in the LV pressure-volume plane. PV loop analysis takes into account a time varying LV elastance, offers a visual tool for identifying changes in SV, Ea, and Emax between patients, and allows for a more clinician-friendly platform for observing and monitoring key LV-AS interactions. However, one limitation of PV loop analysis is that some physiological mechanisms central to LV-AS interactions, such as pulsatile load and wave reflections, are not captured in the LV pressure-volume plane alone, and limiting assumptions need to be made to derive Ea and Emax parameters (Chirinos, 2013). However, overall pressure-volume domain analysis has been a favorable and historically popular means of gaining insight into LV-AS interactions by focusing on mechanical and energetic aspects.

Ea as a measure for effective arterial elastance was derived based on several unrealistic simplifications: time invariant heart rate, and constant diastolic and systolic duration; a linear relation between arterial end-systolic pressure and stroke volume; and lumping together arterial tree impedances into one term (Sunagawa et al., 1983, 1985). Ideally, the coupling index k (defined Ea/Emax) should give a ratio of pure influences of the arterial system versus pure influences of the left ventricle. However, Ea, as defined by Sunagawa and used globally, describes more a system property than a pure index of arterial load. While in its derivation the assumption was made that heart rate is invariant over time (which would eliminate some influences of the heart on a supposedly pure parameter of the arterial system) it has been shown that Ea is greatly influenced by heart rate fluctuations (Chemla et al., 2003; Segers et al., 2002). It has also been shown to be insensitive to changes in pulsatile arterial load, and dominantly defined by resistance. Additionally, it's inability to be useful in detecting pulsatile load renders a large problem for the parameter, because of the important role arterial pulse wave dynamics play in

LV-AS interactions in hypertension, heart failure, and aging. It has been shown that Ea is a poor representation for arterial stiffening due to its insufficiencies in describing physical elastance, as well as in its lack of responsiveness to arterial or total arterial stiffness (Chemla et al., 2003; Chirinos, 2013; Segers et al., 2002). Because of these drawbacks, more modern approaches are being implemented to avoid using Ea, and instead incorporating compliance.

Pressure-flow relations need to be considered for more accurate and useful analysis of LV-AS interactions. Arterial input impedance, characteristic impedance of the proximal aorta, magnitude and time of forward and reflected waves, and total arterial compliance calculations via pressure-flow analysis, like those demonstrated in the canine portions of this thesis, are the current gold standards for assessing pulsatile LV load (Chirinos, 2013; Nichols et al., 2011). Though flow waveforms were not directly reported in the data collected for the current human studies, total arterial compliance and discrete volume measurements were reported via echocardiograms. Using k versus total arterial compliance, trends in distinguishing HFpEF and HFrEF patients were demonstrated in Figure 4.2.21. Unlike the results for k vs. Ea, where the HFrEF group was linearly distributed over the whole range of k and Ea, the HFrEF group on the k vs. C plot had a more distinguishable behavior — confined in a range of C values between 0.4 and 1.9, and the whole range of k values. This suggests that when using C as a parameter to distinguish HFrEF from HFpEF, the former group will be confined to smaller C values, and the later group will be confined to smaller k values. We saw a similar trend in HFpEF for both k vs. C and k vs. Ea plots: patients were confined to low k values, but spanned the range for Ea and C values, though C values were more distributed. This indicates that HFpEF preserves variability in total arterial compliance and effective arterial elastance, whereas HFrEF patients tend to have a limited range of variability in compliances and more dependent on the effectiveness of the LV-AS coupling.

5.3 Some Suggestions for Future Research

While arterial compliance is a more reliable and physical measure of arterial system properties than Ea, further comparisons of k vs. C and k vs. Ea need to be more widely utilized in a larger population pool in future clinical investigations. Additionally, the merit of pulsatile interactions, in terms of wave reflections and its popular substitute of augmentation index should be included.

It is noteworthy to consider the variability of the results and the caveats of the methods used in the present study. In calculating Emax, V_0 was assumed to be equal to 0, though this is not physically accurate; most patients have a non-zero residual LV volume. Changing this point affects the slope of the ESPV line that Emax is derived from; therefore, depending on the value taken for V_0, results can vary. Figures 5.2.1 through 5.2.6 demonstrate the changes in Emax for both HFpEF and HFrEF patients. Increasing V_0 increases the slope of the ESPV line (increases Emax), and effectively decreases k. However, due to consistently assuming $V_0 = 0$, the results shown in chapter 4 are valid. The only variation that would occur if V_0 where taken to be non-zero would be a uniform decrease in k and increase in Emax for each patient.

The results shown in this thesis are based on a specific patient population, where Figure 5.2.7 shows demographic and pertinent patient distributions. The included patients were mainly male, older than 55 years, did not have high blood pressure, and were equally divided in HFpEF and HFrEF groups. These specific biases may have an effect on the results obtained, while giving insight into trends among populations of similar characteristics. Future studies inclusive of both male and female patients will allow prominence due to sex difference to be more clearly delineated, as it is known that female patients tend to have higher incidence of heart problems post-menopause (Chantler, 2012; Maurer, 2005; Nichols, 2002).

Though the results from this study have presented a comprehensive analysis of the primary clinical parameters of the heart and arterial system as far as pressure and flow wave

analysis, more research can be done investigating the interactions that the simplified lump parameter model was not able to examine. The results and analytic methods presented from this model-based strategy set up further studies to be done to develop an automatic method or software program capable of extracting relevant data from LV and aortic pressure and flow waveforms for use in clinical diagnostic and monitoring settings, especially in diagnosing hypertension and heart failure patients. Work done in the distinguishing HFpEF from HFrEF patients should be expanded and validated. Future work should focus on incorporating pulse wave analysis into diagnostic tools, and presenting it in a clinician-friendly platform to increase the effectiveness and overall success of detection, treatment, and prevention of cardiovascular disease.

(a)

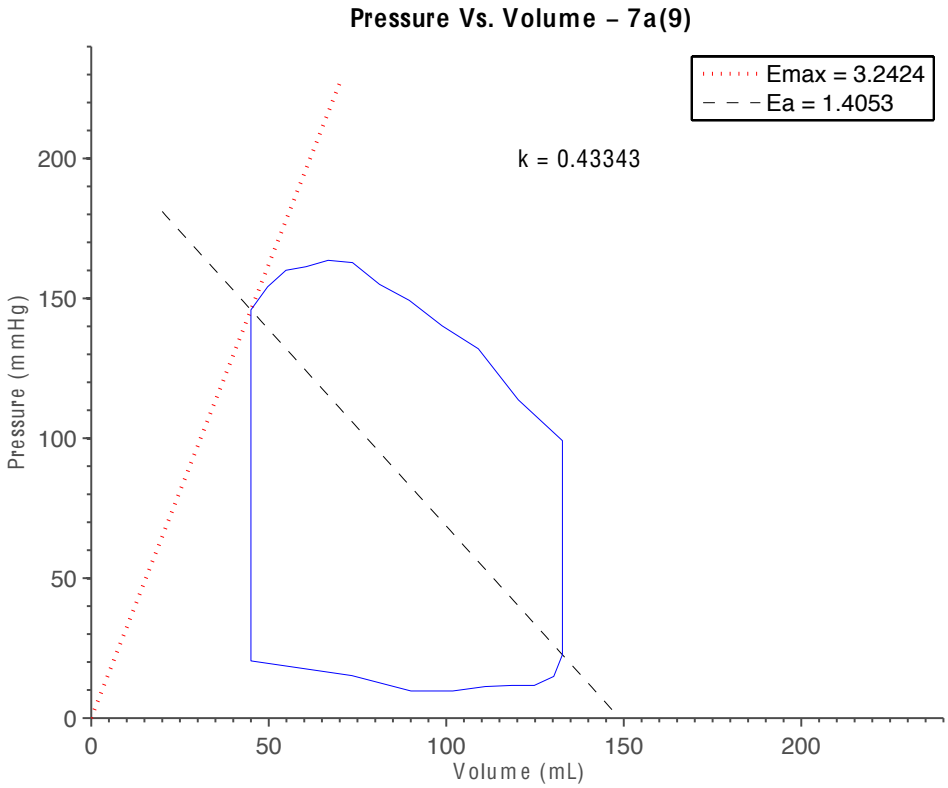

(b)

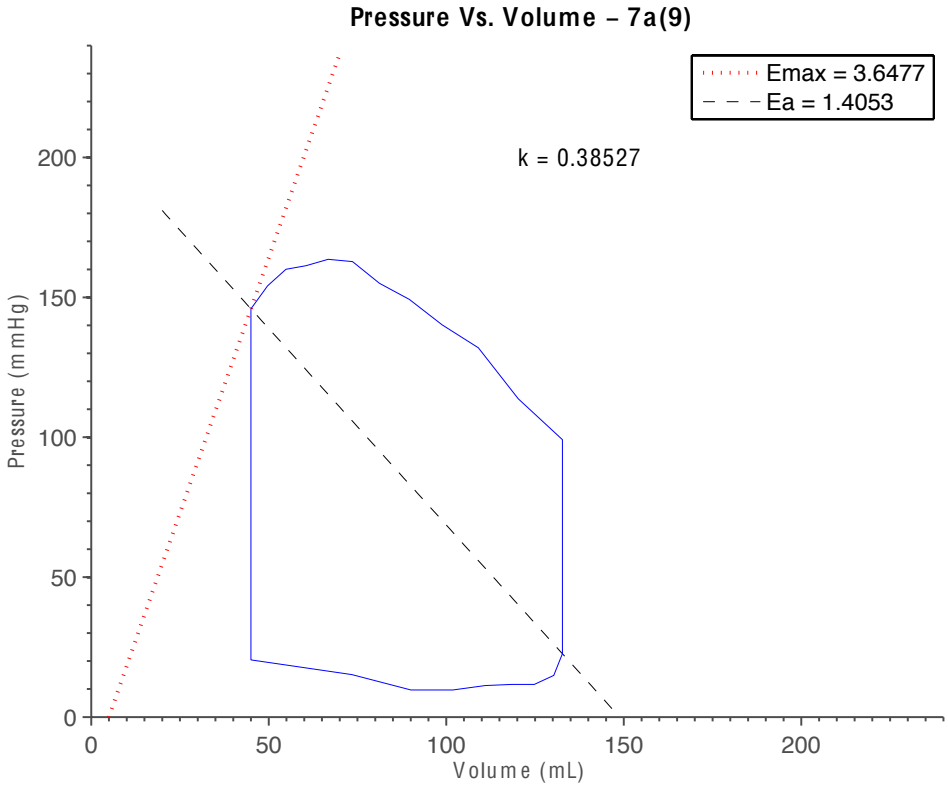

Figure 5.2.1: Patient 7a-9 (EF = 60%): LV Pressure-Volume loops with varying V_0 values *(a)* V_0 = 0 mL; Emax = 3.24; k = 0.433 *(b)* V_0 = 5 mL; Emax = 3.65; k = 0.385

(a)

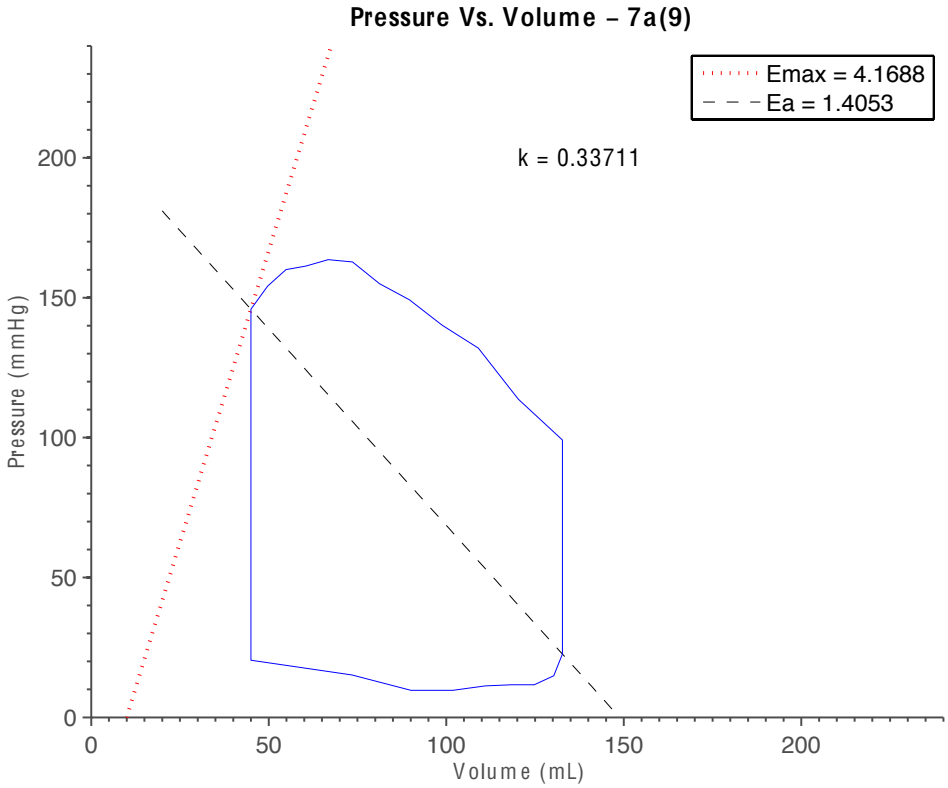

(b)

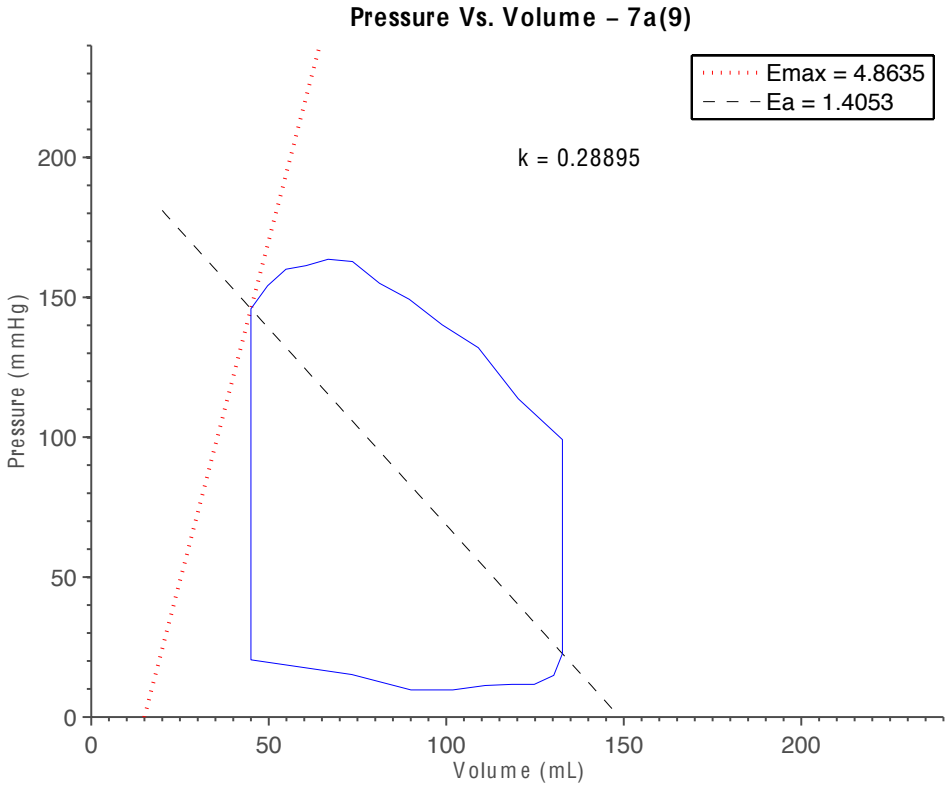

Figure 5.2.2: Patient 7a-9 (EF = 60%): LV Pressure-Volume loops with varying V_0 values *(a)* V_0 = 10 mL; Emax = 4.17; k = 0.337 *(b)* V_0 = 15 mL; Emax = 4.86; k = 0.289

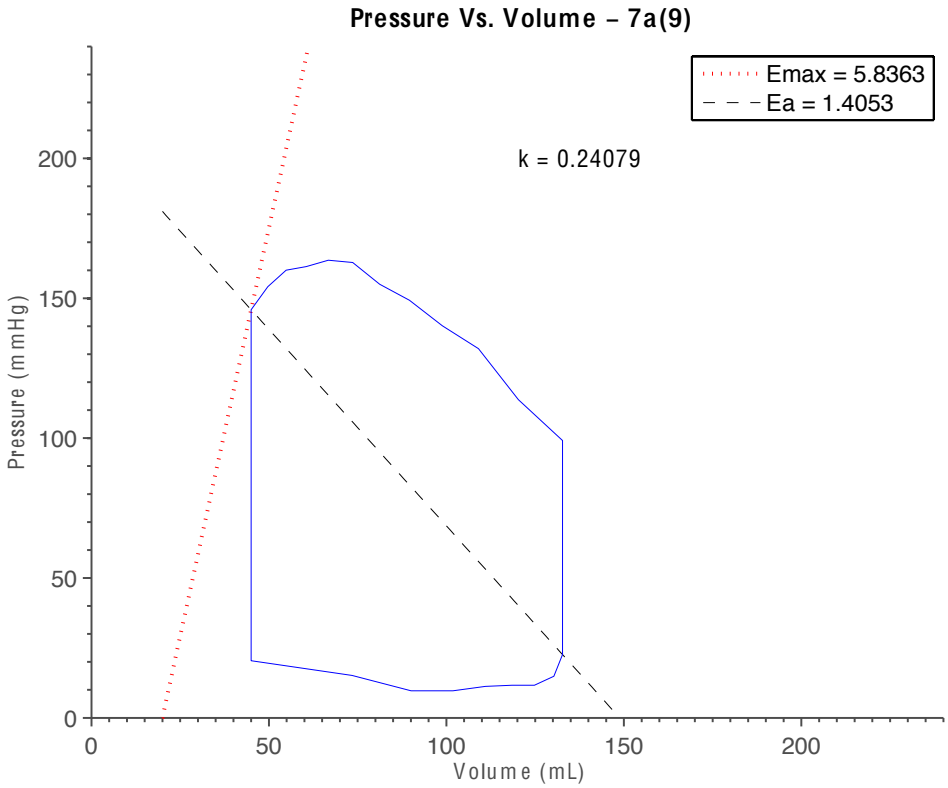

Figure 5.2.3: Patient 7a-9 (EF = 60%): LV Pressure-Volume loops with varying V_0 values
V_0 = 20 mL; Emax = 5.84; k = 0.241

(a)

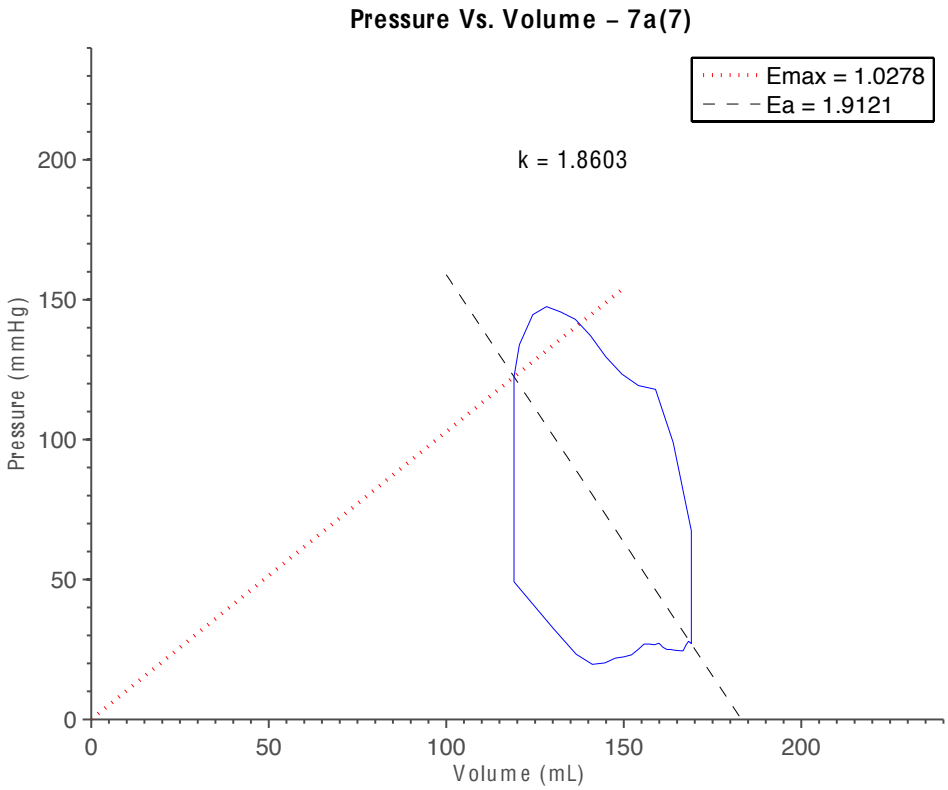

(b)

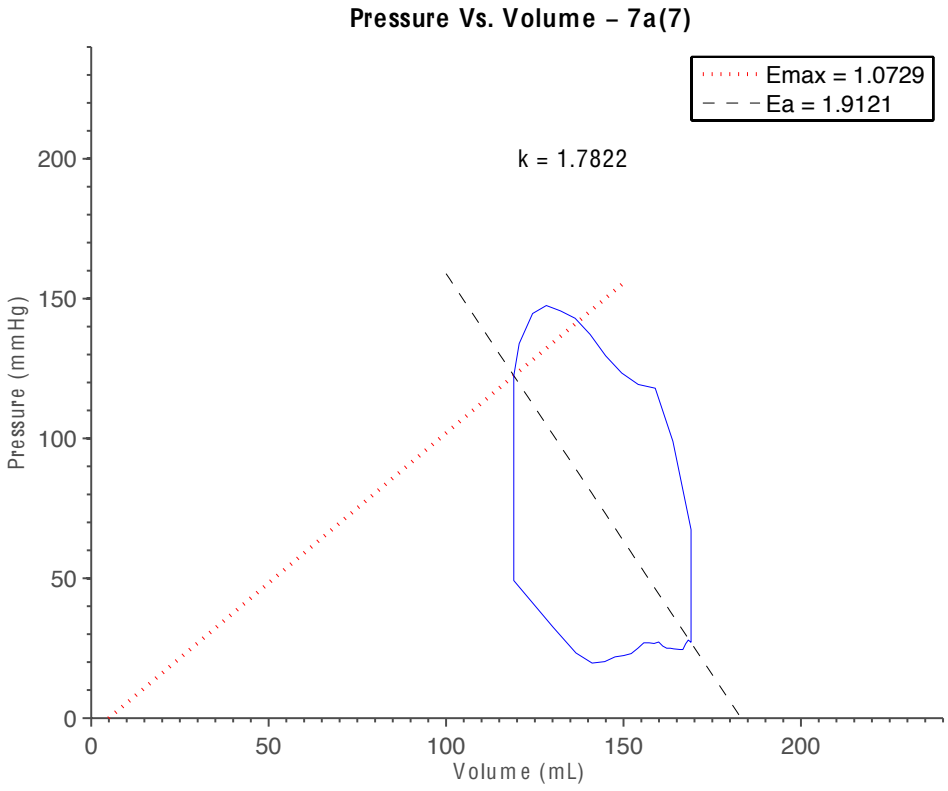

Figure 5.2.4: Patient 7a-7 (EF = 30.2%): LV Pressure-Volume loops with varying V_0 values *(a)* V_0 = 0 mL; Emax = 1.03; k = 1.86 *(b)* V_0 = 5 mL; Emax = 1.07; k = 1.78

(a)

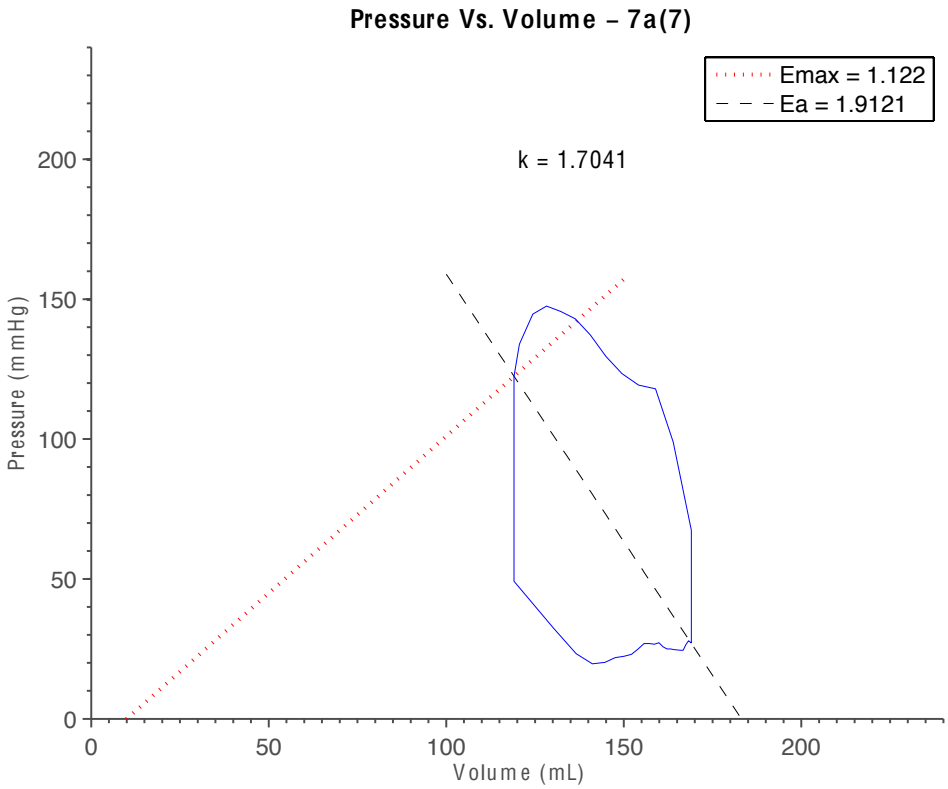

(b)

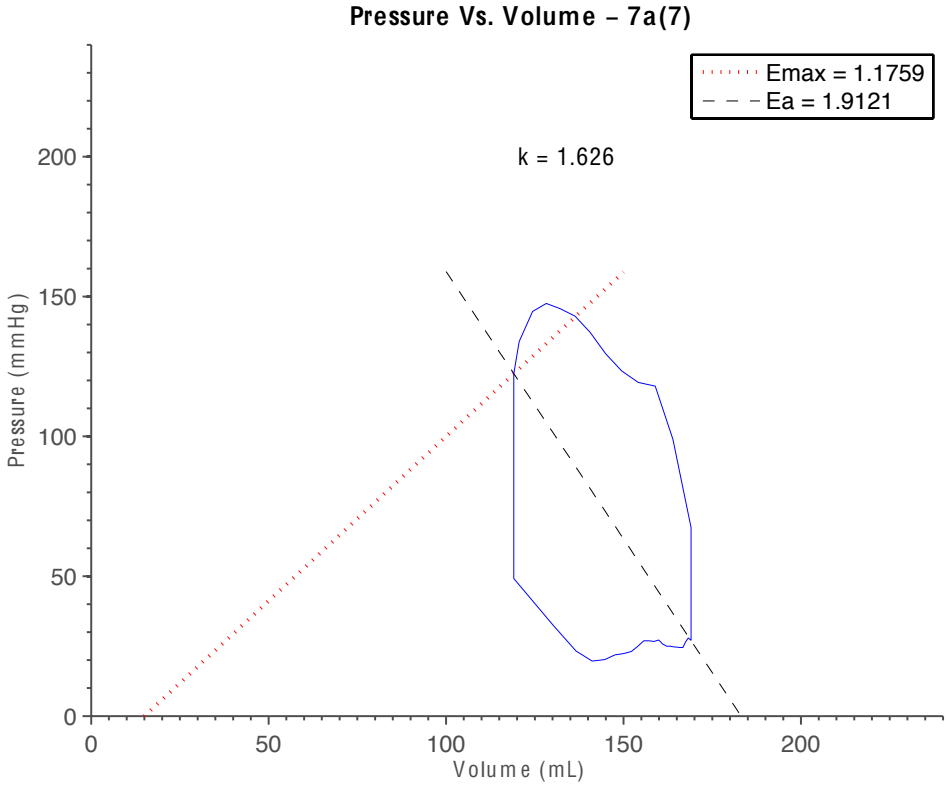

Figure 5.2.5: Patient 7a-7 (EF = 30.2%): LV Pressure-Volume loops with varying V_0 values *(a)* V_0 = 10 mL; Emax = 1.12; k = 1.70 *(b)* V_0 = 15 mL; Emax = 1.18; k = 1.63

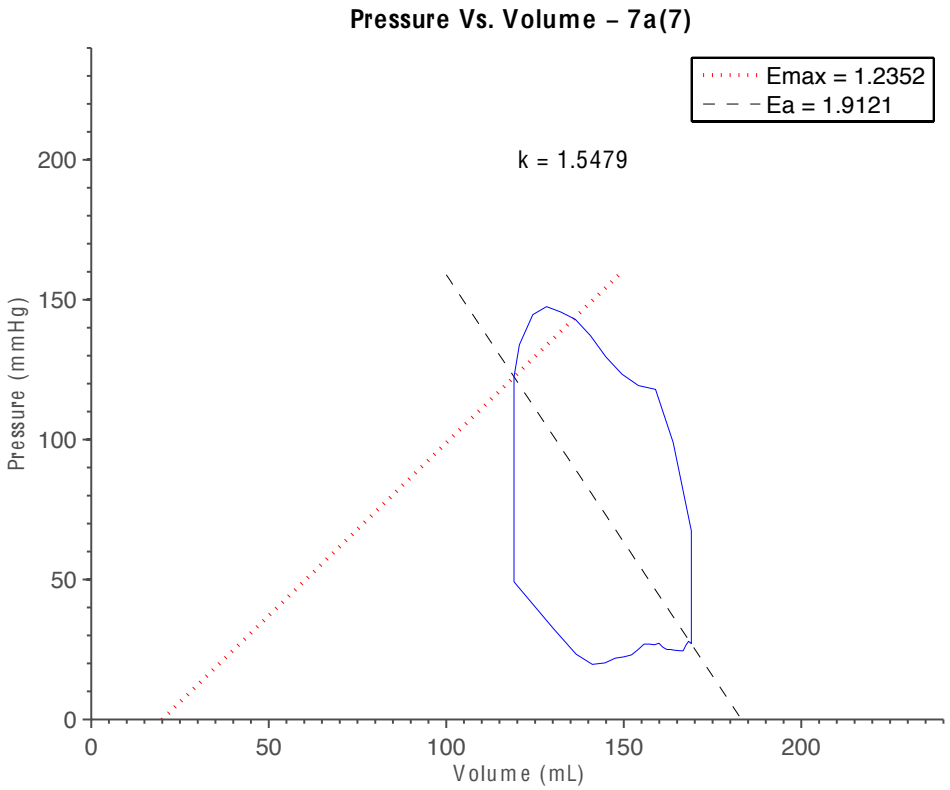

Figure 5.2.6: Patient 7a-7 (EF = 30.2%): LV Pressure-Volume loops with varying V_0 values
V_0 = 20 mL; Emax = 1.14; k = 1.55

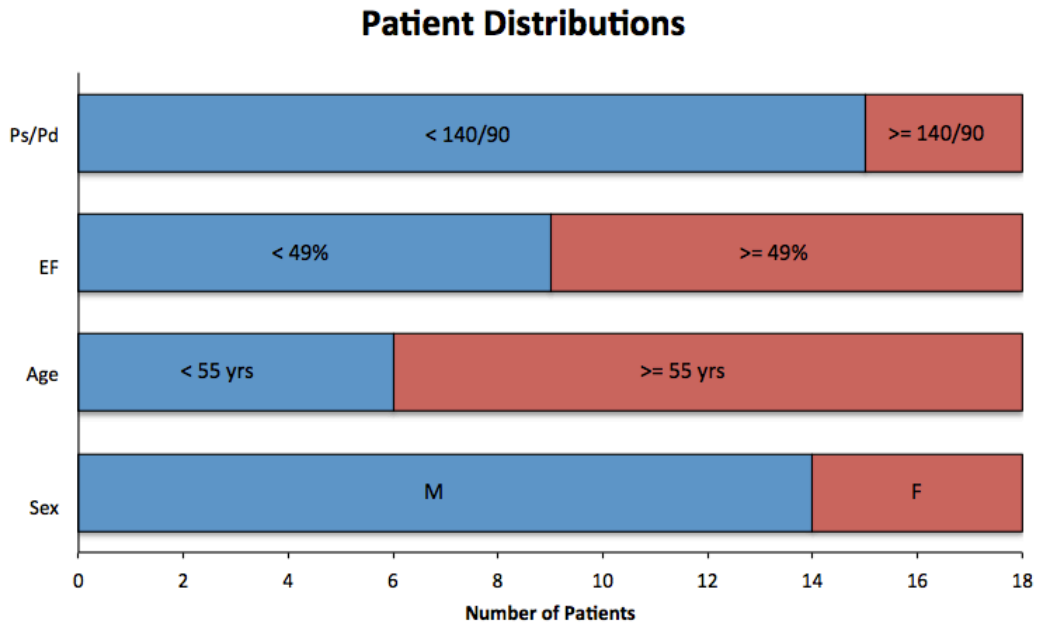

Figure 5.2.7: Patient Distributions by Blood pressure (arterial systolic/diastolic, measured in mmHg), Ejection fraction, Age, and Sex.

References

Berger, D.S., Robinson, K.A. and Shroff, S.G. (1996), "Wave propagation in coupled left ventricle-arterial system. Implications for aortic pressure", *Hypertension*, Vol. 27 No. 5, pp. 1079–89.

Burattini, R. and Gnudi, G. (1982), "Computer identification of models for the arterial tree input impedance: Comparison between two new simple models and first experimental results", *Medical & Biological Engineering & Computing*, Vol. 20 No. 2, pp. 134–144.

Burattini, R., Knowlen, G.G. and Campbell, K.B. (1991), "Two arterial effective reflecting sites may appear as one to the heart", *Circulation research*, Vol. 68 No. 1, pp. 85–99.

Caro, C.G., Pedley, T.J., Schroter, R.C. and Seed, W.A. (2012), *The Mechanics of the Circulation*, Cambridge University Press, New York, 2nded.

Chang, D. "Wiggers Diagram" by DanielChangMD revised original work of DestinyQx - Wikimedia Commons, File:Cardiac Cycle Left Ventricle.PNG. Licensed under CC BY-SA 2.5 via Wikimedia Commons - http://commons.wikimedia.org/wiki/File:Wiggers_Diagram.png#/media/File:Wiggers_Diagram.png

Chantler, P.D., Lakatta, E.G. and Najjar, S.S. (2008), "Arterial-ventricular coupling: mechanistic insights into cardiovascular performance at rest and during exercise", *Journal of applied physiology (Bethesda, Md. : 1985)*, Vol. 105 No. 4, pp. 1342–51.

Chau, N.P., Safar, M.E., London, G.M. and Weiss, Y.A. (1979), "Essential hypertension: an approach to clinical data by the use of models", *Hypertension*, Vol. 1 No. 2, pp. 86–97.

Chemla, D., Antony, I., Lecarpentier, Y. and Nitenberg, A. (2003), "Contribution of systemic vascular resistance and total arterial compliance to effective arterial elastance in humans", *American journal of physiology. Heart and circulatory physiology*, Vol. 285 No. 2, pp. H614–20.

Chirinos, J.A. (2013), "Ventricular-arterial coupling: Invasive and non-invasive assessment.", *Artery research*, Vol. 7 No. 1, doi:10.1016/j.artres.2012.12.002.

Fogliardi, R., Di Donfrancesco, M. and Burattini, R. (1996), "Comparison of linear and nonlinear formulations of the three-element windkessel model", *The American journal of physiology*, Vol. 271 No. 6 Pt 2, pp. H2661–8.

Hardy, H.H., Collins, R.E. and Calvert, R.E. (1982), "A digital computer model of the human circulatory system", *Medical & Biological Engineering & Computing*, Vol. 20 No. 5, pp. 550–564.

Iwano, H. and Little, W.C. (2013), "Heart failure: what does ejection fraction have to do with it?", *Journal of cardiology*, Vol. 62 No. 1, pp. 1–3.

Jager, G.N., Westerhof, N. and Noordergraaf, A. (1965), "Oscillatory Flow Impedance in Electrical Analog of Arterial System:: Representation of Sleeve Effect and Non-Newtonian Properties of Blood", *Circulation Research*, Vol. 16 No. 2, pp. 121–133.

Joyner, M.J. (2006), "Baroreceptor function during exercise: resetting the record.", *Experimental physiology*, Vol. 91 No. 1, pp. 27–36.

Kerkhof, P.L.M., Kresh, J.Y., Li, J.K.-J., and Heyndrickx, G.R. (2013), "Left Ventricular Volume Regulation in heart failure with preserved ejection fraction", *Physiol. Reports*, Vol. 2, e00007, pp. 1-10.

Lee, T.-C., Huang, K.-F., Hsiao, M.-L., Tang, S.-T. and Young, S.-T. (2004), "Electrical lumped model for arterial vessel beds", *Computer methods and programs in biomedicine*, Vol. 73 No. 3, pp. 209–19.

Levick, R.J. (2010), *An Introduction to Cardiovascular Physiology*, CRC Press, London, 5thed.

Li, J.K-J., Cui, T. and Drzewiecki, G.M. (1990), “A nonlinear model of the arterial system incorporating a pressure-dependent compliance”, *IEEE transactions on bio-medical engineering*, Vol. 37 No. 7, pp. 673–8.

Li, J.K.-J. (1989), “Increased Arterial Pulse Wave Reflections and Pulsatile Energy Loss in Acute Hypertension”, *Angiology*, Vol. 40 No. 8, pp. 730–735.

Li, J.K.-J. (2000), *The Arterial Circulation: Physical Principles and Clinical Applications*, Humana Press, Totowa, NJ.

Li, J.K.-J. (2004), *Dynamics of the Vascular System*, World Scientific, Singapore.

Li, J.K.-J., Zhu, Y. and Geipel, P.S. (2010), “Pulse pressure, arterial compliance and wave reflection under differential vasoactive and mechanical loading”, *Cardiovascular engineering (Dordrecht, Netherlands)*, Vol. 10 No. 4, pp. 170–5.

MATLAB and Statistics Toolbox Release 2014a, The MathWorks, Inc., Natick, Massachusetts, United States.

Maurer, M., King, D., El-Khoury Rumbarger, L. (2005), " Left heart failure with a normal ejection fraction: identification of different pathophysiologic mechanisms", *Journal of cardiac failure,*Vol. 11 No. 3, pp. 177-87.

McIlroy, M.B., Seitz, W.S. and Targett, R.C. (1986), “A transmission line model of the normal aorta and its branches”, *Cardiovascular research*, Vol. 20 No. 8, pp. 581–7.

Nichols, W., and Singh, B. (2002), “Augmentation Index as a Measure of Peripheral Vascular Disease State” *Current Opinion in Cardiology*, Vol. 17 No. 5 pp. 543–51.

Nichols, W., O’Rourke, M. and Vlachopoulos, C. (2011), *McDonald’s Blood Flow in Arteries, Sixth Edition: Theoretical, Experimental and Clinical Principles*, CRC Press.

Noordergraaf, A. (1978), *Circulatory System Dynamics*, Academic Press, New York.

O’Rourke, M.F. (1967), “Pressure and flow waves in systemic arteries and the anatomical design of the arterial system”, *Journal of applied physiology*, Vol. 23 No. 2, pp. 139–49.

O’Rourke, M.F. and Avolio, A.P. (1980), “Pulsatile flow and pressure in human systemic arteries. Studies in man and in a multibranched model of the human systemic arterial tree”, *Circulation Research*, Vol. 46 No. 3, pp. 363–372.

Parati, G. and Esler, M. (2012), “The human sympathetic nervous system: its relevance in hypertension and heart failure.”, *European heart journal*, Vol. 33 No. 9, pp. 1058–66.

Rohatgi, A. WebPlotDigitizer. http://arohatgi.info/WebPlotDigitizer/app/ Accessed April 2015.

Segers, P., Stergiopulos, N. and Westerhof, N. (2002), “Relation of effective arterial elastance to arterial system properties”, *American journal of physiology. Heart and circulatory physiology*, Vol. 282 No. 3, pp. H1041–6.

Shim, E.B., Sah, J.Y. and Youn, C.H. (2004), “Mathematical Modeling of Cardiovascular System Dynamics Using a Lumped Parameter Method”, *The Japanese Journal of Physiology*, Vol. 54 No. 6, pp. 545–553.

Sud, V.K., Srinivasan, R.S., Charles, J.B. and Bungo, M.W. (1992), “Mathematical modelling of flow distribution in the human cardiovascular system”, *Medical & Biological Engineering & Computing*, Vol. 30 No. 3, pp. 311–316.

Sunagawa, K., Maughan, W.L., Burkhoff, D. and Sagawa, K. (1983), “Left ventricular interaction with arterial load studied in isolated canine ventricle.”, *The American journal of physiology*, Vol. 245 No. 5 Pt 1, pp. H773–80.

Sunagawa, K., Maughan, W.L. and Sagawa, K. (1985), “Optimal arterial resistance for the maximal stroke work studied in isolated canine left ventricle”, *Circulation research*, Vol. 56 No. 4, pp. 586–95.

Udelson, J.E. (2011), “Heart failure with preserved ejection fraction”, *Circulation*, Vol. 124 No. 21, pp. e540–3.

“Understand Your Risk for Heart Failure”. (n.d.). , available at: http://www.heart.org/HEARTORG/Conditions/HeartFailure/UnderstandYourRiskforHeartF

ailure/Understand-Your-Risk-for-Heart-Failure_UCM_002046_Article.jsp (accessed 6 February 2015).
Westerhof, N., Bosman, F., De Vries, C.J. and Noordergraaf, A. (1969), "Analog studies of the human systemic arterial tree", *Journal of Biomechanics*, Vol. 2 No. 2, pp. 121–143.
Westerhof, N., Elzinga, G. and Sipkema, P. (1971), "An artificial arterial system for pumping hearts", *Journal of applied physiology*, Vol. 31 No. 5, pp. 776–81.
Westerhof, N., Lankhaar, J.-W. and Westerhof, B.E. (2009), "The arterial Windkessel", *Medical & biological engineering & computing*, Vol. 47 No. 2, pp. 131–41.
Widmaier, E.P., Raff, H. and Strang, K.T. (2007), *Vander's Human Physiology: The Mechanisms of Body Function*, McGraw-Hill, 11thed.
World Health Organization. (2011a), *Global status report on noncommunicable diseases 2010*, Geneva.
World Health Organization. (2011b), *Global atlas on cardiovascular disease prevention and control*, Geneva.
World Health Organization. (2013), *A global brief on Hypertension*, Geneva, Switzerland.
Yancy, C.W., Jessup, M., Bozkurt, B., Butler, J., Casey, D.E., Drazner, M.H., Fonarow, G.C., et al. (2013), "2013 ACCF/AHA guideline for the management of heart failure: a report of the American College of Cardiology Foundation/American Heart Association Task Force on practice guidelines", *Circulation*, Vol. 128 No. 16, pp. e240–327.